Appendix B

Quantile IDA Curves for Single-Spring Systems

This appendix presents quantile (16th, 50th and 84th percentile) incremental dynamic analysis (IDA) curves from focused analytical studies on individual spring single-degree-of-freedom (SDOF) systems. These systems consist of spring types 1 through 8, with characteristics described in Chapter 3. This collection of curves is intended to present the range of results for representative short (T=0.5s), moderate (T=1.0s), and long (T=2.0s) period systems, both with and without cyclic degradation. In the figures, the vertical axis is the intensity measure $S_a(T,5\%)$, which is not normalized, and the horizontal axis is the maximum story drift ratio, θ_{max}, in radians. IDA curves with cyclic degradation (black lines) are shown along with IDA curves without cyclic degradation (grey lines). Differences between the black and grey lines in the plots indicate the effect of cyclic degradation given the characteristics of the particular spring and period of vibration.

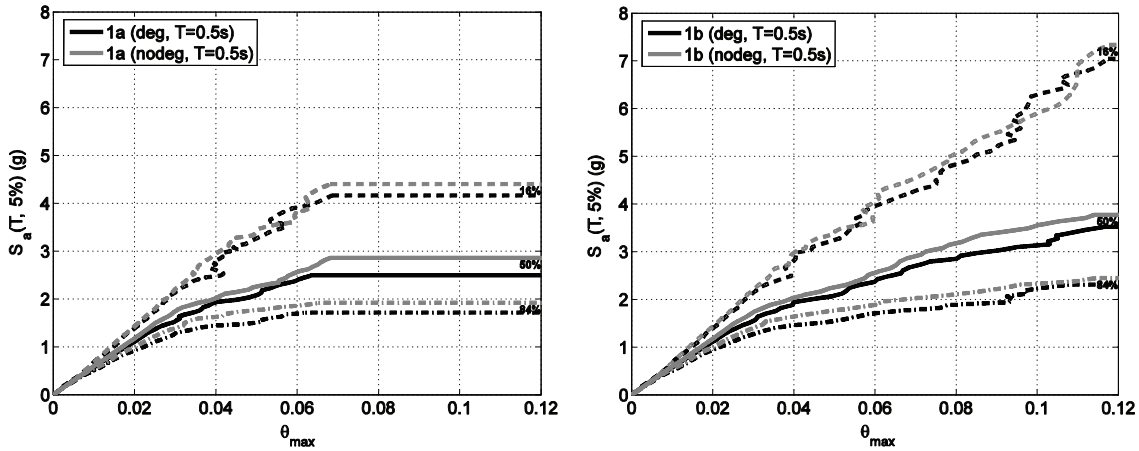

Figure B-1 Quantile IDA curves plotted versus $S_a(T,5\%)$ for Spring 1a and Spring 1b with a period of T = 0.5s

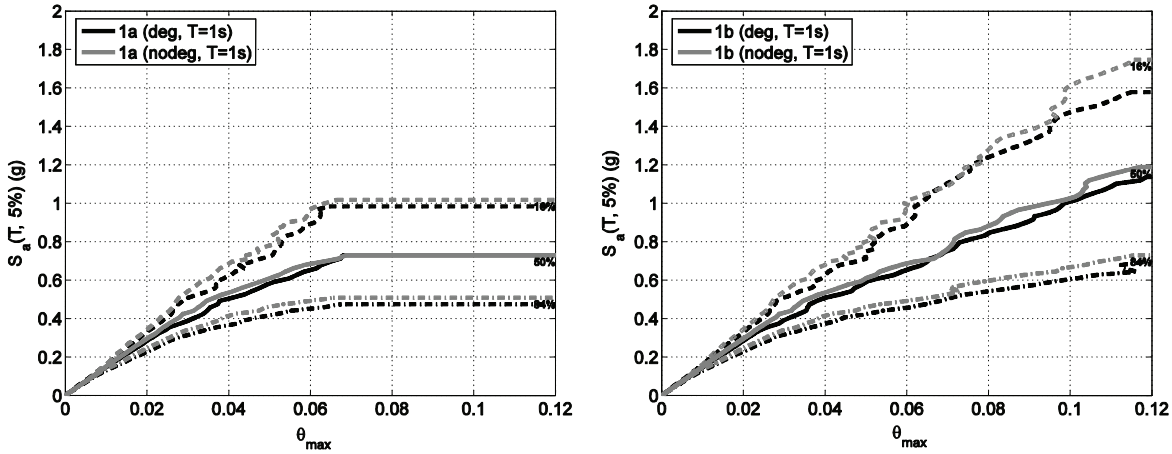

Figure B-2 Quantile IDA curves plotted versus $S_a(T,5\%)$ for Spring 1a and Spring 1b with a period of T = 1.0s.

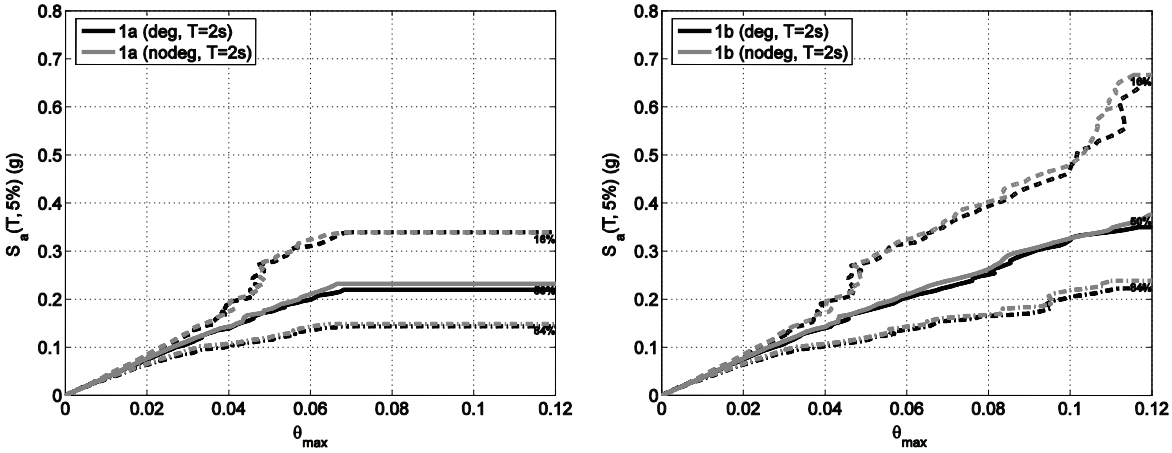

Figure B-3 Quantile IDA curves plotted versus $S_a(T,5\%)$ for Spring 1a and Spring 1b with a period of T = 2.0s.

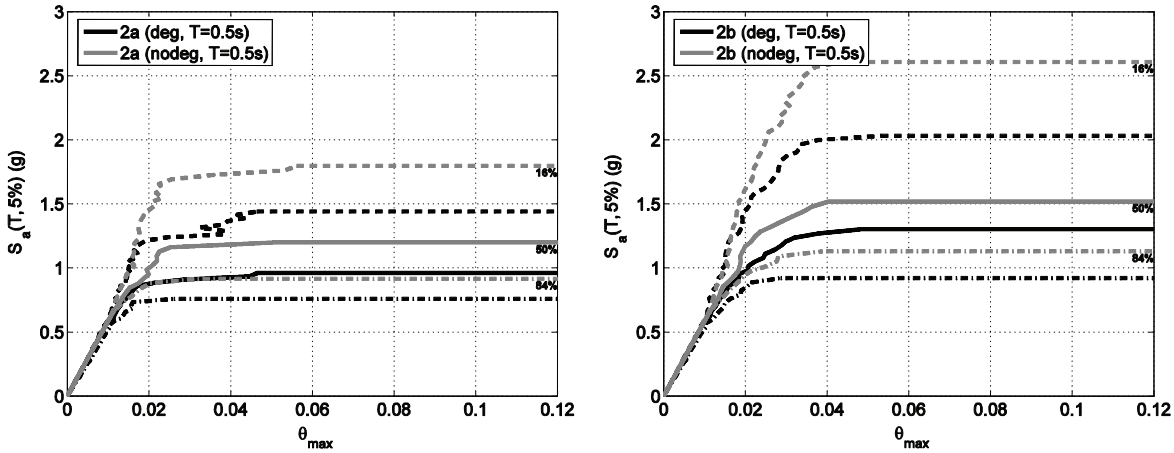

Figure B-4 Quantile IDA curves plotted versus S_a(T,5%) for Spring 2a and Spring 2b with a period of T = 0.5s.

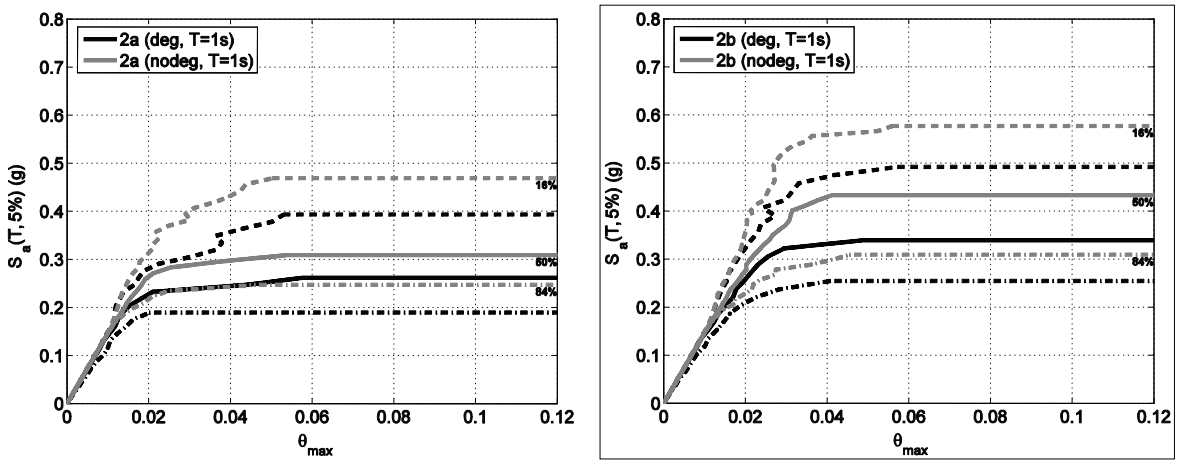

Figure B-5 Quantile IDA curves plotted versus S_a(T,5%) for Spring 2a and Spring 2b with a period of T = 1.0s.

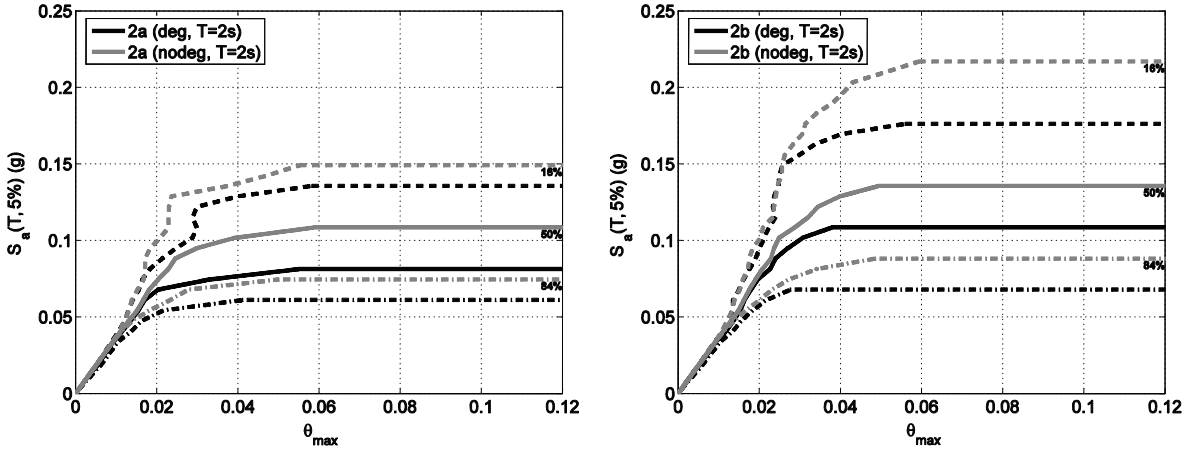

Figure B-6 Quantile IDA curves plotted versus S_a(T,5%) for Spring 2a and Spring 2b with a period of T = 2.0s.

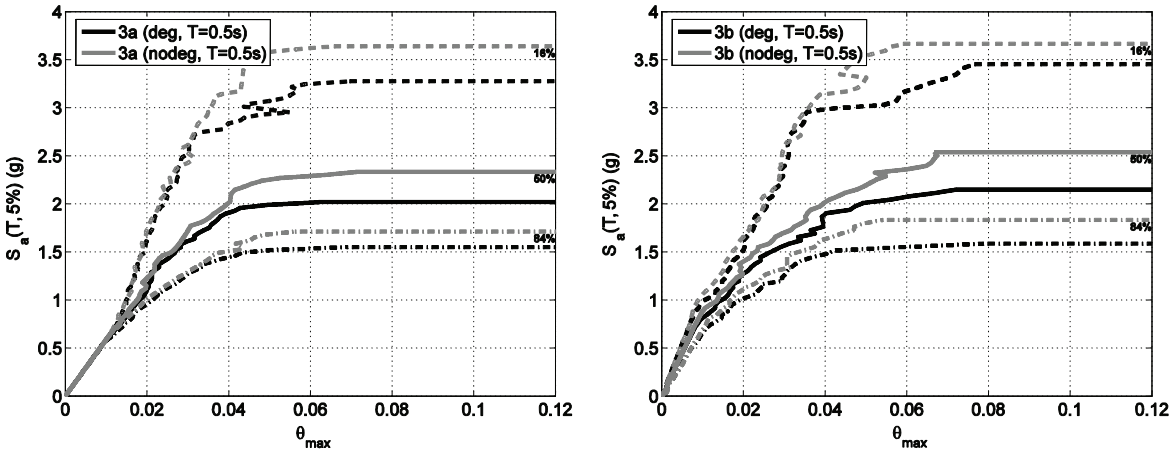

Figure B-7 Quantile IDA curves plotted versus $S_a(T,5\%)$ for Spring 3a and Spring 3b with a period of T = 0.5s.

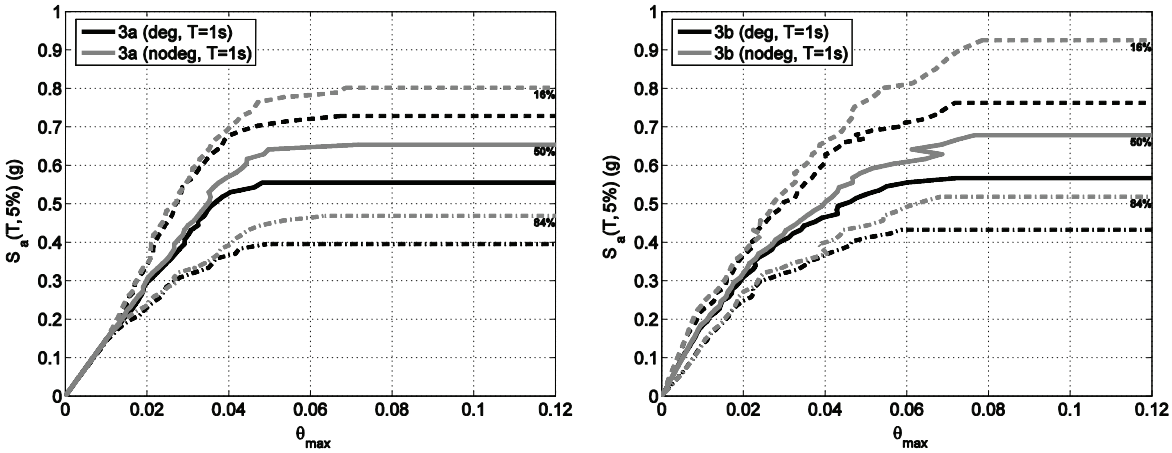

Figure B-8 Quantile IDA curves plotted versus $S_a(T,5\%)$ for Spring 3a and Spring 3b with a period of T = 1.0s.

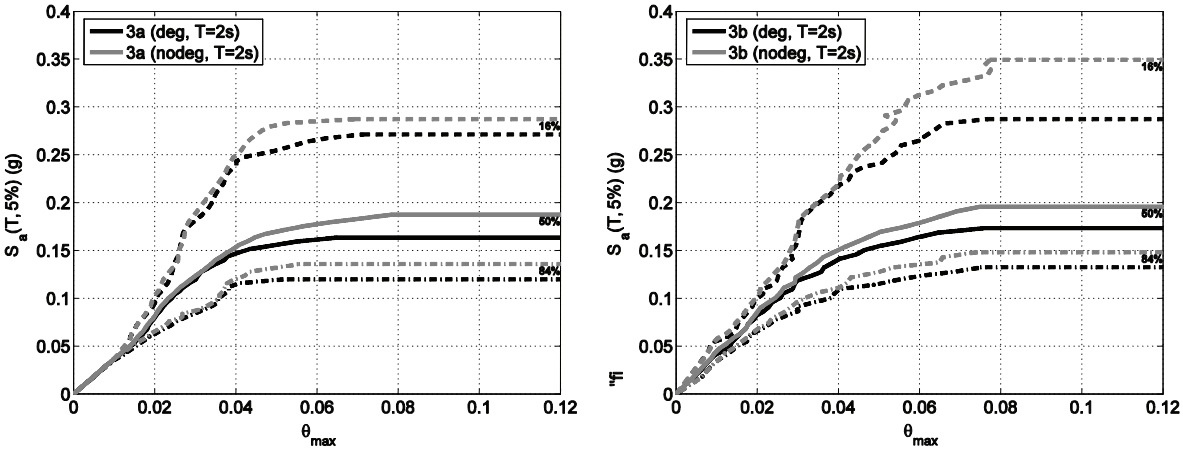

Figure B-9 Quantile IDA curves plotted versus $S_a(T,5\%)$ for Spring 3a and Spring 3b with a period of T = 2.0s.

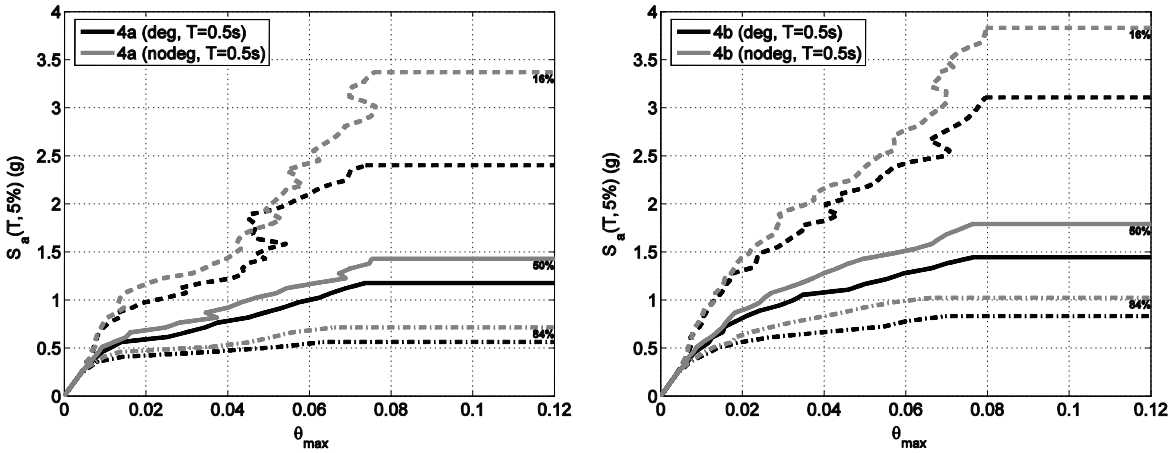

Figure B-10 Quantile IDA curves plotted versus S_a(T,5%) for Spring 4a and Spring 4b with a period of T = 0.5s.

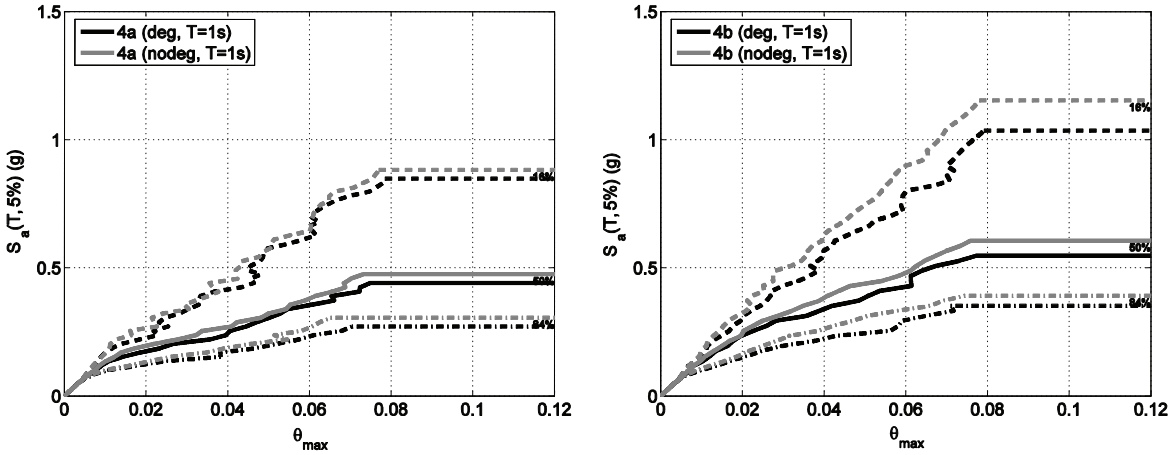

Figure B-11 Quantile IDA curves plotted versus S_a(T,5%) for Spring 4a and Spring 4b with a period of T = 1.0s.

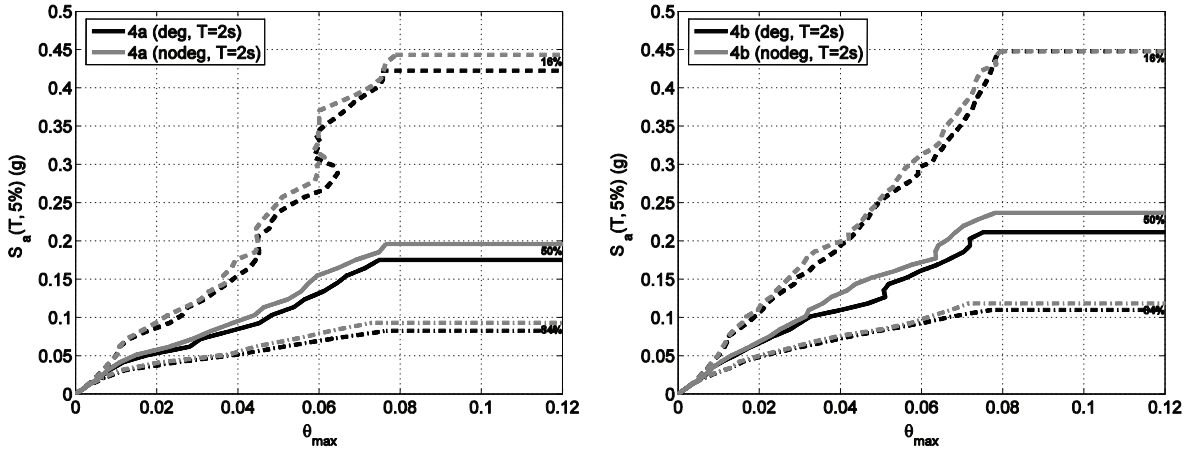

Figure B-12 Quantile IDA curves plotted versus S_a(T,5%) for Spring 4a and Spring 4b with a period of T = 2.0s.

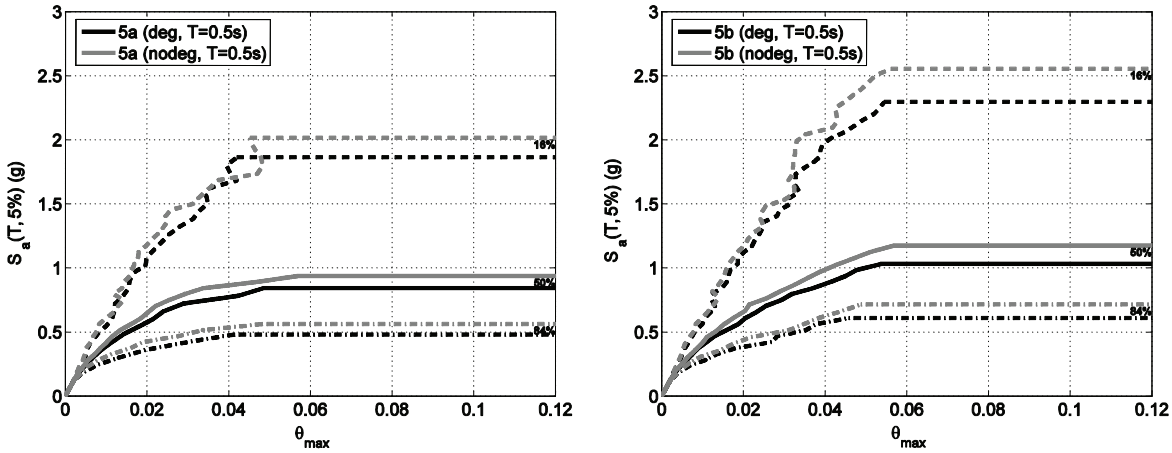

Figure B-13 Quantile IDA curves plotted versus Sa(T,5%) for Spring 5a and Spring 5b with a period of T = 0.5s.

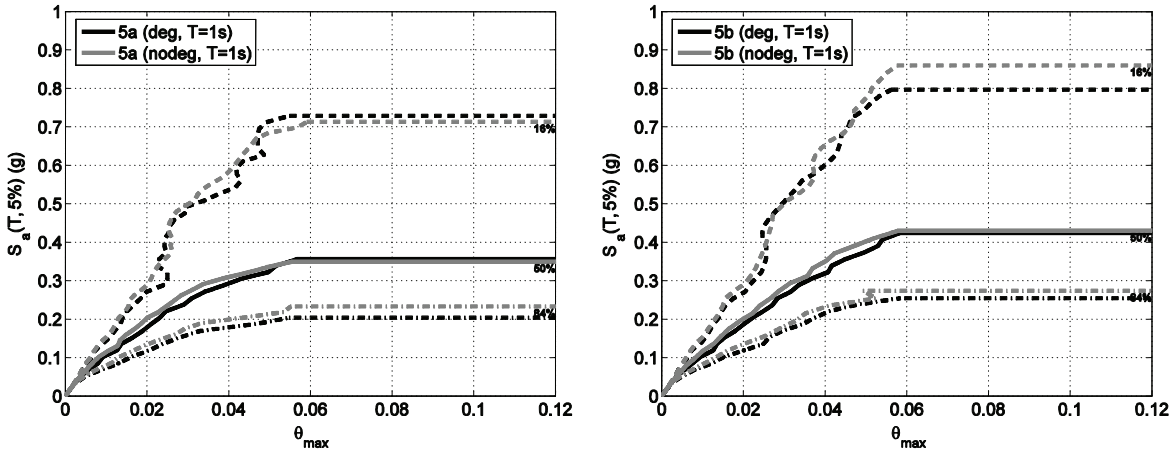

Figure B-14 Quantile IDA curves plotted versus S_a(T,5%) for Spring 5a and Spring 5b with a period of T = 1.0s.

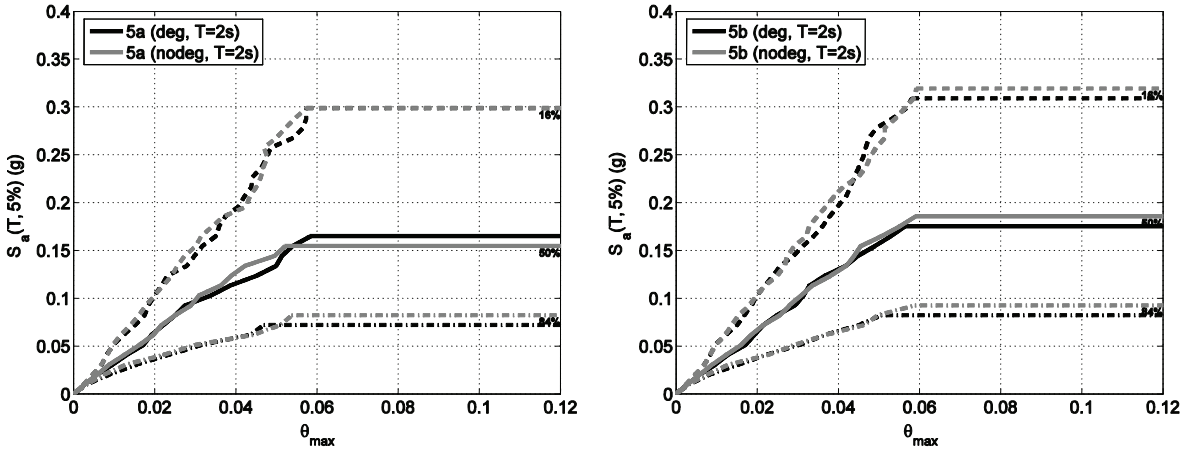

Figure B-15 Quantile IDA curves plotted versus S_a(T,5%) for Spring 5a and Spring 5b with a period of T = 2.0s.

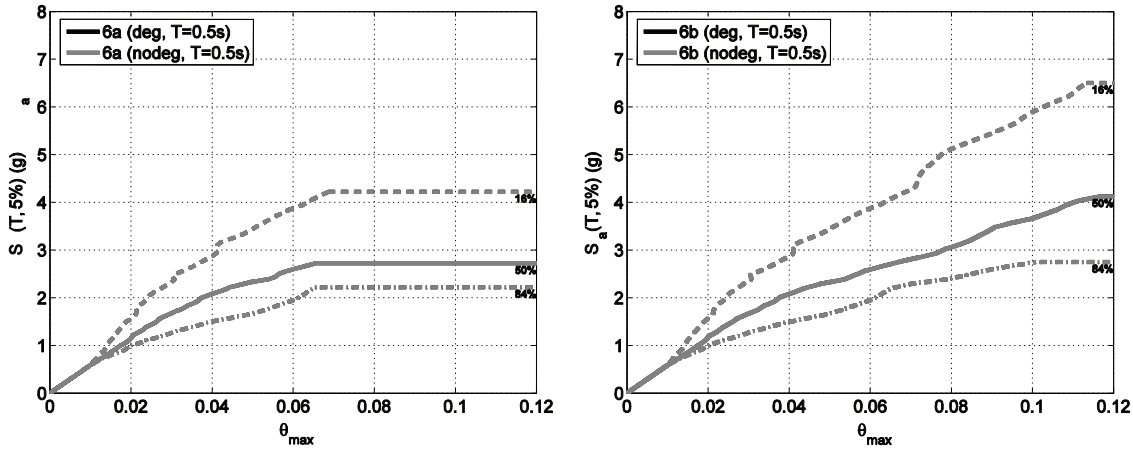

Figure B-16 Quantile IDA curves plotted versus Sa(T,5%) for Spring 6a and Spring 6b with a period of T = 0.5s.

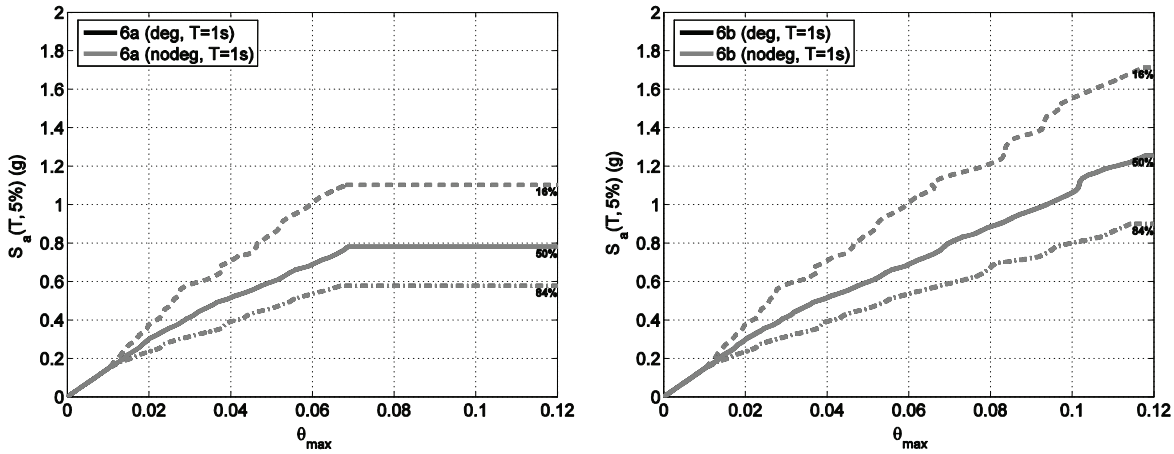

Figure B-17 Quantile IDA curves plotted versus S_a(T,5%) for Spring 6a and Spring 6b with a period of T = 1.0s.

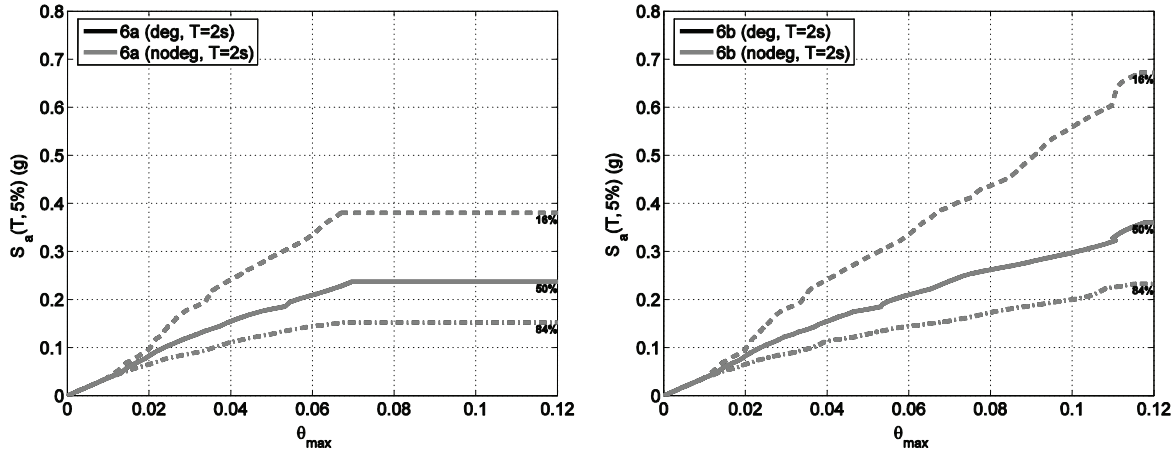

Figure B-18 Quantile IDA curves plotted versus S_a(T,5%) for Spring 6a and Spring 6b with a period of T = 2.0s.

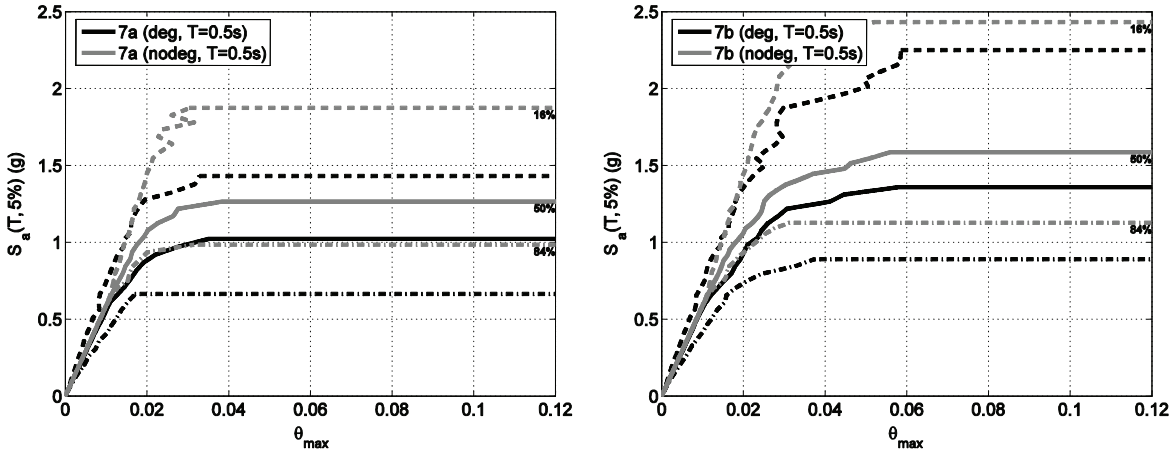

Figure B-19 Quantile IDA curves plotted versus Sa(T,5%) for Spring 7a and Spring 7b with a period of T = 0.5s.

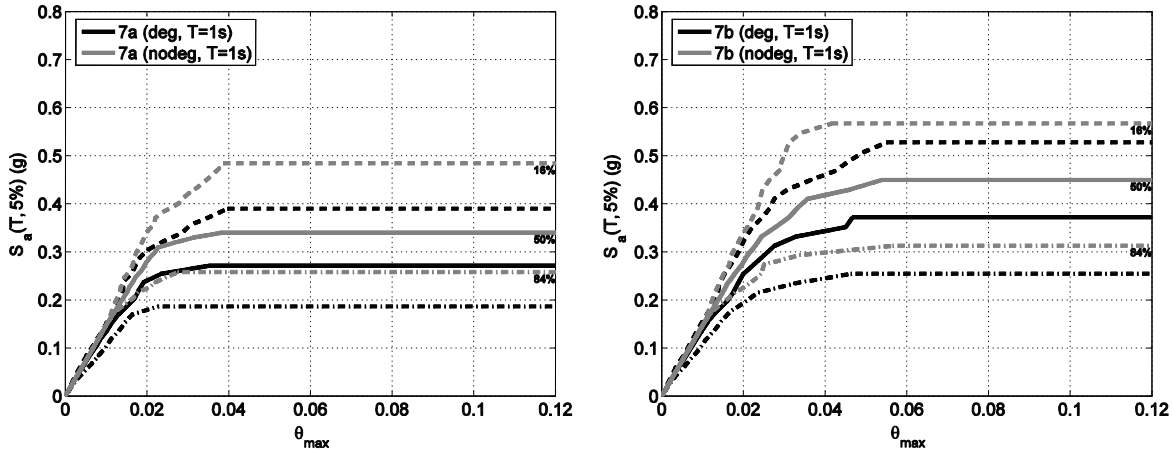

Figure B-20 Quantile IDA curves plotted versus S_a(T,5%) for Spring 7a and Spring 7b with a period of T = 1.0s.

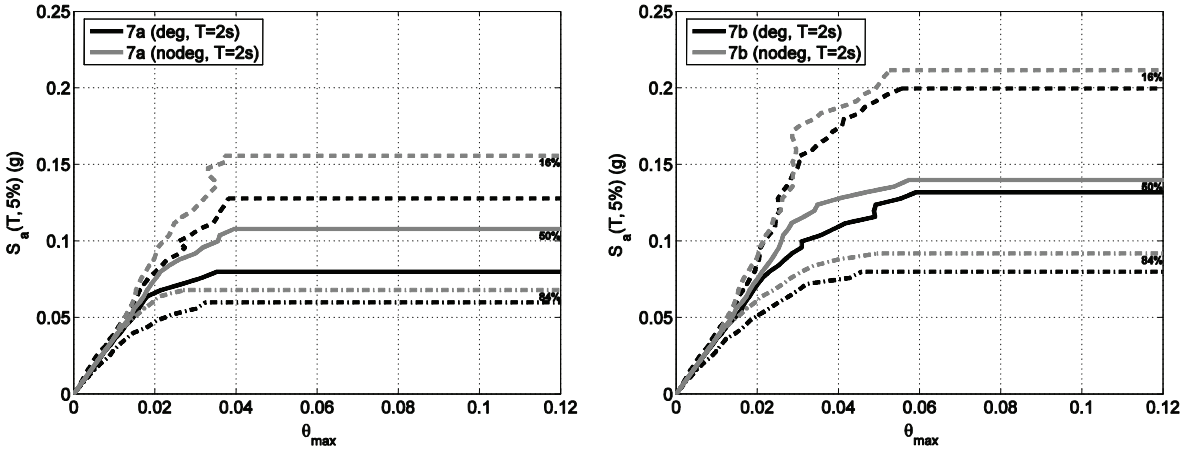

Figure B-21 Quantile IDA curves plotted versus S_a(T,5%) for Spring 7a and Spring 7b with a period of T = 2.0s.

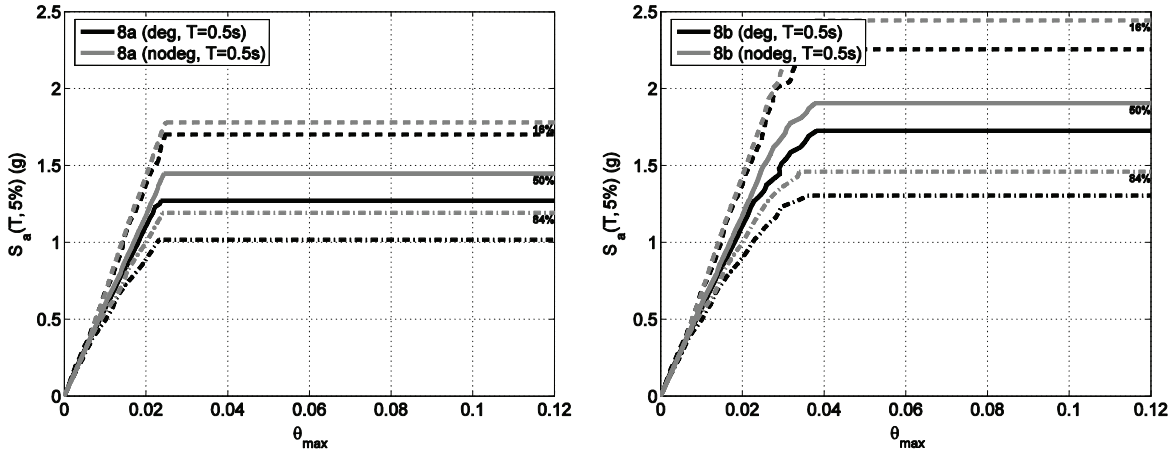

Figure B-22 Quantile IDA curves plotted versus Sa(T,5%) for Spring 8a and Spring 8b with a period of T = 0.5s.

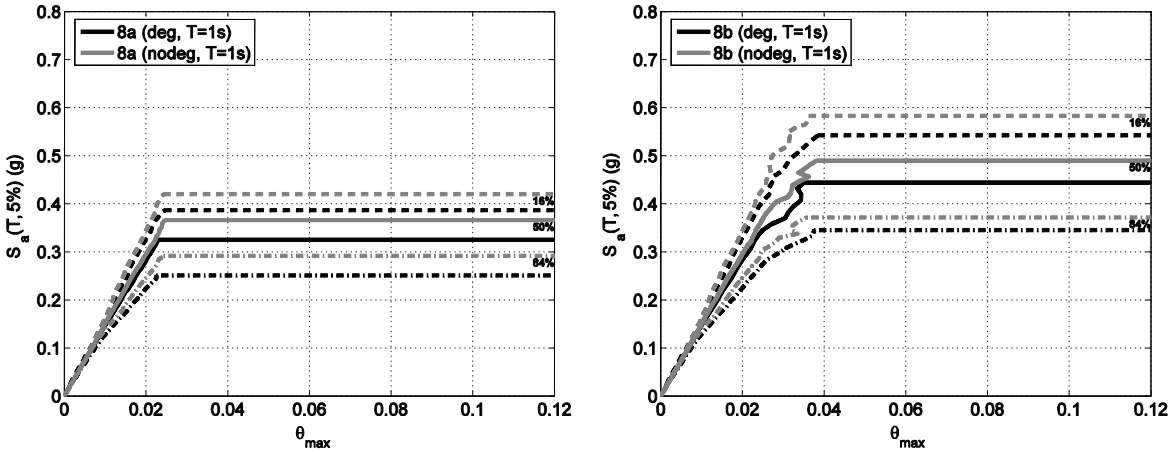

Figure B-23 Quantile IDA curves plotted versus S_a(T,5%) for Spring 8a and Spring 8b with a period of T = 1.0s.

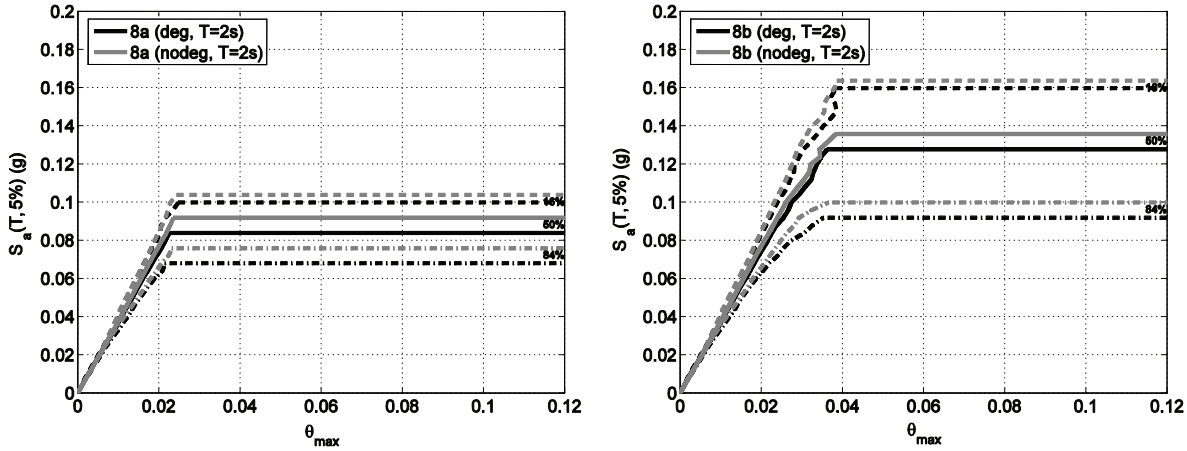

Figure B-24 Quantile IDA curves plotted versus S_a(T,5%) for Spring 8a and Spring 8b with a period of T = 2.0s.

Appendix C

Median IDA Curves for Multi-Spring Systems versus Normalized Intensity Measures

This appendix contains normalized plots of median incremental dynamic analysis (IDA) curves from focused analytical studies on multi-spring single-degree-of-freedom (SDOF) systems. All systems are composed of two springs representing a primary lateral-force-resisting system and a secondary gravity system with the characteristics described in Chapter 3. Multi-spring systems carry a designation of "NxJa+1a" or "NxJa+1b" where "N" is the peak strength multiplier (N = 1, 2, 3, 5, or 9), "J" is the lateral-force-resisting spring number (J = 2, 3, 4, 5, 6, or 7), and 1a or 1b is the gravity system identifier. In all figures, the vertical axis is the normalized intensity measure $R = S_a(T_1,5\%)/S_{ay}(T_1,5\%)$, and the horizontal axis is the maximum story drift ratio, θ_{max}, in radians. The period of vibration for each system is indicated in parentheses.

C.1 Visualization Tool

Given the large volume of analytical data, customized algorithms were developed for post-processing, statistical analysis, and visualization of results. The accompanying CD includes an electronic visualization tool that was developed to view results of multi-spring studies. The tool is a Microsoft Excel based application with a user-interface that accesses a database of all available multi-spring data. By selecting a desired spring combination ("NxJa+1a" or "NxJa+1b"), stiffness level (stiff or flexible), and intensity measure (normalized or non-normalized), users can view the resulting quantile (median, 16th, and 84th percentile) IDA curves for the combination of interest.

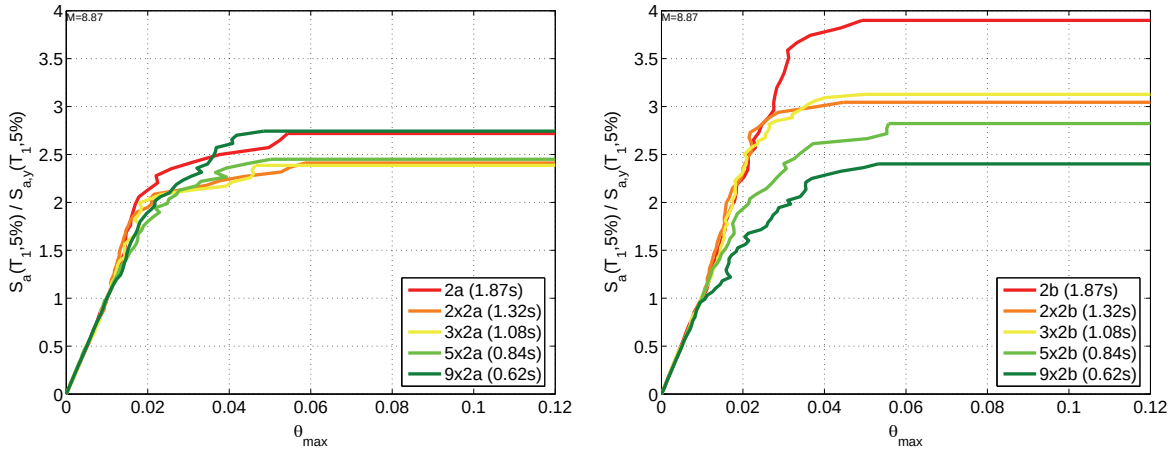

Figure C-1 Median IDA curves plotted versus the normalized intensity measure $R = S_a(T_1,5\%)/S_{ay}(T_1,5\%)$ for systems Nx2a and Nx2b with mass M=8.87ton.

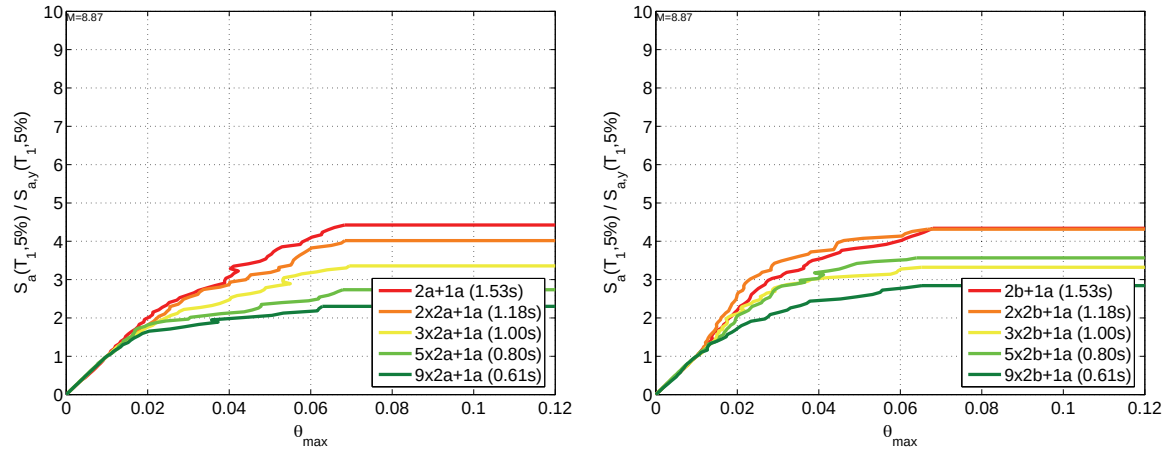

Figure C-2 Median IDA curves plotted versus the normalized intensity measure $R = S_a(T_1,5\%)/S_{ay}(T_1,5\%)$ for systems Nx2a+1a and Nx2b+1a with mass M=8.87ton.

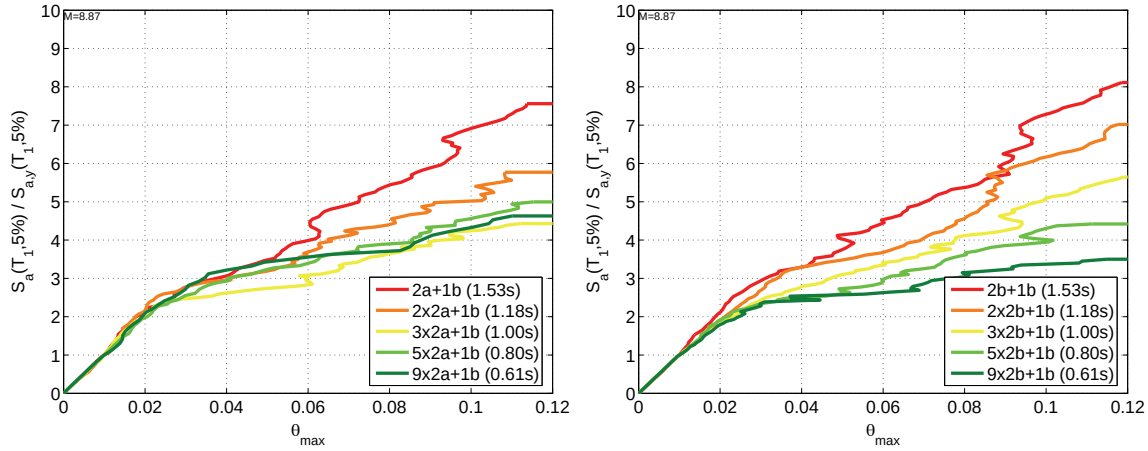

Figure C-3 Median IDA curves plotted versus the normalized intensity measure $R = S_a(T_1,5\%)/S_{ay}(T_1,5\%)$ for systems Nx2a+1b and Nx2b+1b with mass M=8.87ton.

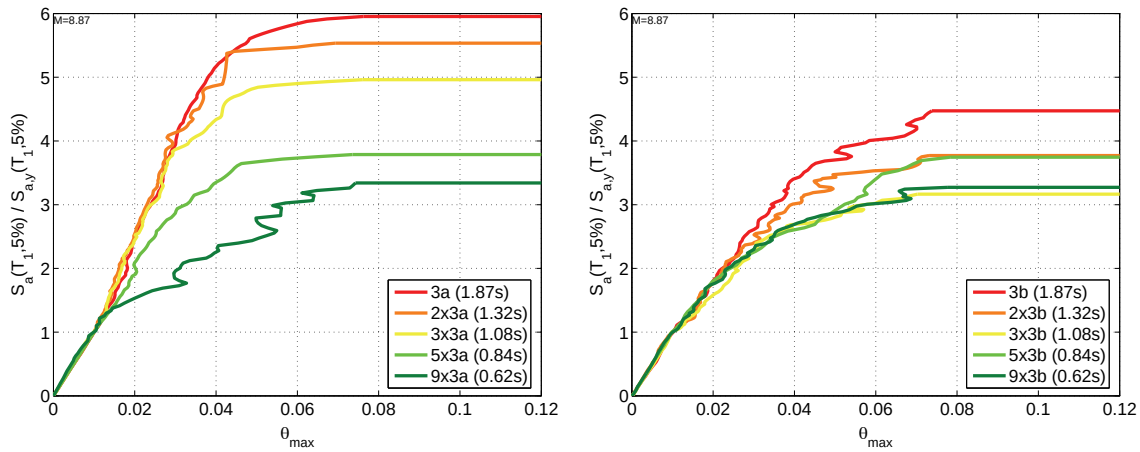

Figure C-4 Median IDA curves plotted versus the normalized intensity measure $R = S_a(T_1,5\%)/S_{ay}(T_1,5\%)$ for systems Nx3a and Nx3b with mass M=8.87ton.

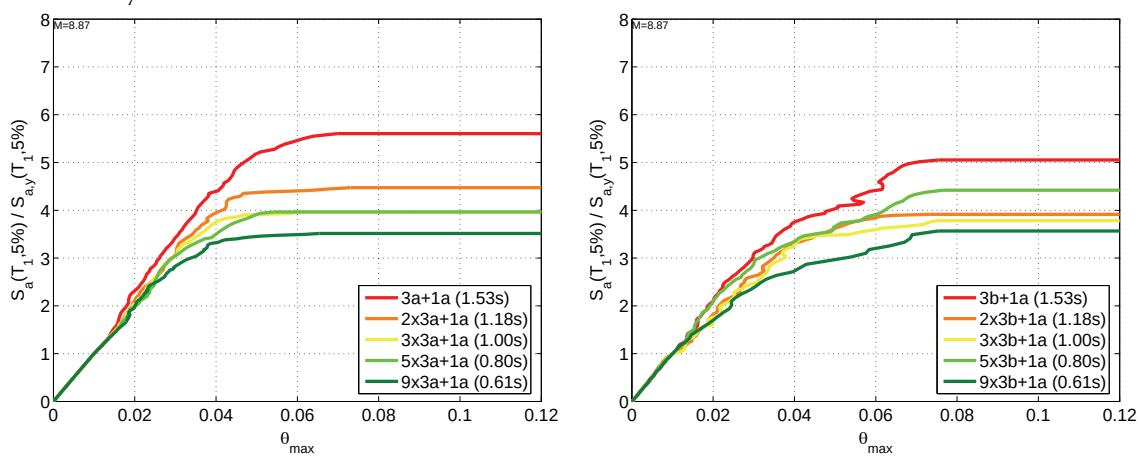

Figure C-5 Median IDA curves plotted versus the normalized intensity measure $R = S_a(T_1,5\%)/S_{ay}(T_1,5\%)$ for systems Nx3a+1a and Nx3b+1a with mass M=8.87ton.

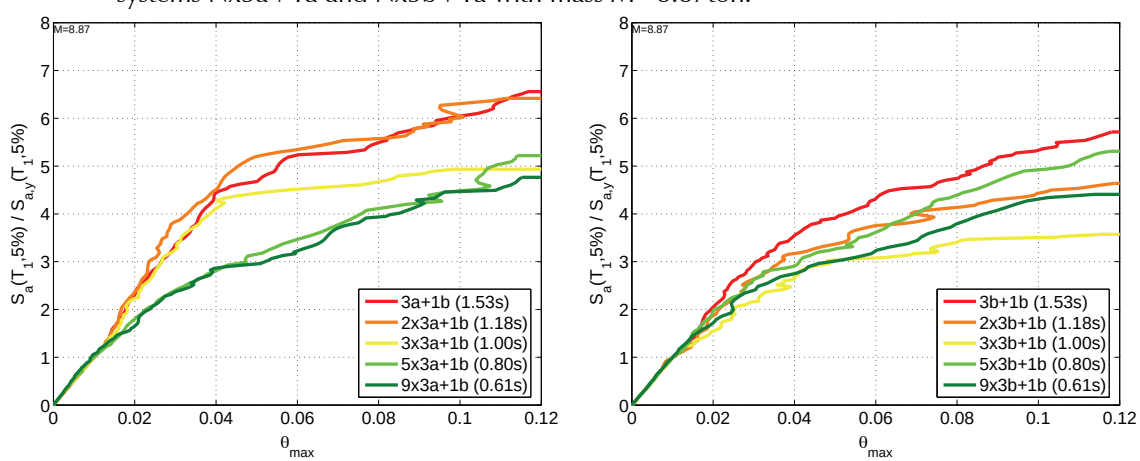

Figure C-6 Median IDA curves plotted versus the normalized intensity measure $R = S_a(T_1,5\%)/S_{ay}(T_1,5\%)$ for systems Nx3a+1b and Nx3b+1b with mass M=8.87ton.

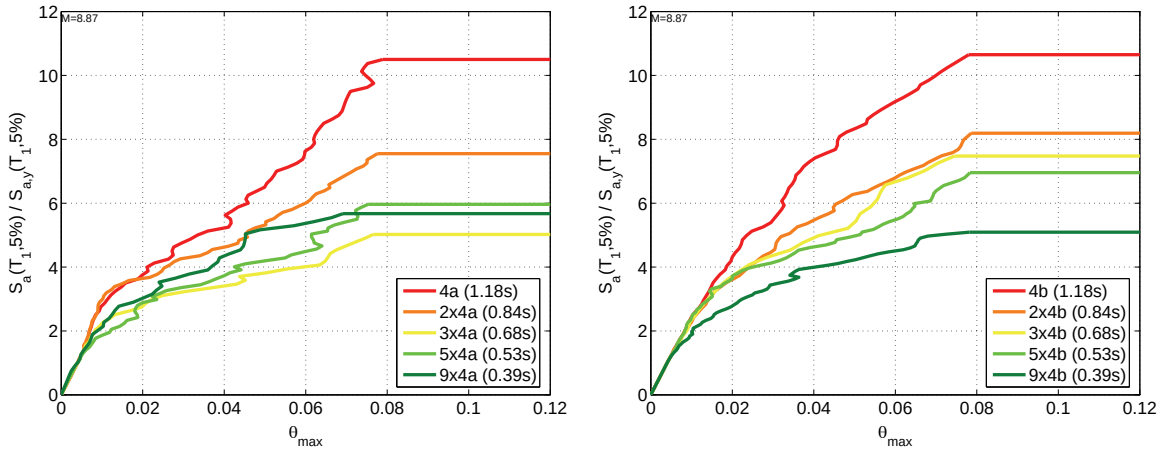

Figure C-7 Median IDA curves plotted versus the normalized intensity measure $R = S_a(T_1,5\%)/S_{ay}(T_1,5\%)$ for systems Nx4a and Nx4b with mass M=8.87ton.

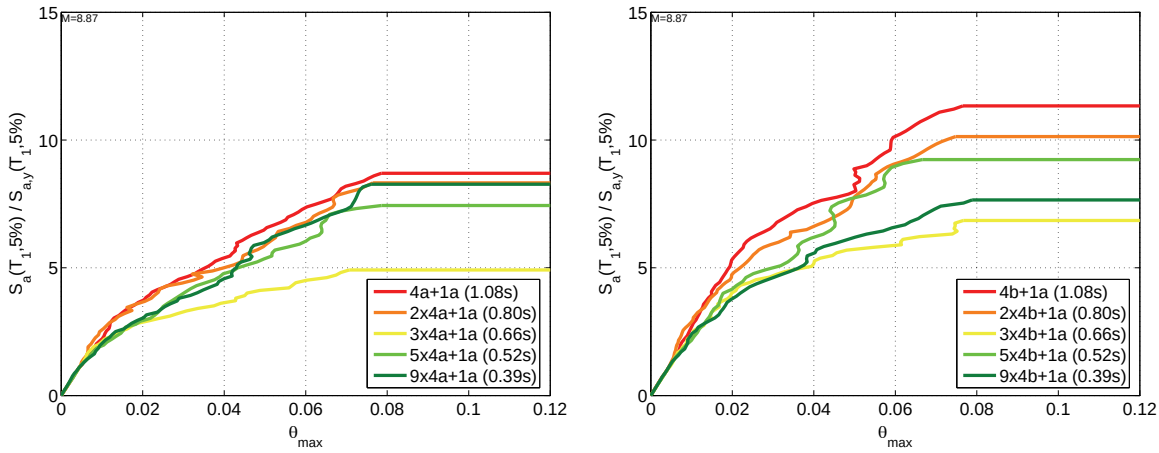

Figure C-8 Median IDA curves plotted versus the normalized intensity measure $R = S_a(T_1,5\%)/S_{ay}(T_1,5\%)$ for systems Nx4a+1a and Nx4b+1a with mass M=8.87ton.

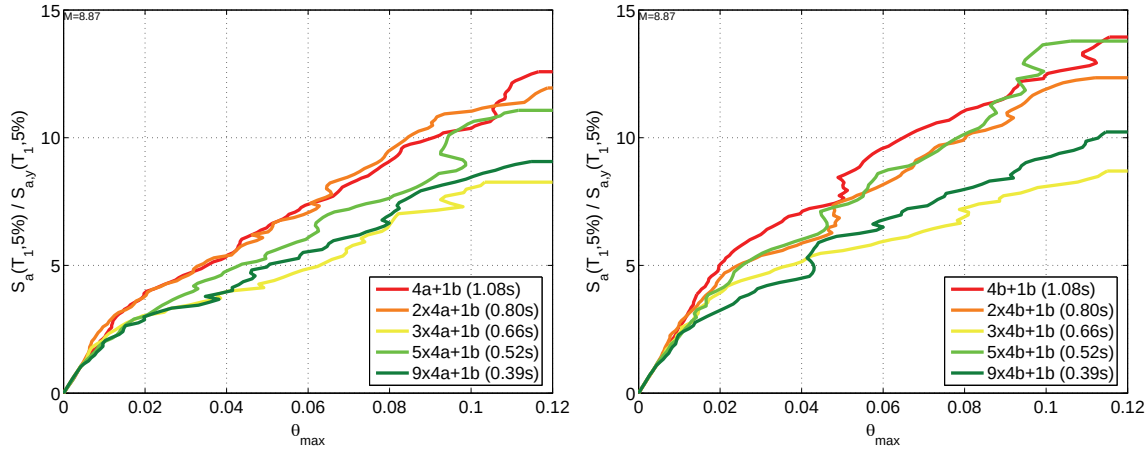

Figure C-9 Median IDA curves plotted versus the normalized intensity measure $R = S_a(T_1,5\%)/S_{ay}(T_1,5\%)$ for systems Nx4a+1b and Nx4b+1b with mass M=8.87ton.

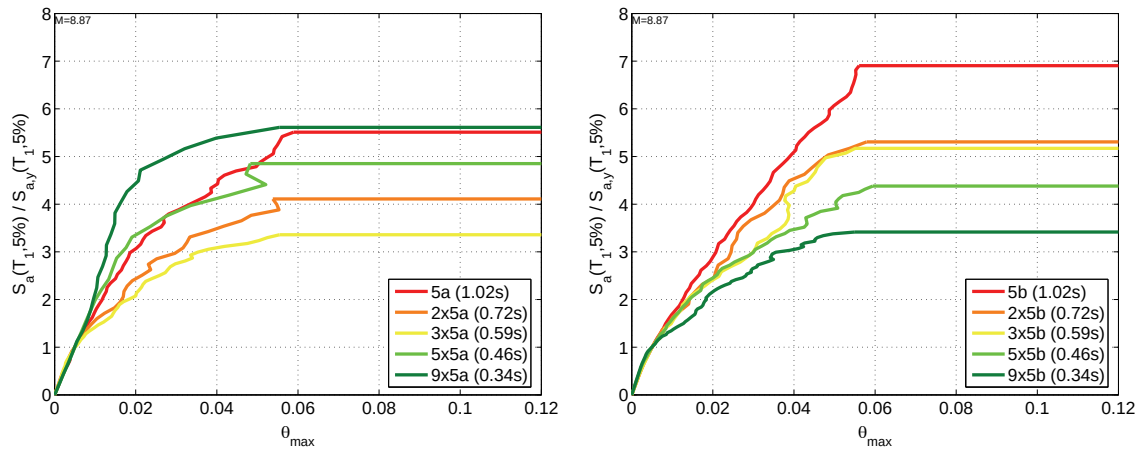

Figure C-10 Median IDA curves plotted versus the normalized intensity measure $R = S_a(T_1,5\%)/S_{ay}(T_1,5\%)$ for systems Nx5a and Nx5b with mass M=8.87ton.

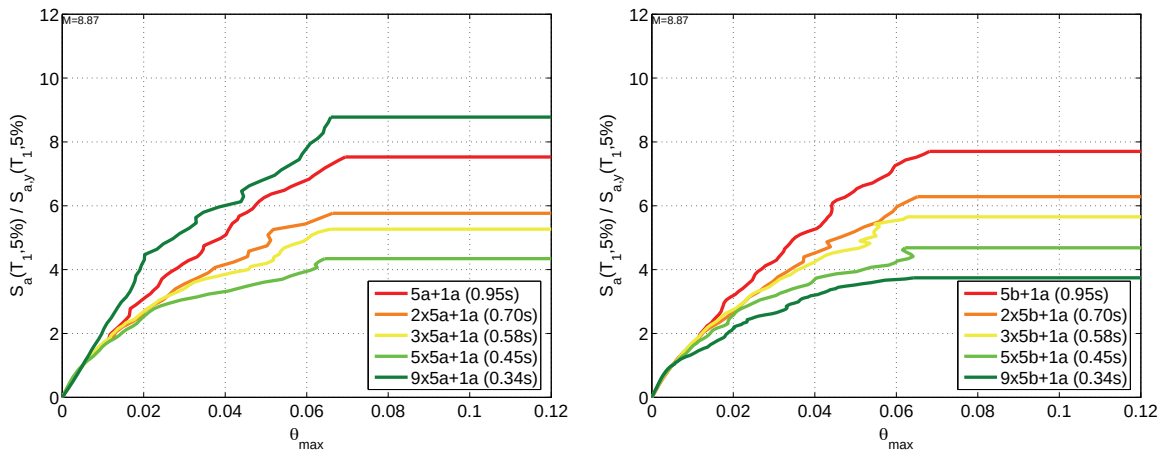

Figure C-11 Median IDA curves plotted versus the normalized intensity measure $R = S_a(T_1,5\%)/S_{ay}(T_1,5\%)$ for systems Nx5a+1a and Nx5b+1a with mass M=8.87ton.

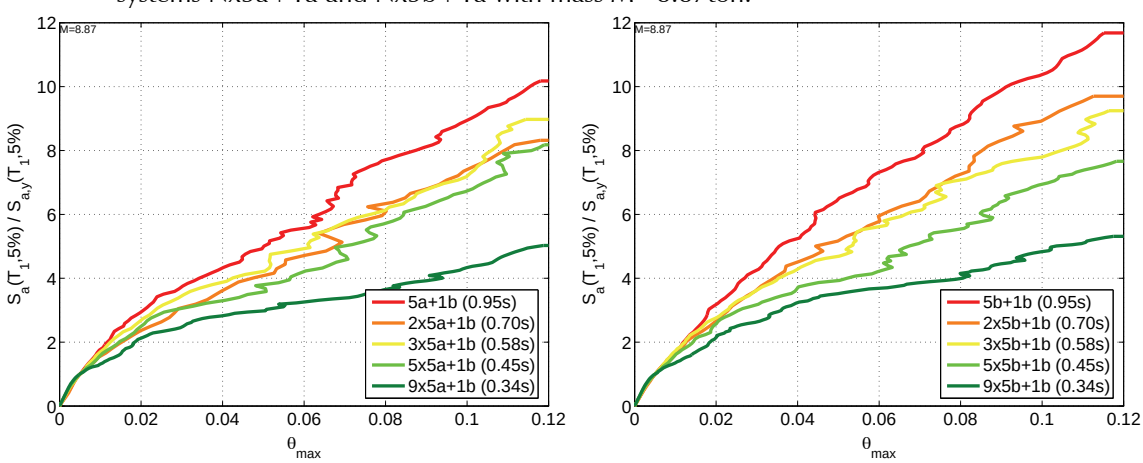

Figure C-12 Median IDA curves plotted versus the normalized intensity measure $R = S_a(T_1,5\%)/S_{ay}(T_1,5\%)$ for systems Nx5a+1b and Nx5b+1b with mass M=8.87ton.

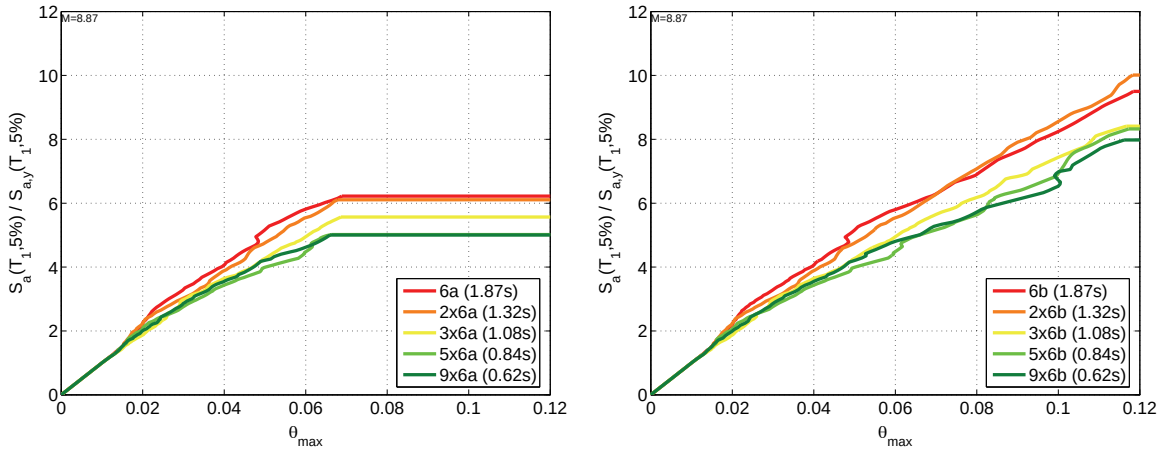

Figure C-13 Median IDA curves plotted versus the normalized intensity measure $R = S_a(T_1,5\%)/S_{ay}(T_1,5\%)$ for systems Nx6a and Nx6b with mass M=8.87ton.

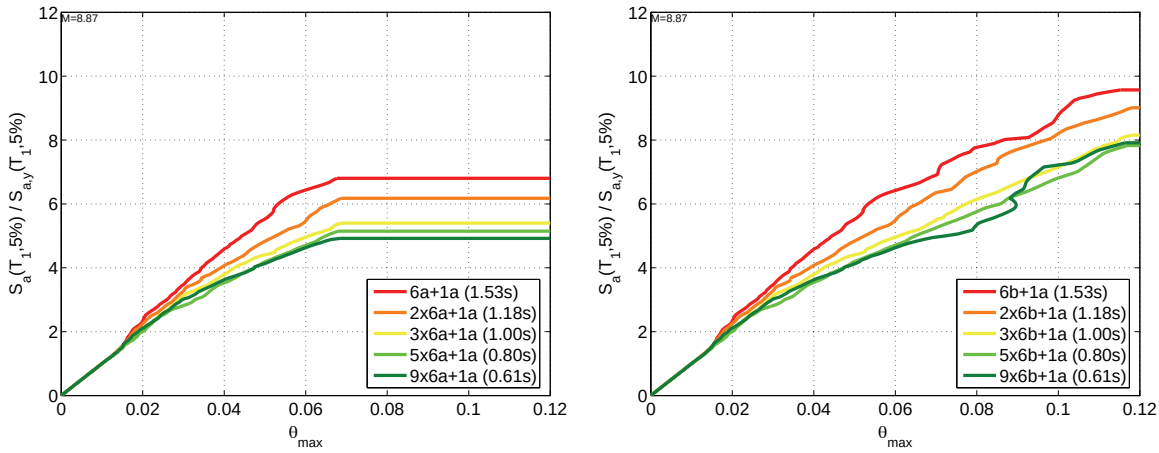

Figure C-14 Median IDA curves plotted versus the normalized intensity measure $R = S_a(T_1,5\%)/S_{ay}(T_1,5\%)$ for systems Nx6a+1a and Nx6b+1a with mass M=8.87ton.

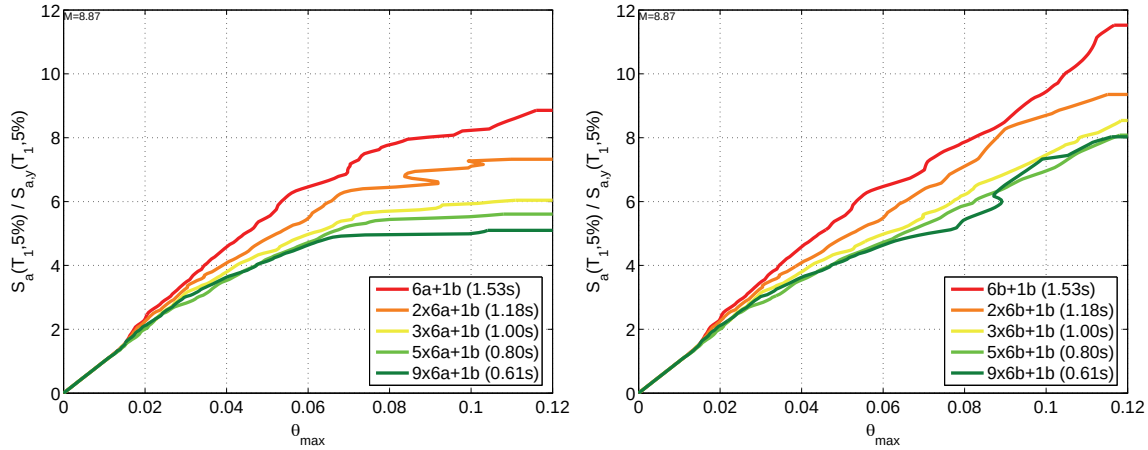

Figure C-15 Median IDA curves plotted versus the normalized intensity measure $R = S_a(T_1,5\%)/S_{ay}(T_1,5\%)$ for systems Nx6a+1b and Nx6b+1b with mass M=8.87ton.

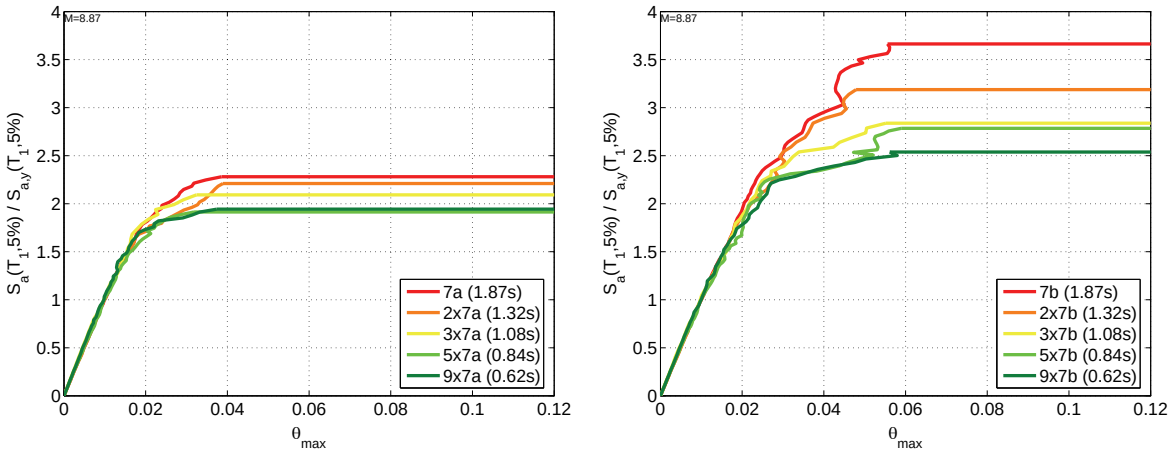

Figure C-16 Median IDA curves plotted versus the normalized intensity measure $R = S_a(T_1,5\%)/S_{ay}(T_1,5\%)$ for systems Nx7a and Nx7b with mass M=8.87ton.

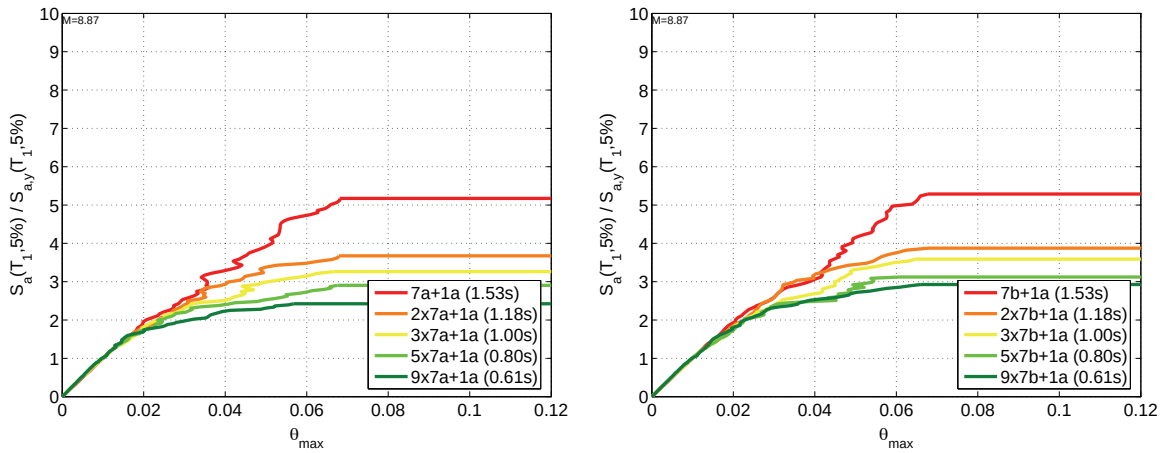

Figure C-17 Median IDA curves plotted versus the normalized intensity measure $R = S_a(T_1,5\%)/S_{ay}(T_1,5\%)$ for systems Nx7a+1a and Nx7b+1a with mass M=8.87ton.

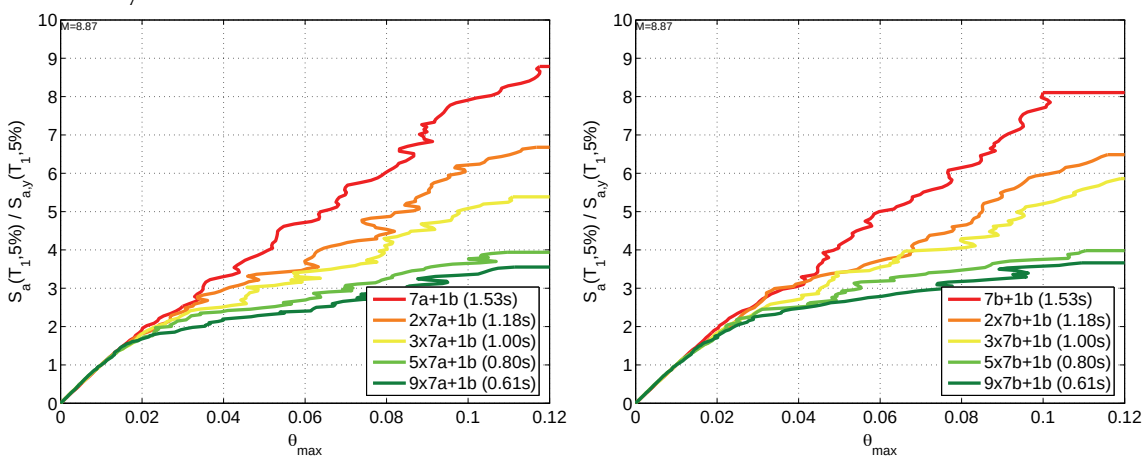

Figure C-18 Median IDA curves plotted versus the normalized intensity measure $R = S_a(T_1,5\%)/S_{ay}(T_1,5\%)$ for systems Nx7a+1b and Nx7b+1b with mass M=8.87ton.

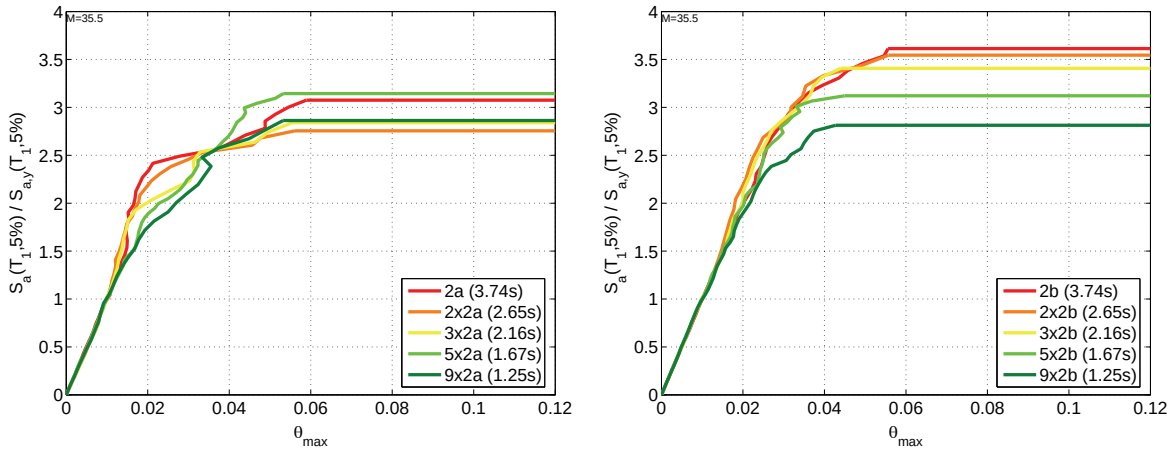

Figure C-19. Median IDA curves plotted versus the normalized intensity measure $R = S_a(T_1,5\%)/S_{ay}(T_1,5\%)$ for systems Nx2a and Nx2b with mass M=35.46ton.

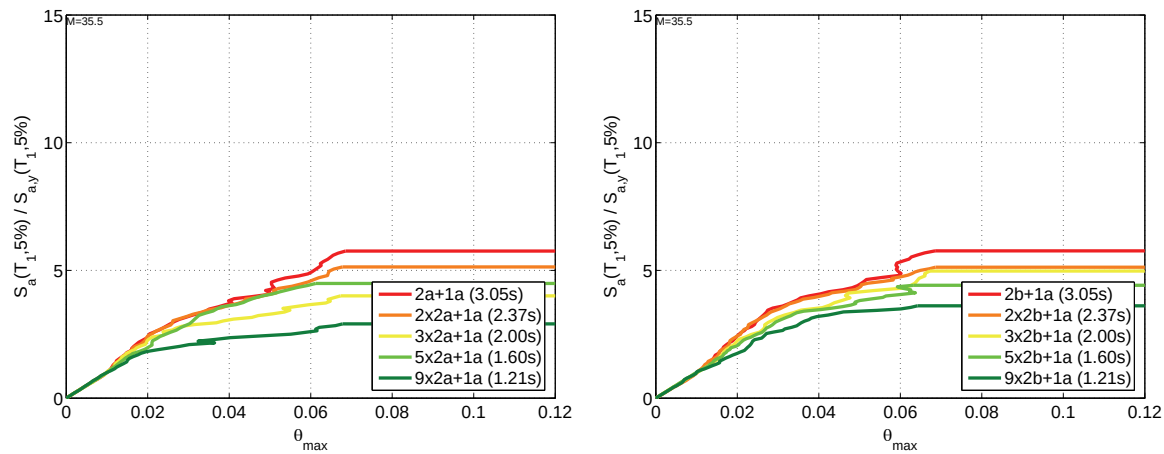

Figure C-20 Median IDA curves plotted versus the normalized intensity measure $R = S_a(T_1,5\%)/S_{ay}(T_1,5\%)$ for systems Nx2a+1a and Nx2b+1a with mass M=35.46ton.

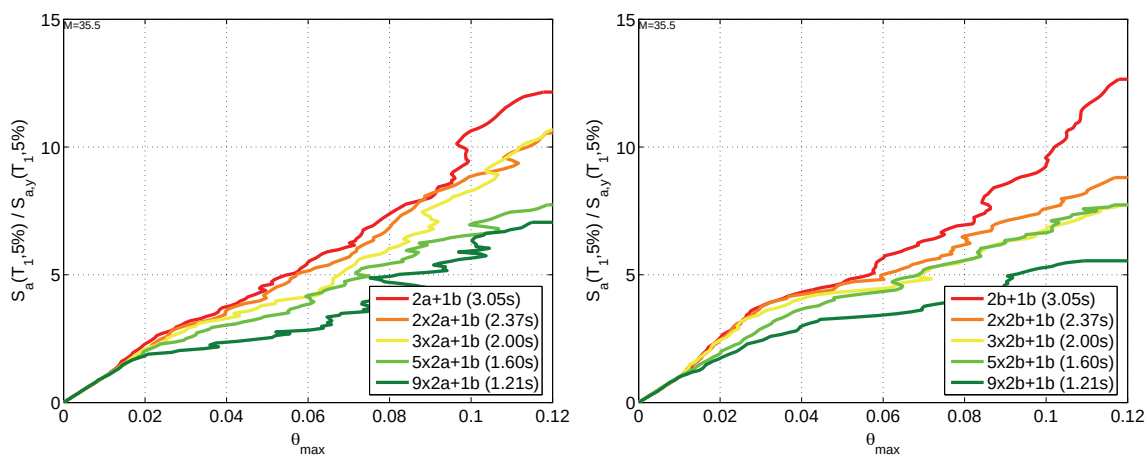

Figure C-21 Median IDA curves plotted versus the normalized intensity measure $R = S_a(T_1,5\%)/S_{ay}(T_1,5\%)$ for systems Nx2a+1b and Nx2b+1b with mass M=35.46ton.

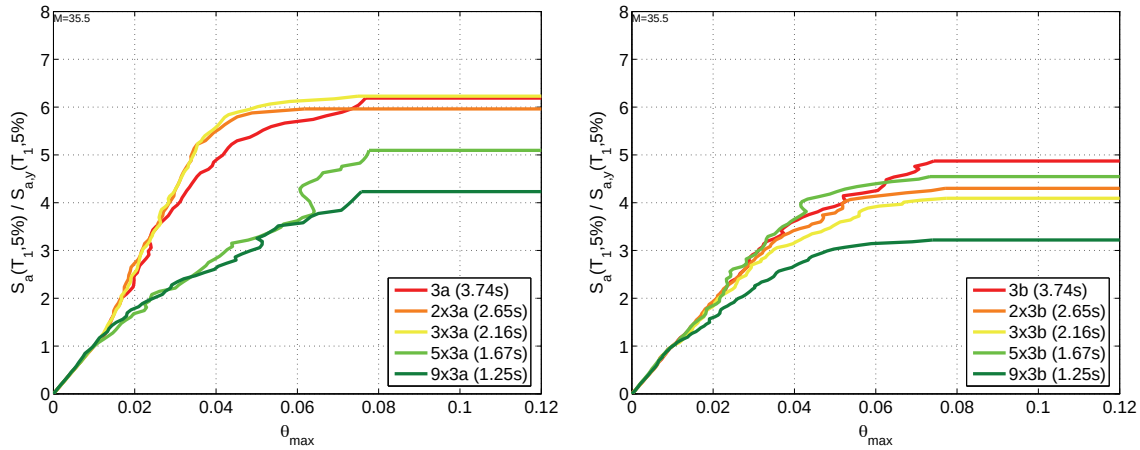

Figure C-22 Median IDA curves plotted versus the normalized intensity measure $R = S_a(T_1,5\%)/S_{ay}(T_1,5\%)$ for systems Nx3a and Nx3b with mass M=35.46ton.

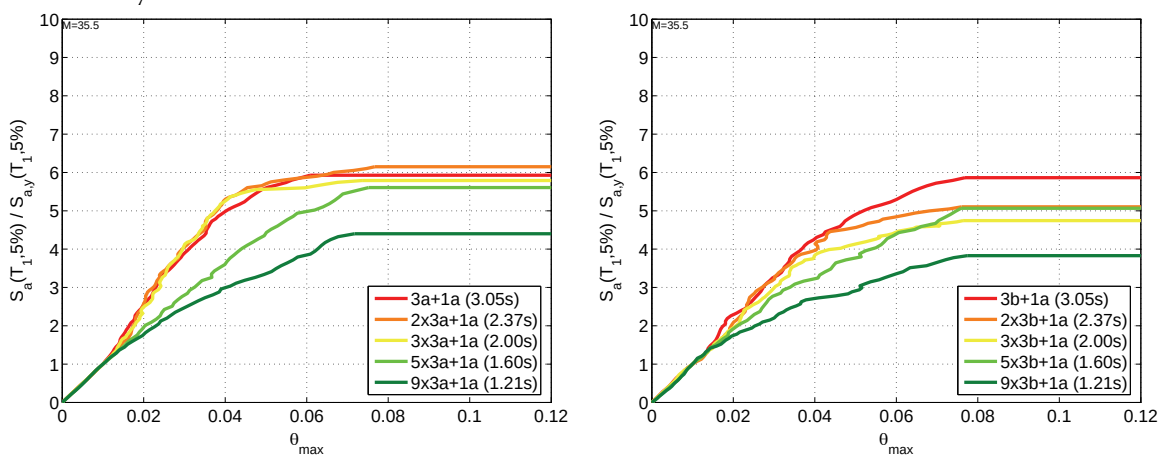

Figure C-23 Median IDA curves plotted versus the normalized intensity measure $R = S_a(T_1,5\%)/S_{ay}(T_1,5\%)$ for systems Nx3a+1a and Nx3b+1a with mass M=35.46ton.

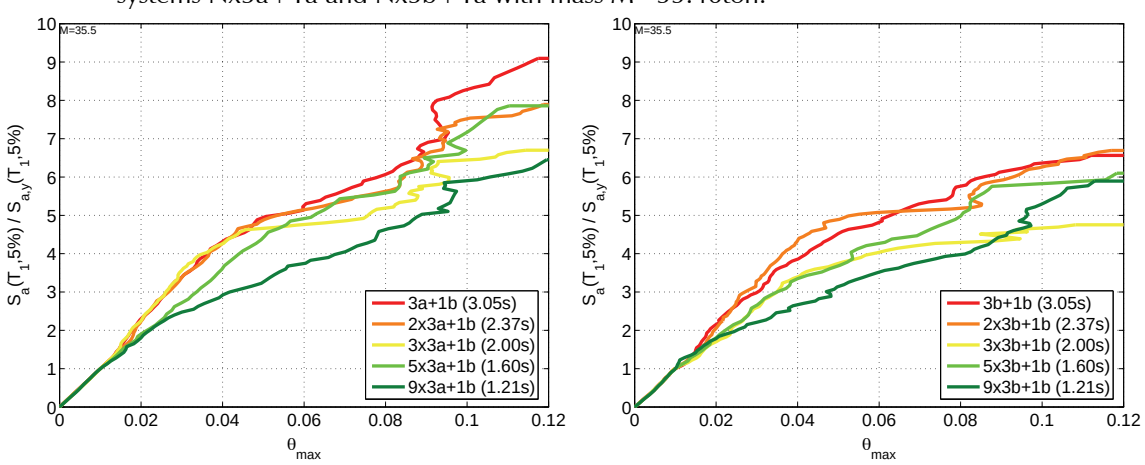

Figure C-24 Median IDA curves plotted versus the normalized intensity measure $R = S_a(T_1,5\%)/S_{ay}(T_1,5\%)$ for systems Nx3a+1b and Nx3b+1b with mass M=35.46ton.

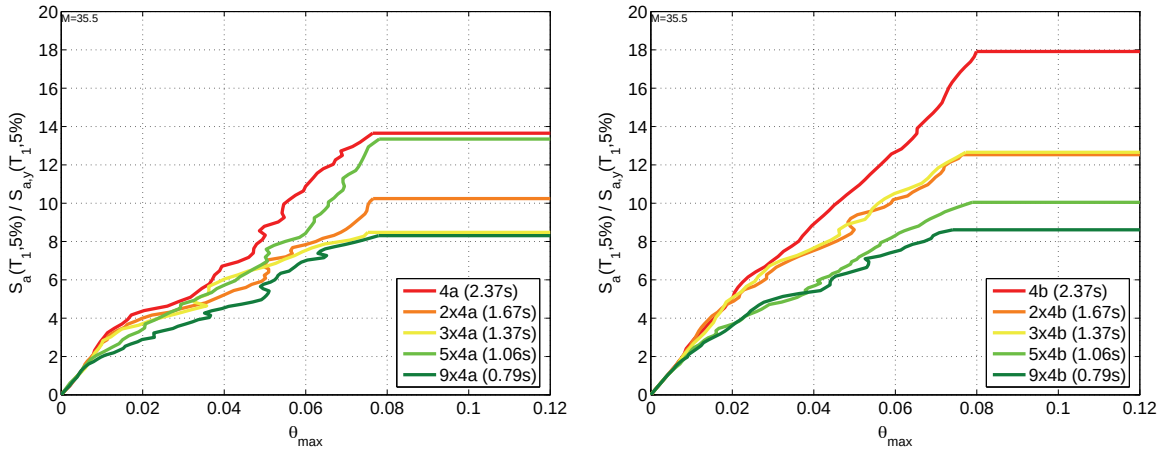

Figure C-25 Median IDA curves plotted versus the normalized intensity measure $R = S_a(T_1,5\%)/S_{ay}(T_1,5\%)$ for systems Nx4a and Nx4b with mass M=35.46ton.

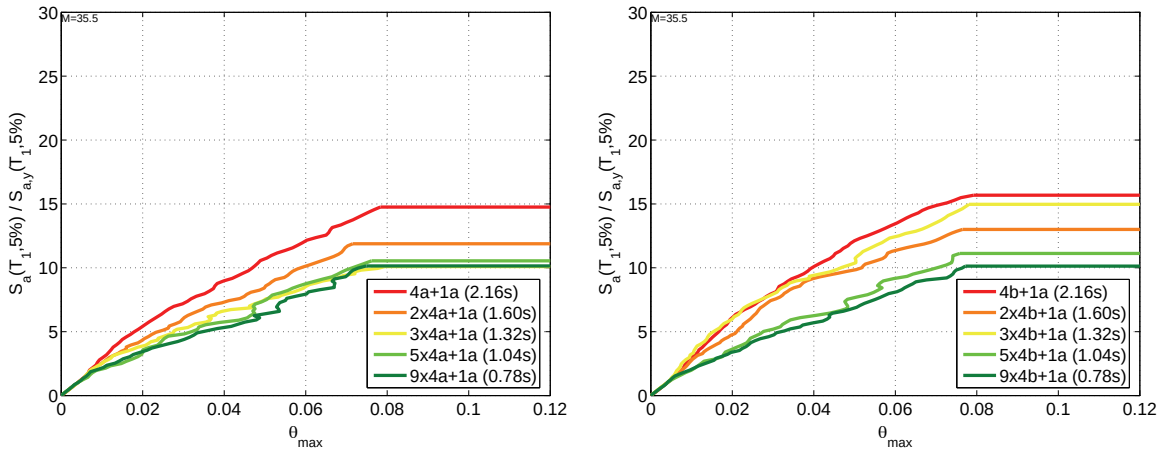

Figure C-26 Median IDA curves plotted versus the normalized intensity measure $R = S_a(T_1,5\%)/S_{ay}(T_1,5\%)$ for systems Nx4a+1a and Nx4b+1a with mass M=35.46ton.

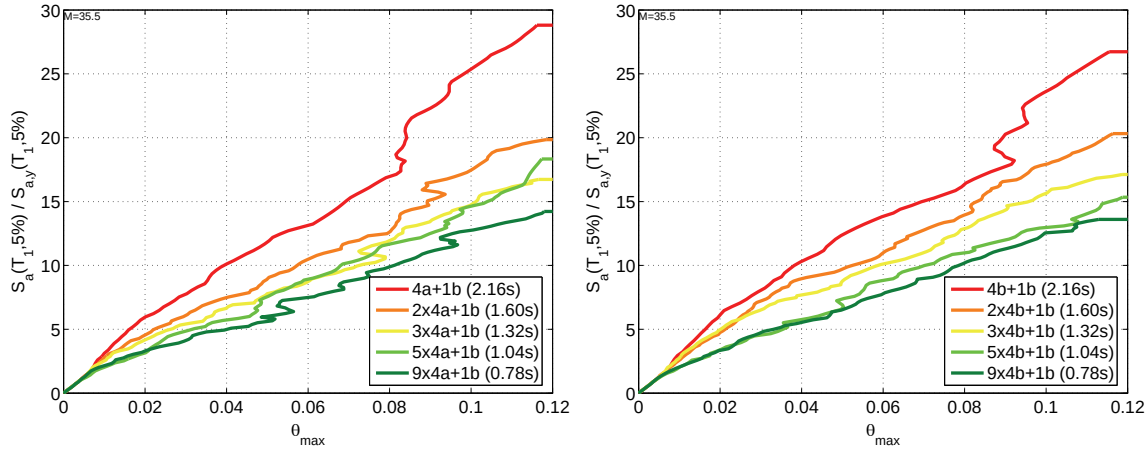

Figure C-27 Median IDA curves plotted versus the normalized intensity measure $R = S_a(T_1,5\%)/S_{ay}(T_1,5\%)$ for systems Nx4a+1b and Nx4b+1b with mass M=35.46ton.

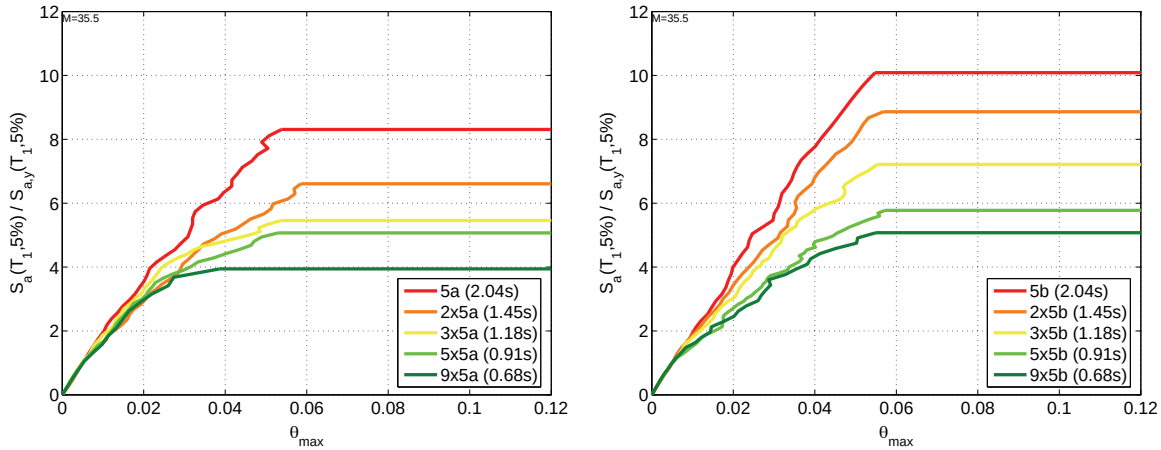

Figure C-28 Median IDA curves plotted versus the normalized intensity measure $R = S_a(T_1,5\%)/S_{ay}(T_1,5\%)$ for systems Nx5a and Nx5b with mass M=35.46ton.

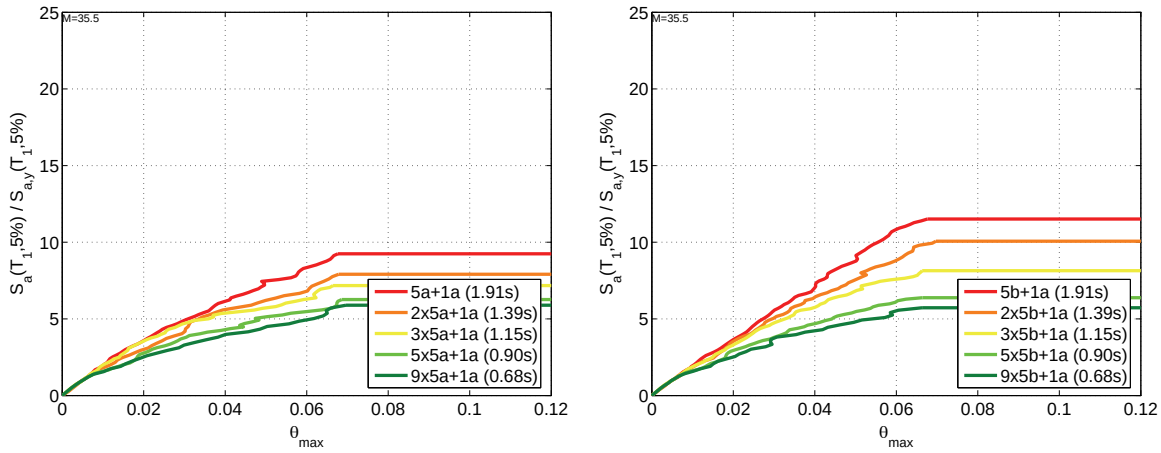

Figure C-29 Median IDA curves plotted versus the normalized intensity measure $R = S_a(T_1,5\%)/S_{ay}(T_1,5\%)$ for systems Nx5a+1a and Nx5b+1a with mass M=35.46ton.

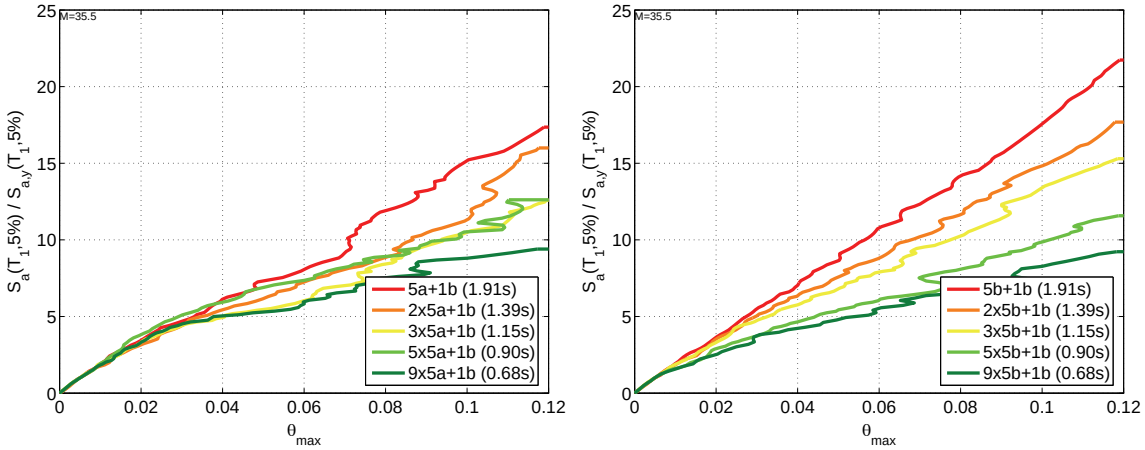

Figure C-30 Median IDA curves plotted versus the normalized intensity measure $R = S_a(T_1,5\%)/S_{ay}(T_1,5\%)$ for systems Nx5a+1b and Nx5b+1b with mass M=35.46ton.

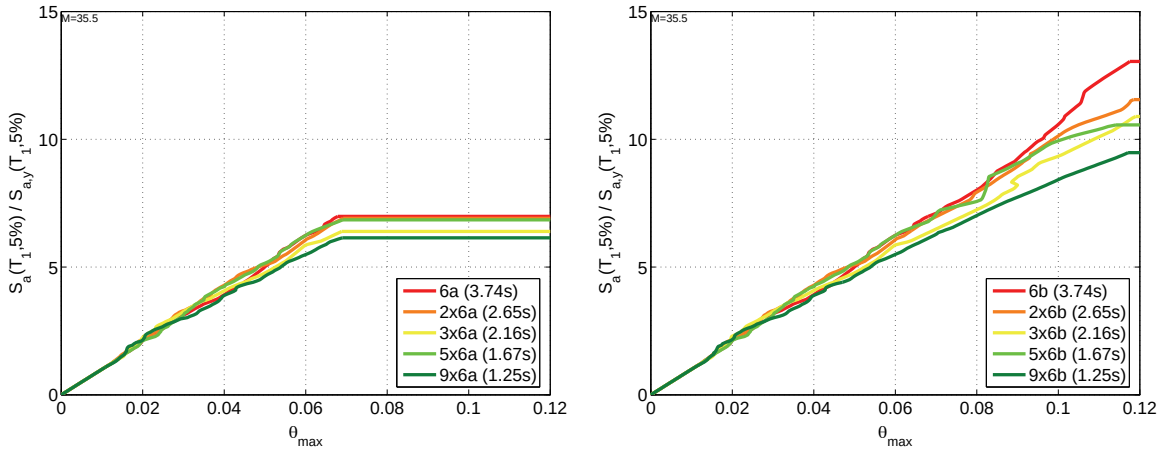

Figure C-31 Median IDA curves plotted versus the normalized intensity measure $R = S_a(T_1,5\%)/S_{ay}(T_1,5\%)$ for systems Nx6a and Nx6b with mass M=35.46ton.

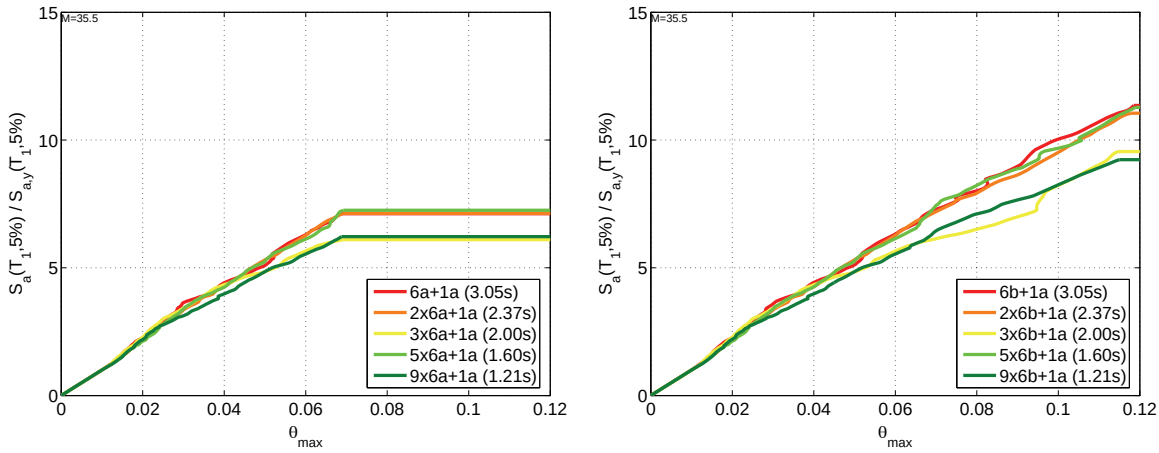

Figure C-32 Median IDA curves plotted versus the normalized intensity measure $R = S_a(T_1,5\%)/S_{ay}(T_1,5\%)$ for systems Nx6a+1a and Nx6b+1a with mass M=35.46ton.

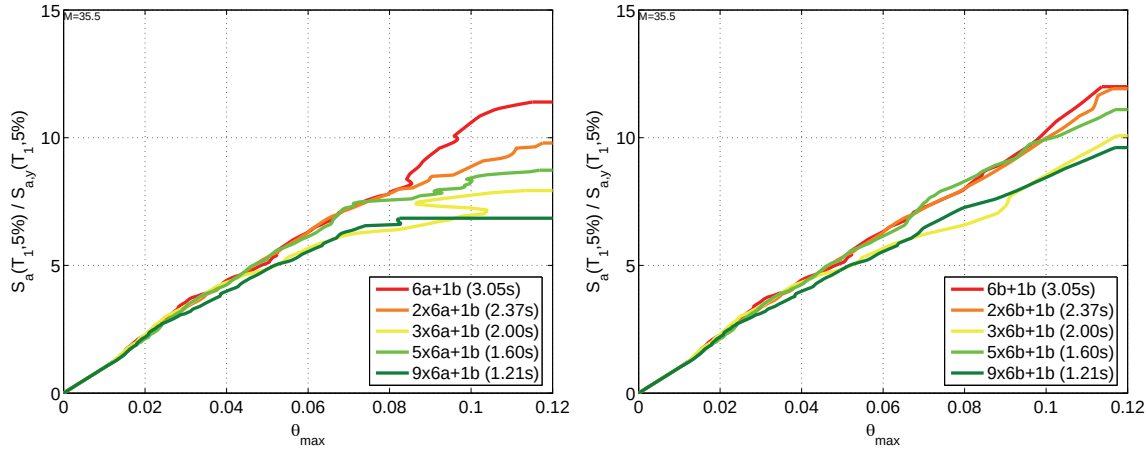

Figure C-33 Median IDA curves plotted versus the normalized intensity measure $R = S_a(T_1,5\%)/S_{ay}(T_1,5\%)$ for systems Nx6a+1b and Nx6b+1b with mass M=35.46ton.

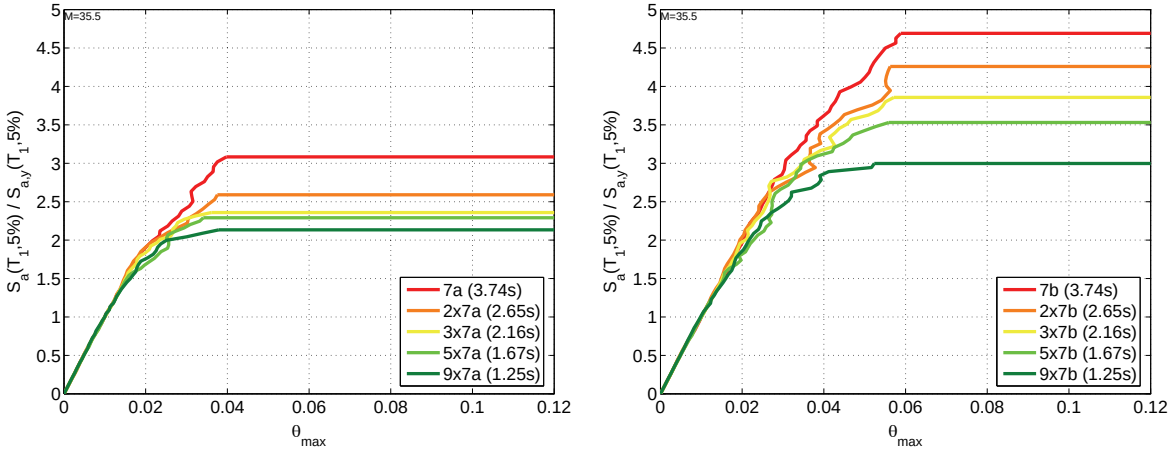

Figure C-34 Median IDA curves plotted versus the normalized intensity measure $R = S_a(T_1,5\%)/S_{ay}(T_1,5\%)$ for systems Nx7a and Nx7b with mass M=35.46ton.

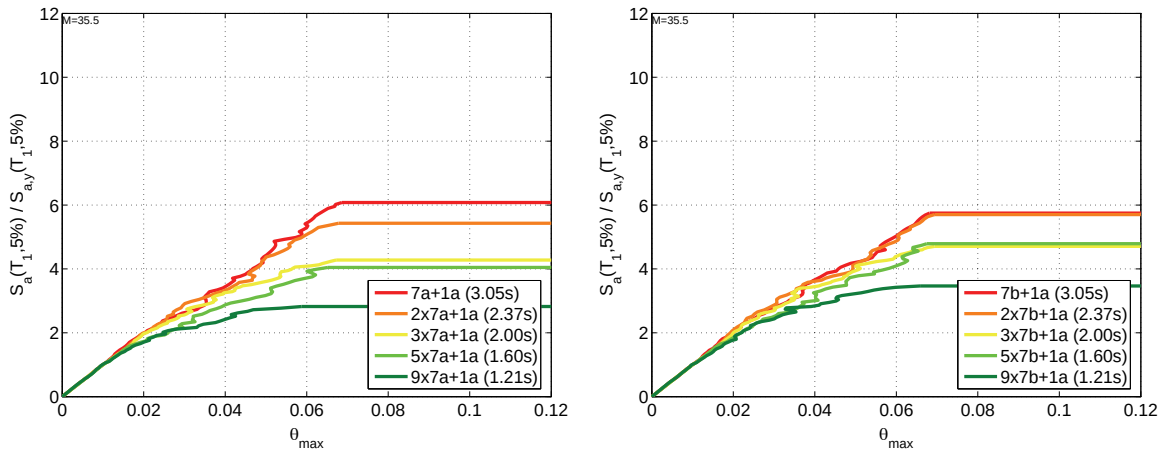

Figure C-35 Median IDA curves plotted versus the normalized intensity measure $R = S_a(T_1,5\%)/S_{ay}(T_1,5\%)$ for systems Nx7a+1a and Nx7b+1a with mass M=35.46ton.

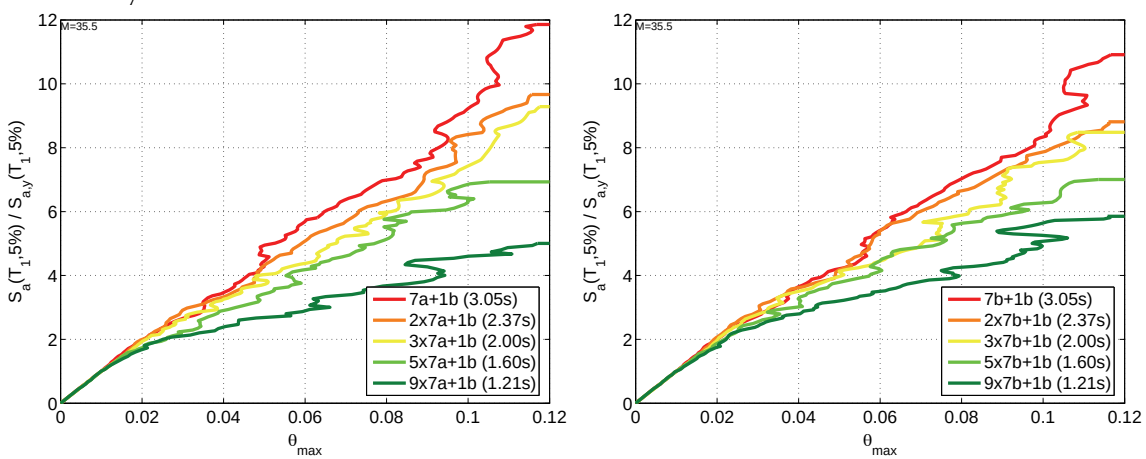

Figure C-36 Median IDA curves plotted versus the normalized intensity measure $R = S_a(T_1,5\%)/S_{ay}(T_1,5\%)$ for systems Nx7a+1b and Nx7b+1b with mass M=35.46ton.

Appendix D

Median IDA Curves for Multi-Spring Systems versus Non-Normalized Intensity Measures

This appendix contains non-normalized plots of median incremental dynamic analysis (IDA) curves from focused analytical studies on multi-spring single-degree-of-freedom (SDOF) systems. All systems are composed of two springs representing a primary lateral-force-resisting system and a secondary gravity system with the characteristics described in Chapter 3. Multi-spring systems carry a designation of "NxJa+1a" or "NxJa+1b" where "N" is the peak strength multiplier (N = 1, 2, 3, 5, or 9), "J" is the lateral-force-resisting spring number (J = 2, 3, 4, 5, 6, or 7), and 1a or 1b is the gravity system identifier. In the figures, the vertical axis is one of two ground motion intensities IM = S_a(1s,5%) or S_a(2s,5%), which are not normalized, and the horizontal axis is the maximum story drift ratio, θ_{max}, in radians. The period of vibration for each system is indicated in parentheses.

D.1 Visualization Tool

Given the large volume of analytical data, customized algorithms were developed for post-processing, statistical analysis, and visualization of results. The accompanying CD includes an electronic visualization tool that was developed to view results of multi-spring studies. The tool is a Microsoft Excel based application with a user-interface that accesses a database of all available multi-spring data. By selecting a desired spring combination ("NxJa+1a" or "NxJa+1b"), stiffness level (stiff or flexible), and intensity measure (normalized or non-normalized), users can view the resulting quantile (median, 16th, and 84th percentile) IDA curves for the combination of interest.

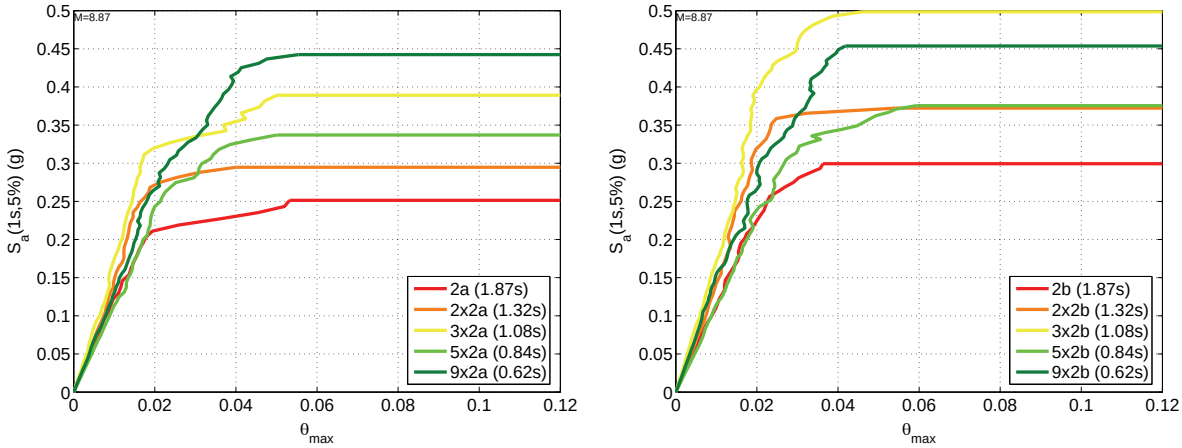

Figure D-1 Median IDA curves plotted versus the intensity measure S_a(1s,5%) for systems Nx2a and Nx2b with mass M=8.87ton.

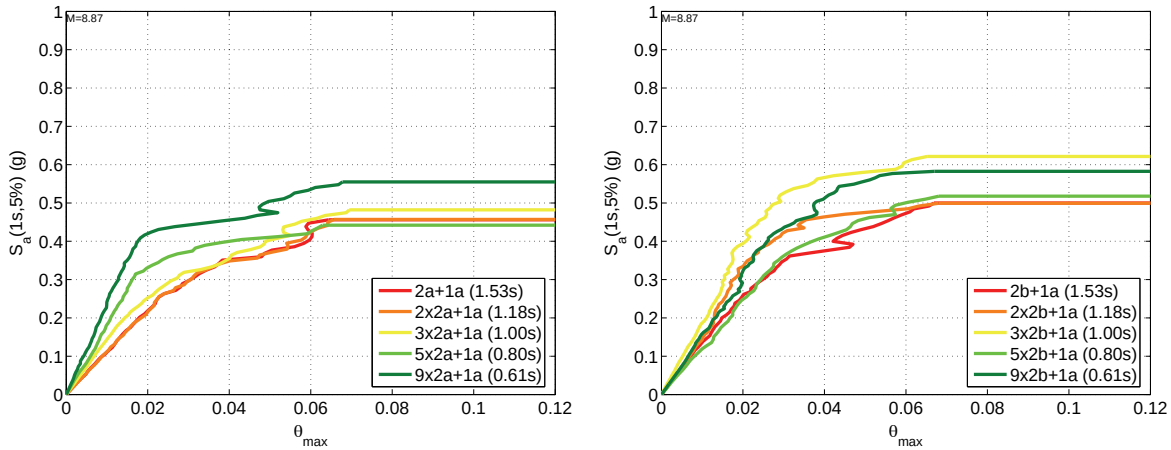

Figure D-2 Median IDA curves plotted versus the intensity measure S_a(1s,5%) for systems Nx2a+1a and Nx2b+1a with mass M=8.87ton.

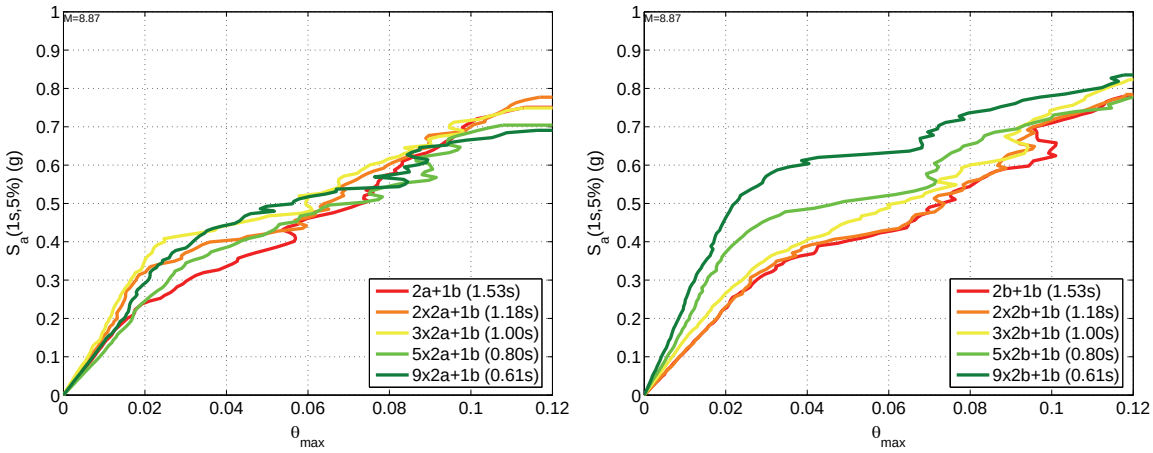

Figure D-3 Median IDA curves plotted versus the intensity measure S_a(1s,5%) for systems Nx2a+1b and Nx2b+1b with mass M=8.87ton.

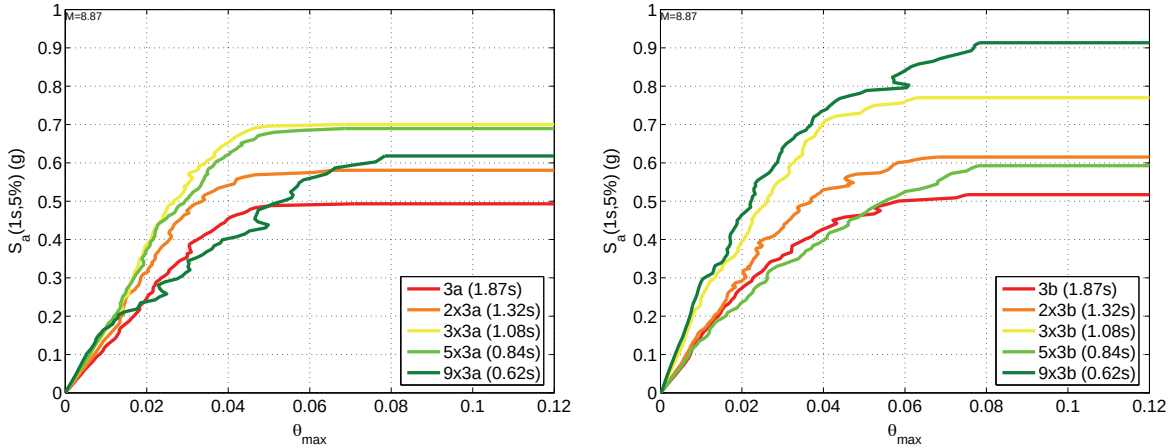

Figure D-4 Median IDA curves plotted versus the intensity measure S_a(1s,5%) for systems Nx3a and Nx3b with mass M=8.87ton.

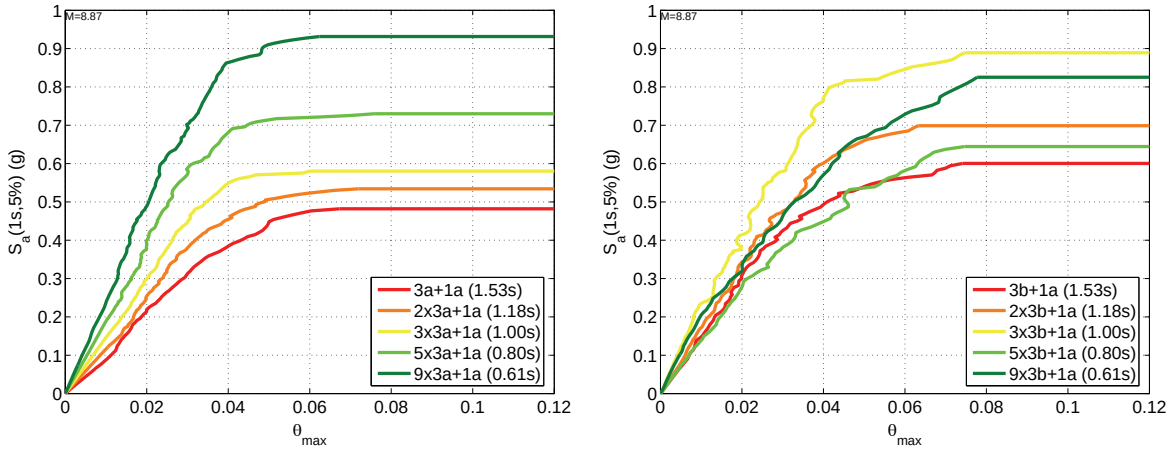

Figure D-5 Median IDA curves plotted versus the intensity measure S_a(1s,5%) for systems Nx3a+1a and Nx3b+1a with mass M=8.87ton.

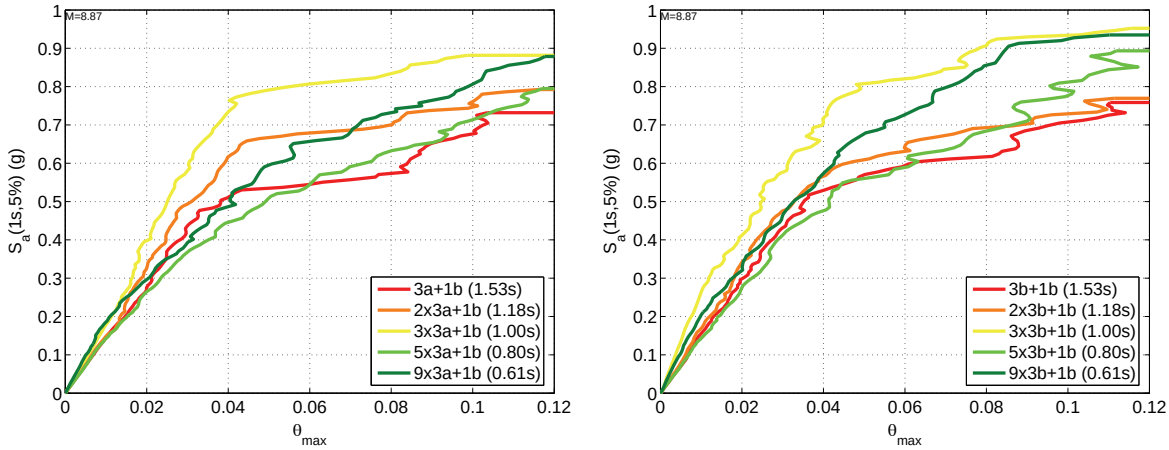

Figure D-6 Median IDA curves plotted versus the intensity measure S_a(1s,5%) for systems Nx3a+1b and Nx3b+1b with mass M=8.87ton.

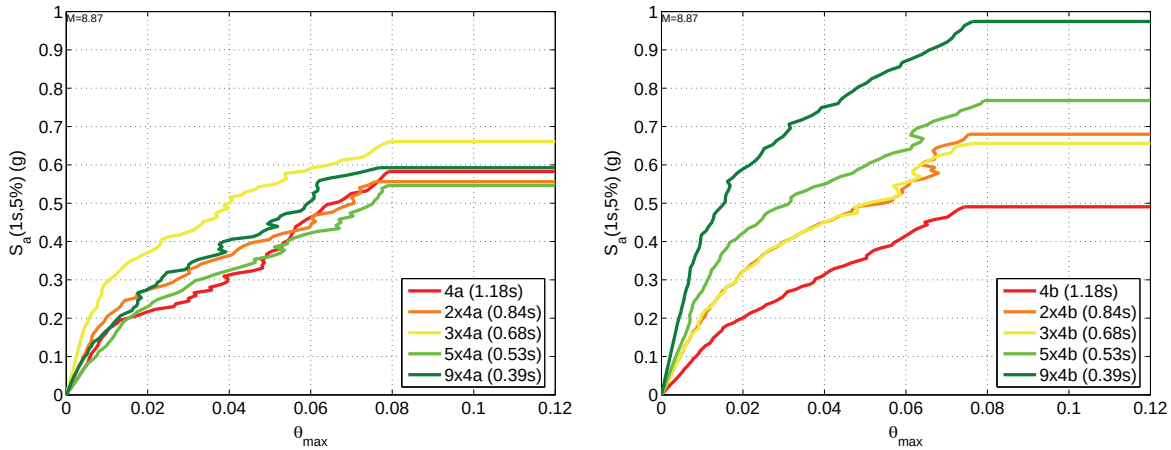

Figure D-7 Median IDA curves plotted versus the intensity measure S_a(1s,5%) for systems Nx4a and Nx4b with mass M=8.87ton.

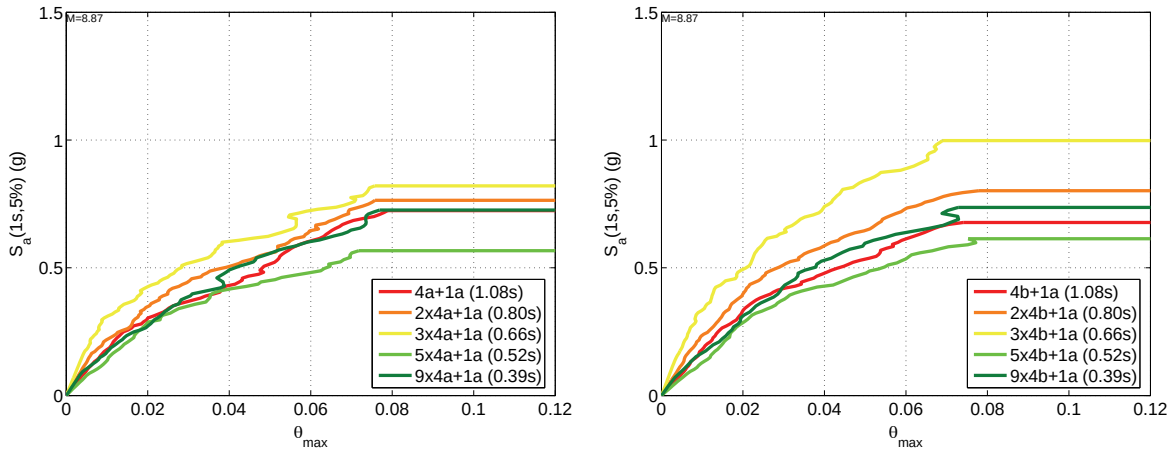

Figure D-8 Median IDA curves plotted versus the intensity measure S_a(1s,5%) for systems Nx4a+1a and Nx4b+1a with mass M=8.87ton.

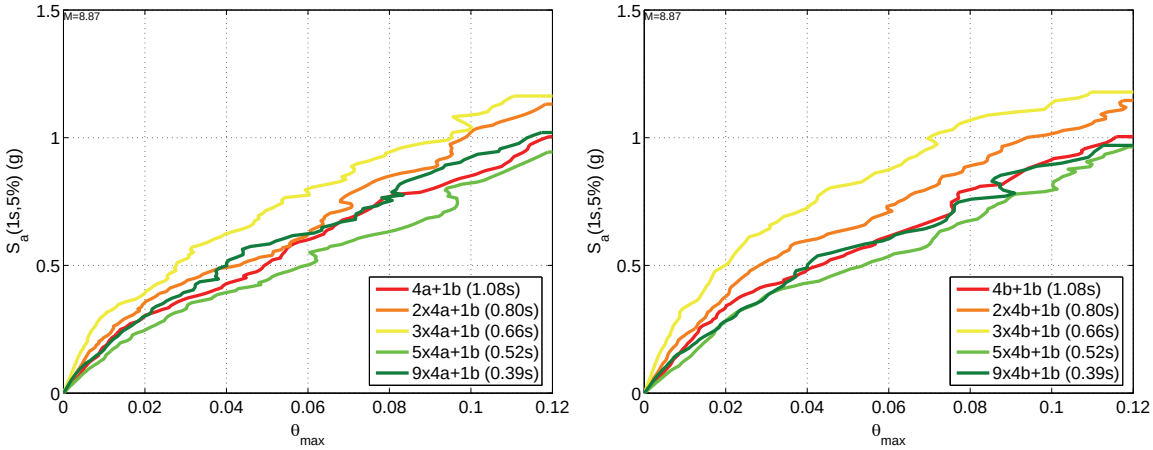

Figure D-9 Median IDA curves plotted versus the intensity measure S_a(1s,5%) for systems Nx4a+1b and Nx4b+1b with mass M=8.87ton.

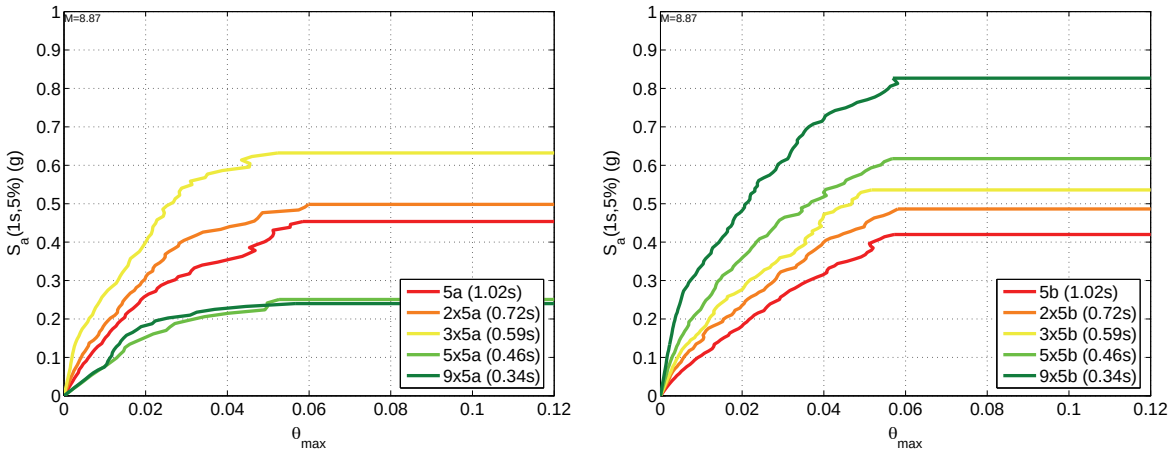

Figure D-10 Median IDA curves plotted versus the intensity measure S_a(1s,5%) for systems Nx5a and Nx5b with mass M=8.87ton.

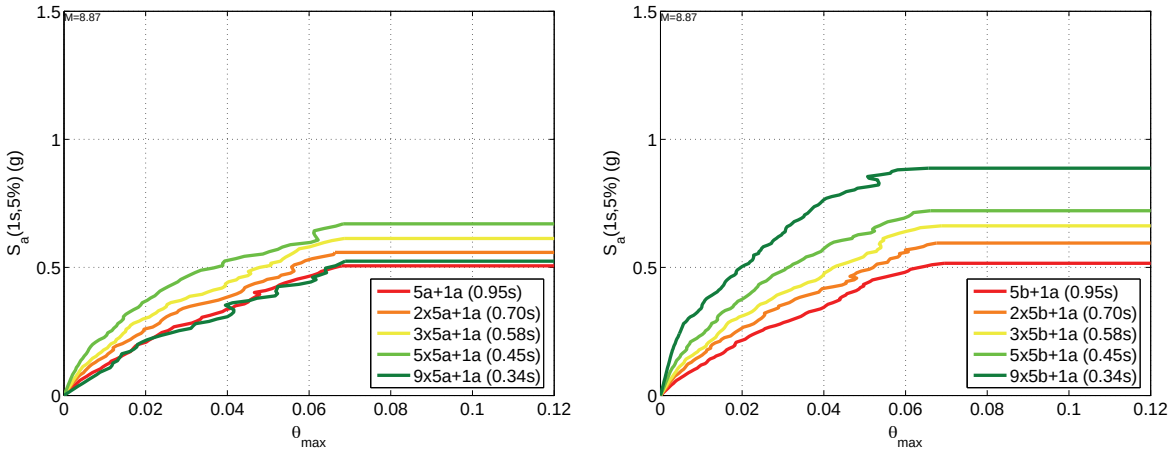

Figure D-11 Median IDA curves plotted versus the intensity measure S_a(1s,5%) for systems Nx5a+1a and Nx5b+1a with mass M=8.87ton.

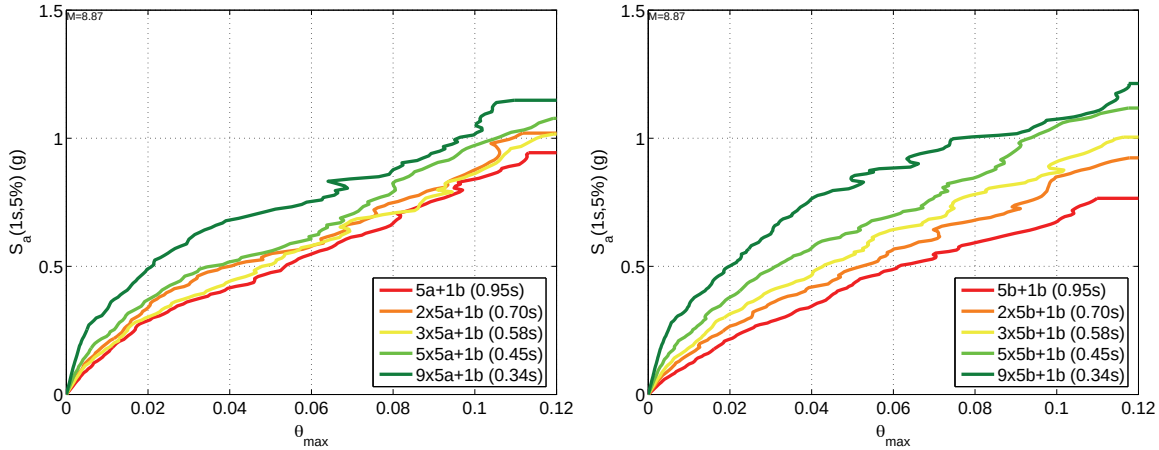

Figure D-12 Median IDA curves plotted versus the intensity measure S_a(1s,5%) for systems Nx5a+1b and Nx5b+1b with mass M=8.87ton.

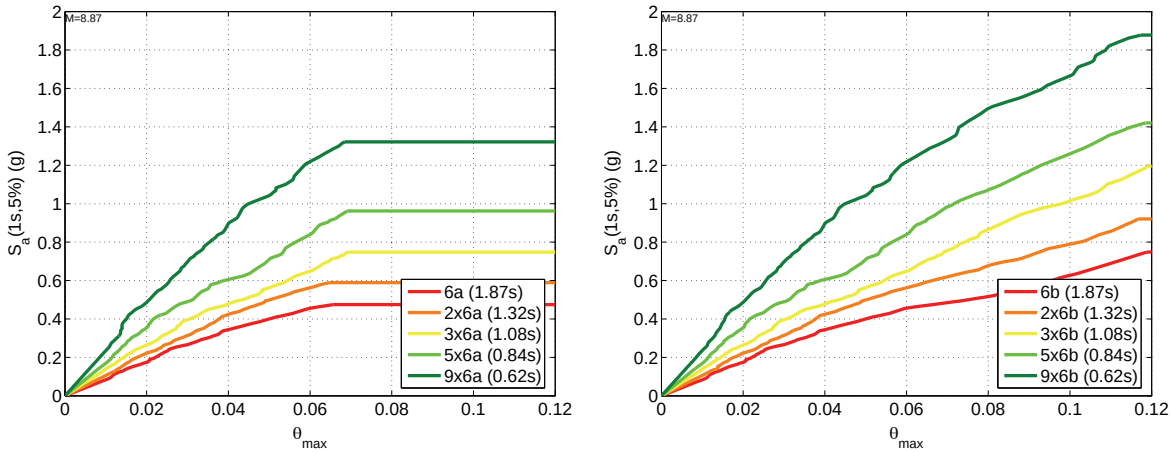

Figure D-13 Median IDA curves plotted versus the intensity measure S_a(1s,5%) for systems Nx6a and Nx6b with mass M=8.87ton.

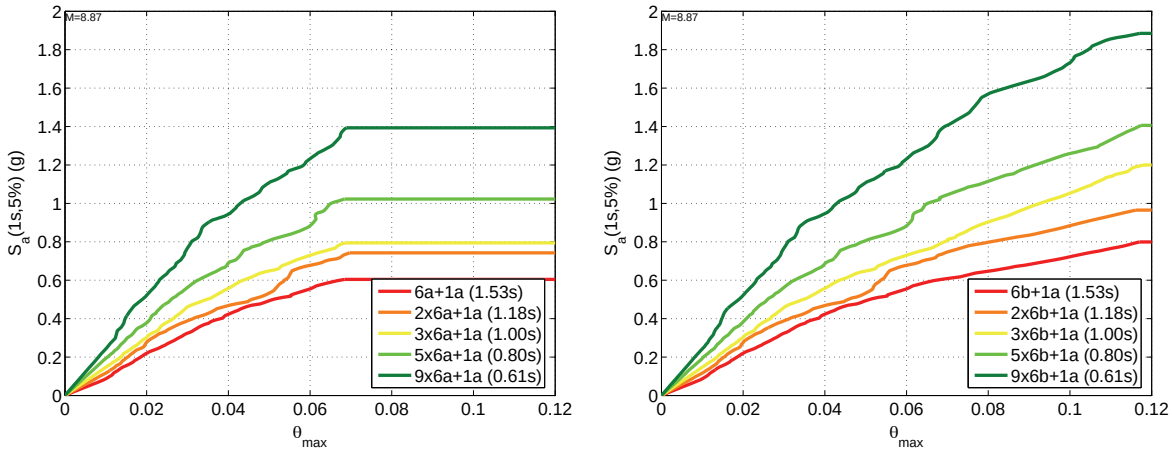

Figure D-14 Median IDA curves plotted versus the intensity measure S_a(1s,5%) for systems Nx6a+1a and Nx6b+1a with mass M=8.87ton.

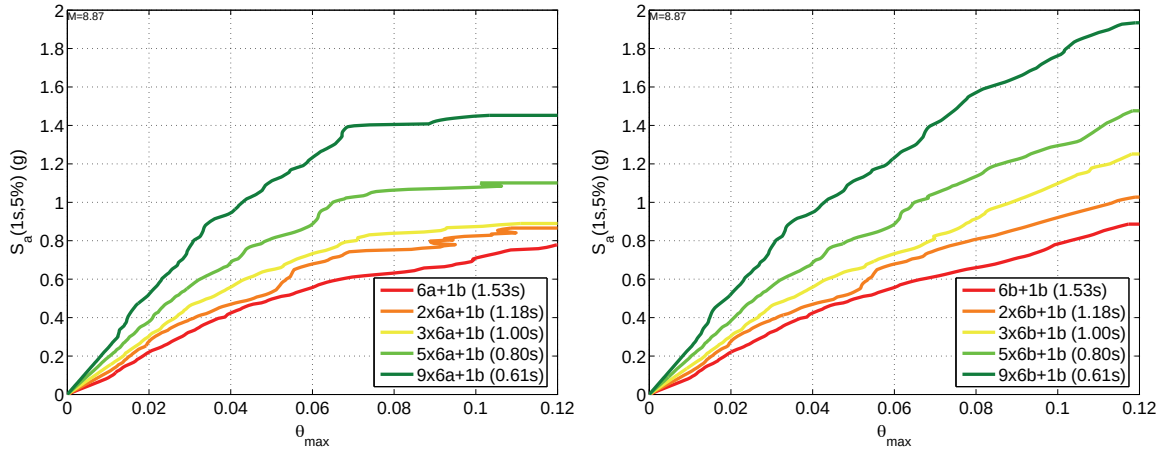

Figure D-15 Median IDA curves plotted versus the intensity measure S_a(1s,5%) for systems Nx6a+1b and Nx6b+1b with mass M=8.87ton.

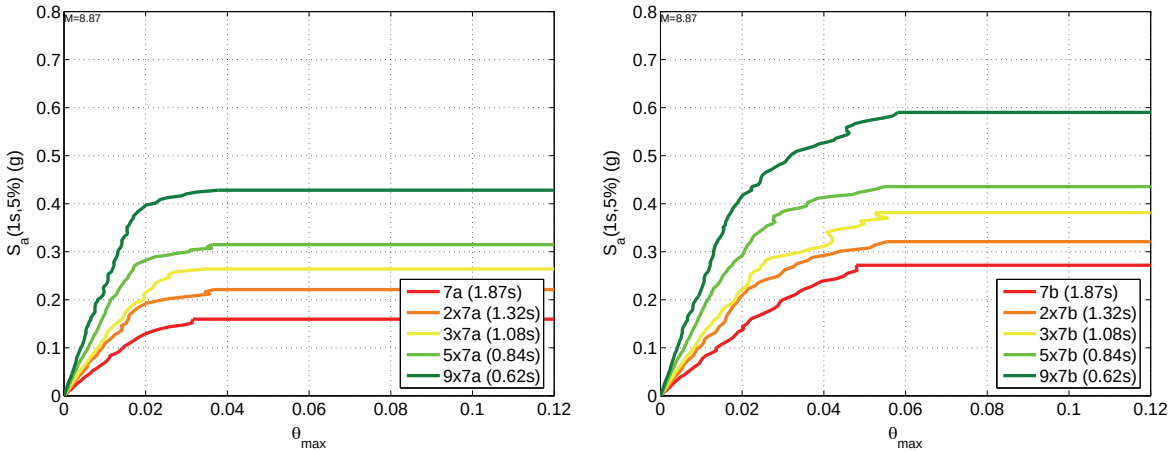

Figure D-16 Median IDA curves plotted versus the intensity measure S_a(1s,5%) for systems Nx7a and Nx7b with mass M=8.87ton.

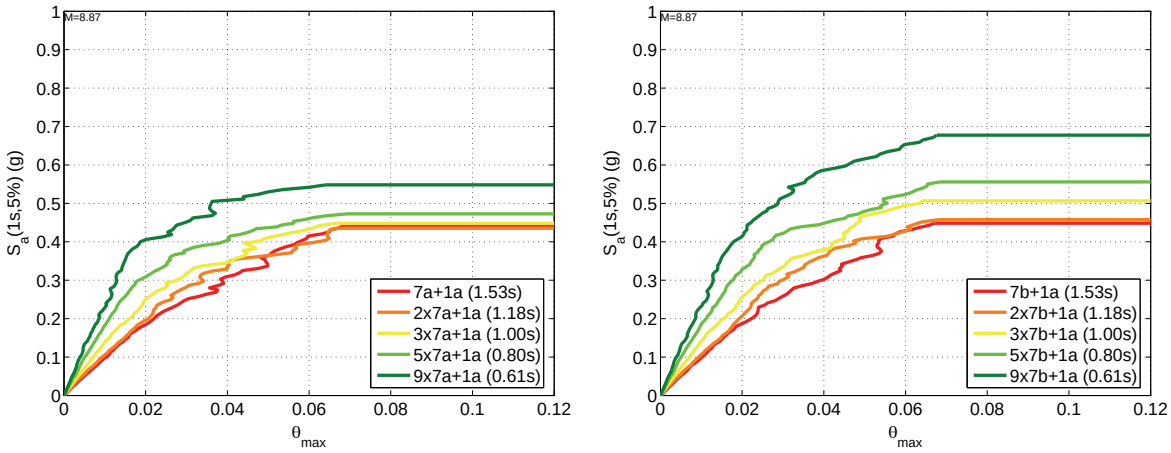

Figure D-17 Median IDA curves plotted versus the intensity measure S_a(1s,5%) for systems Nx7a+1a and Nx7b+1a with mass M=8.87ton.

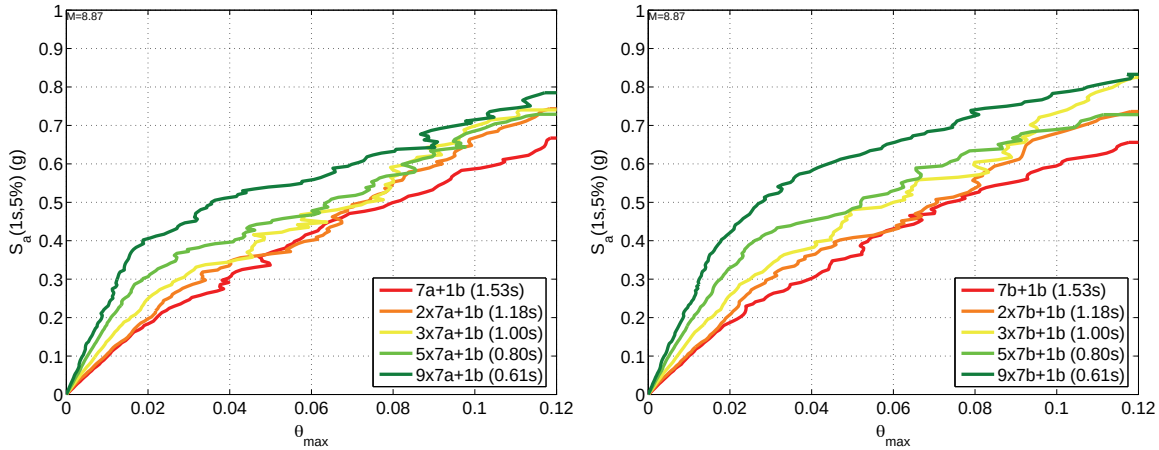

Figure D-18 Median IDA curves plotted versus the intensity measure S_a(1s,5%) for systems Nx7a+1b and Nx7b+1b with mass M=8.87ton.

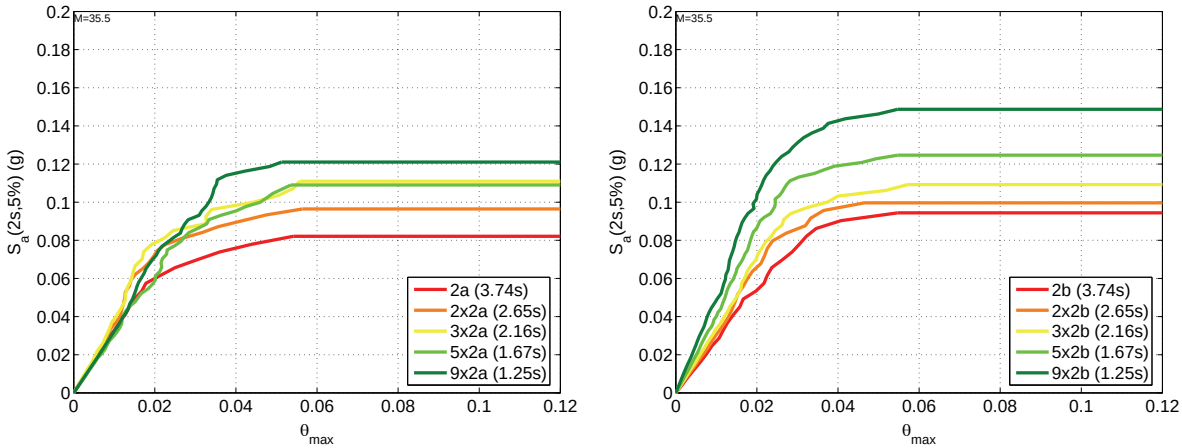

Figure D-19 Median IDA curves plotted versus the intensity measure $S_a(2s,5\%)$ for systems Nx2a and Nx2b with mass M=35.46ton.

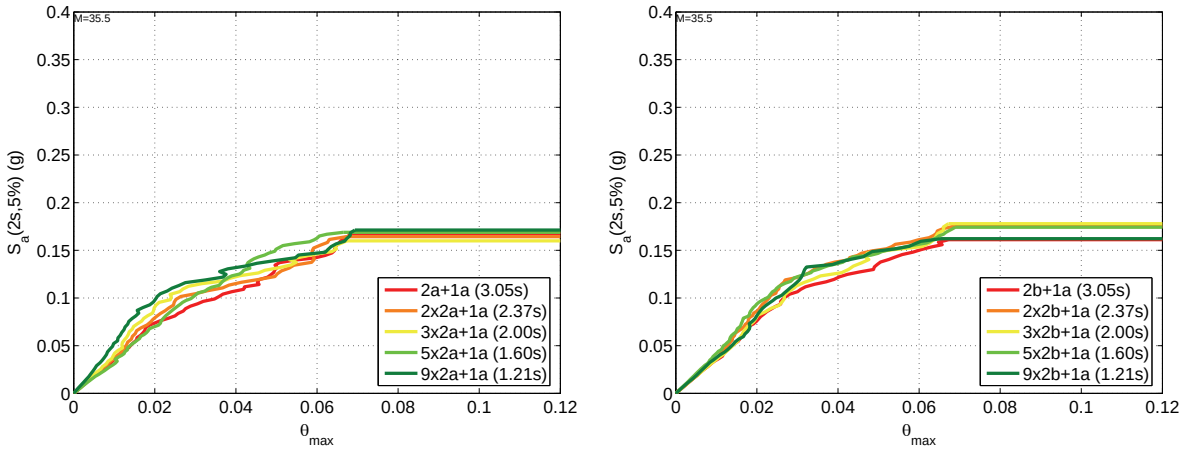

Figure D-20 Median IDA curves plotted versus the intensity measure $S_a(2s,5\%)$ for systems Nx2a+1a and Nx2b+1a with mass M=35.46ton.

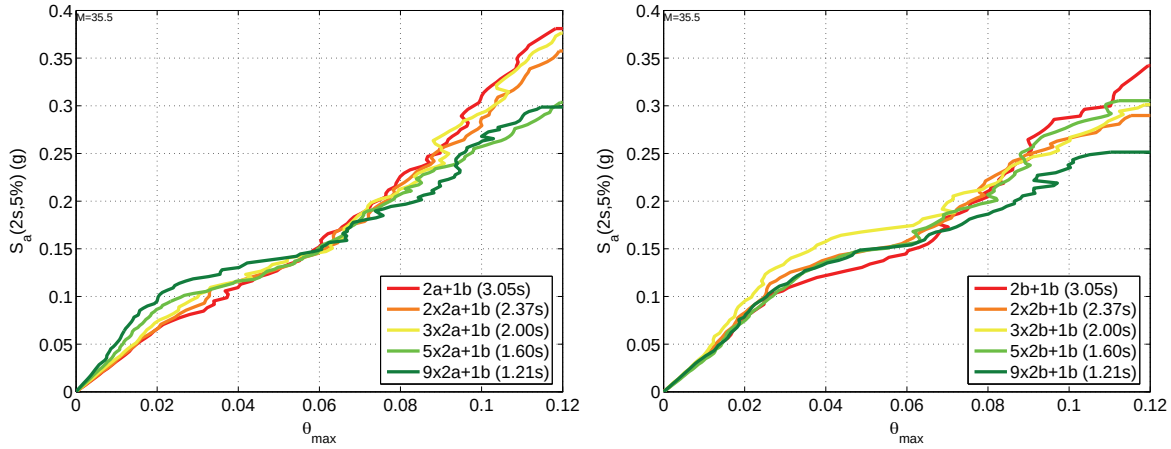

Figure D-21 Median IDA curves plotted versus the intensity measure $S_a(2s,5\%)$ for systems Nx2a+1b and Nx2b+1b with mass M=35.46ton.

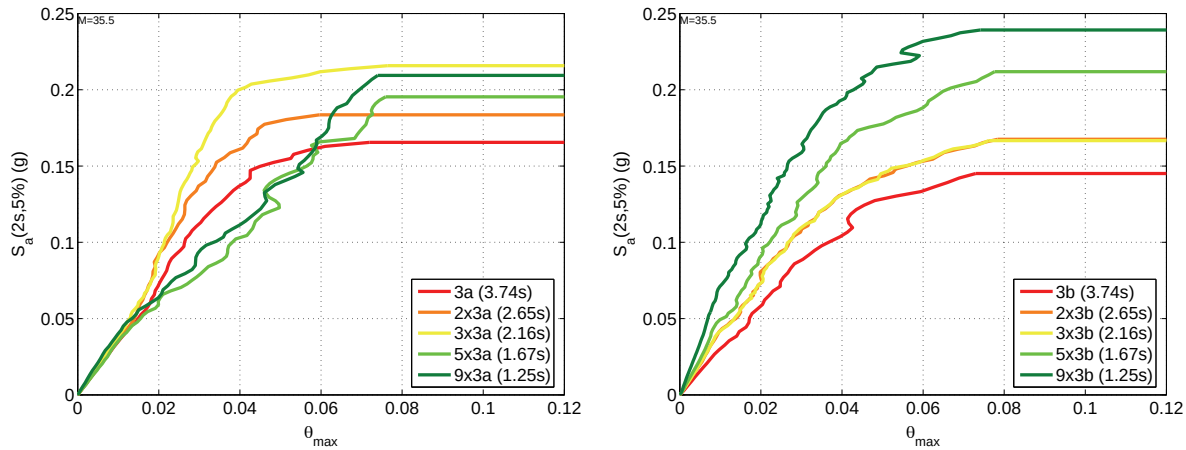

Figure D-22 Median IDA curves plotted versus the intensity measure $S_a(2s,5\%)$ for systems Nx3a and Nx3b with mass M=35.46ton.

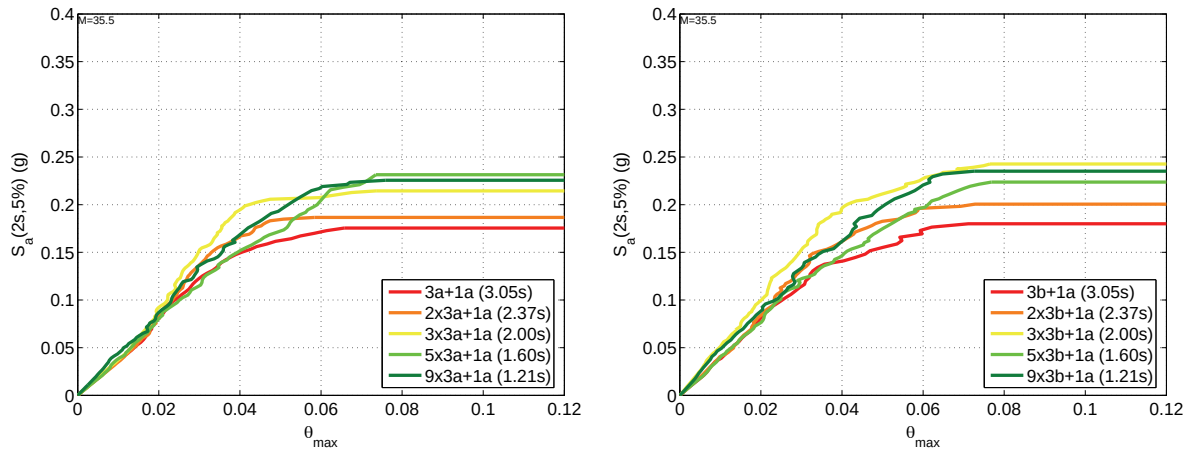

Figure D-23 Median IDA curves plotted versus the intensity measure $S_a(2s,5\%)$ for systems Nx3a+1a and Nx3b+1a with mass M=35.46ton.

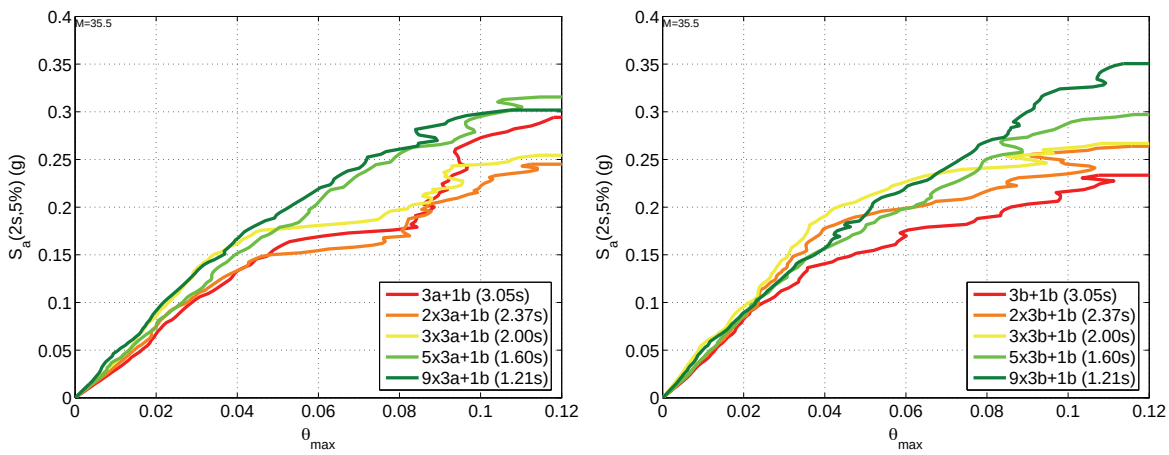

Figure D-24 Median IDA curves plotted versus the intensity measure $S_a(2s,5\%)$ for systems Nx3a+1b and Nx3b+1b with mass M=35.46ton.

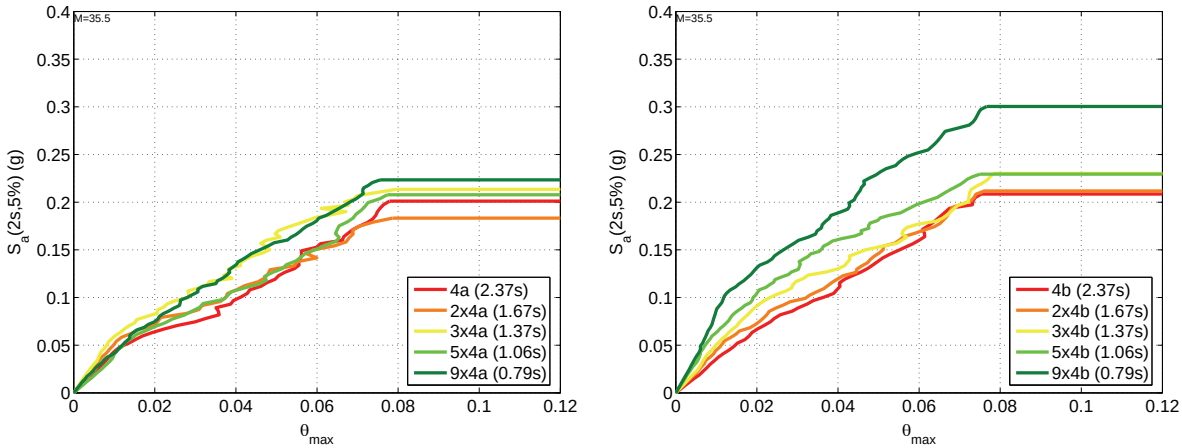

Figure D-25 Median IDA curves plotted versus the intensity measure S_a(2s,5%) for systems Nx4a and Nx4b with mass M=35.46ton.

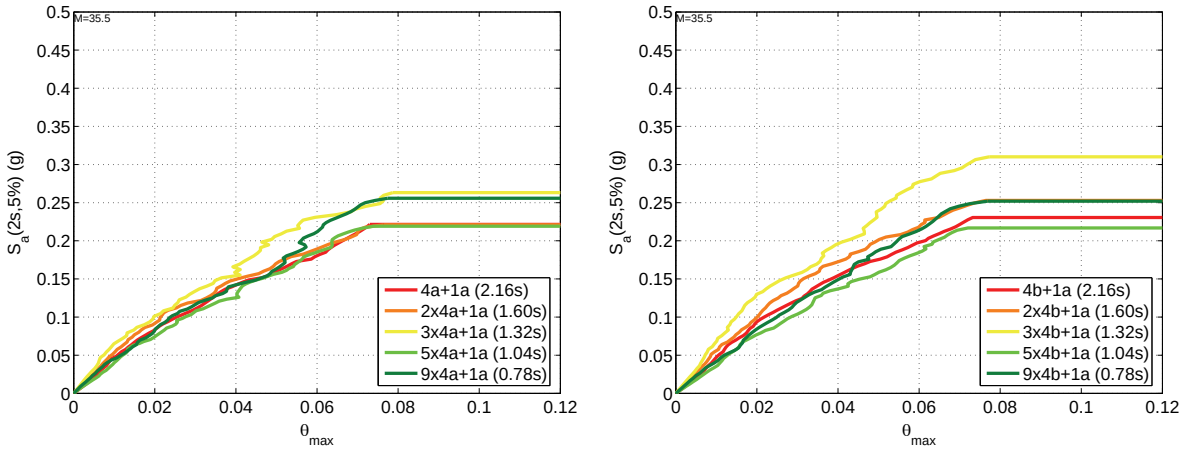

Figure D-26 Median IDA curves plotted versus the intensity measure S_a(2s,5%) for (systems Nx4a+1a and Nx4b+1a with mass M=35.46ton.

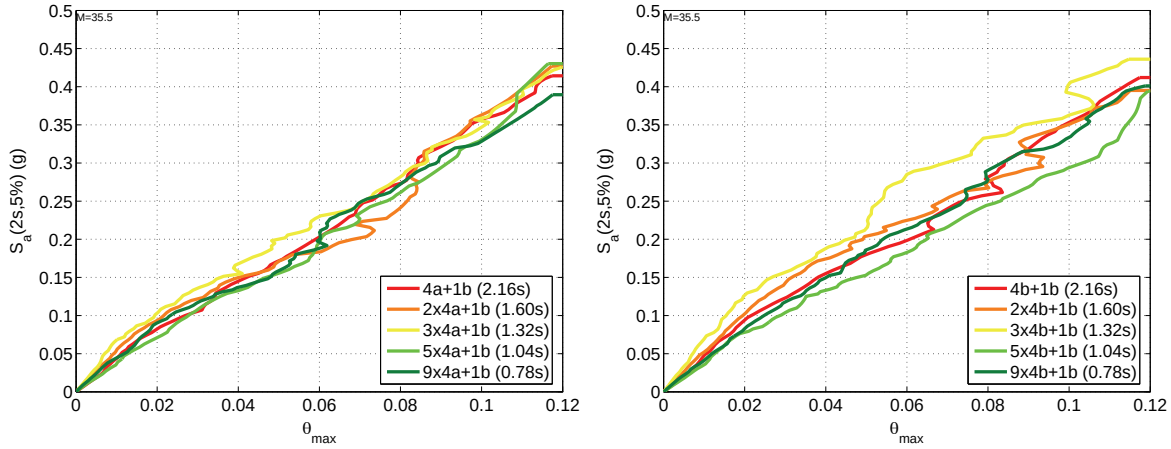

Figure D-27 Median IDA curves plotted versus the intensity measure S_a(2s,5%) for systems Nx4a+1b and Nx4b+1b with mass M=35.46ton.

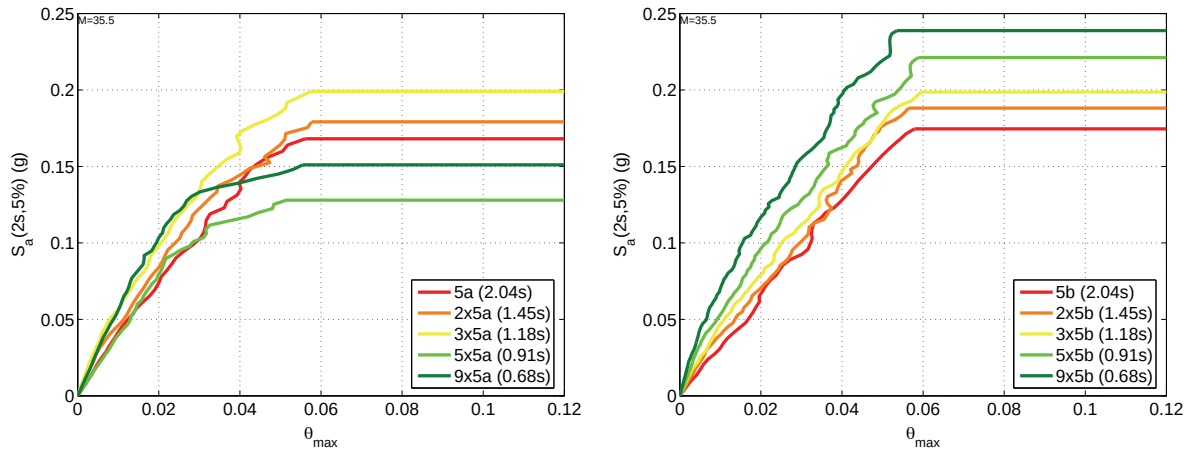

Figure D-28 Median IDA curves plotted versus the intensity measure $S_a(2s,5\%)$ for systems Nx5a and Nx5b with mass M=35.46ton.

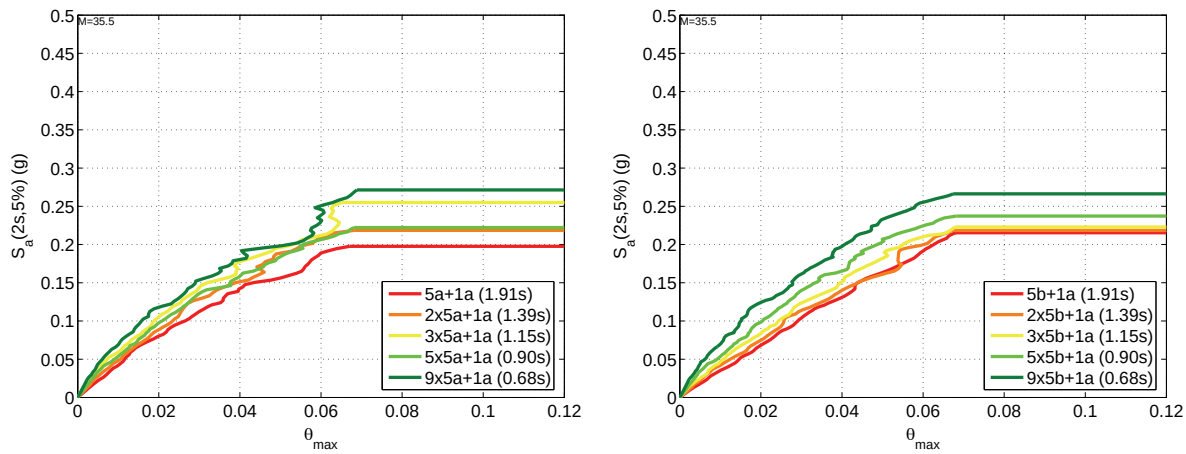

Figure D-29 Median IDA curves plotted versus the intensity measure $S_a(2s,5\%)$ for systems Nx5a+1a and Nx5b+1a with mass M=35.46ton.

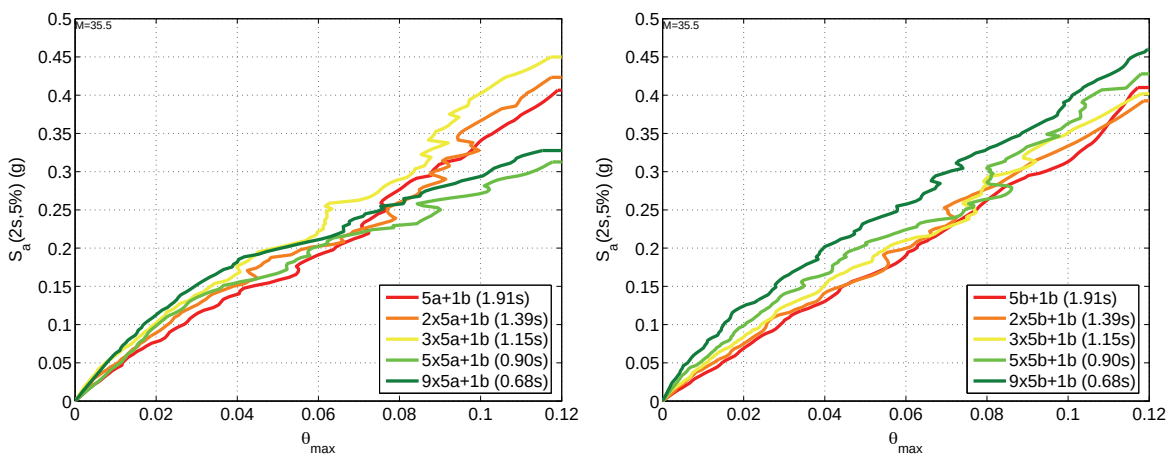

Figure D-30 Median IDA curves plotted versus the intensity measure $S_a(2s,5\%)$ for systems Nx5a+1b and Nx5b+1b with mass M=35.46ton.

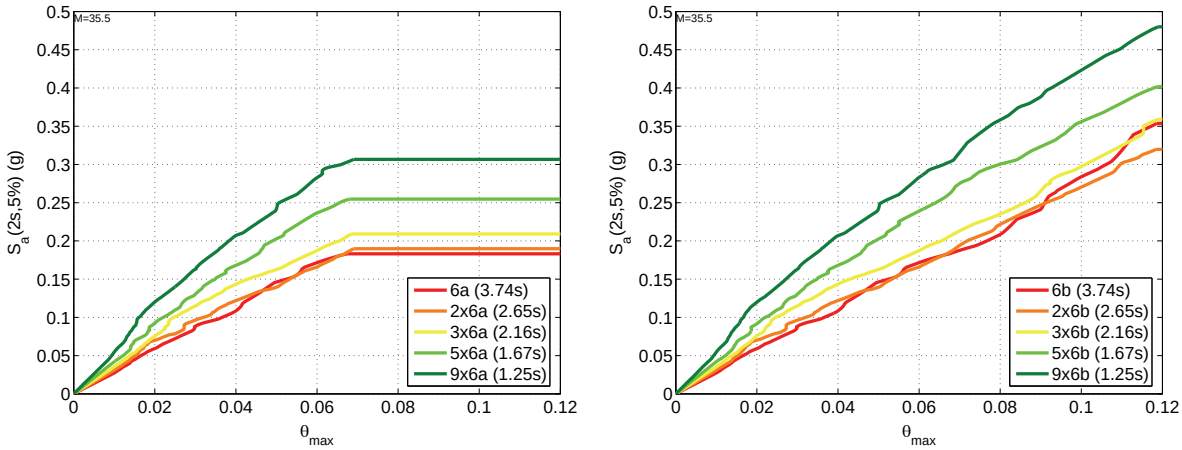

Figure D-31 Median IDA curves plotted versus the intensity measure S_a(2s,5%) for systems Nx6a and Nx6b with mass M=35.46ton.

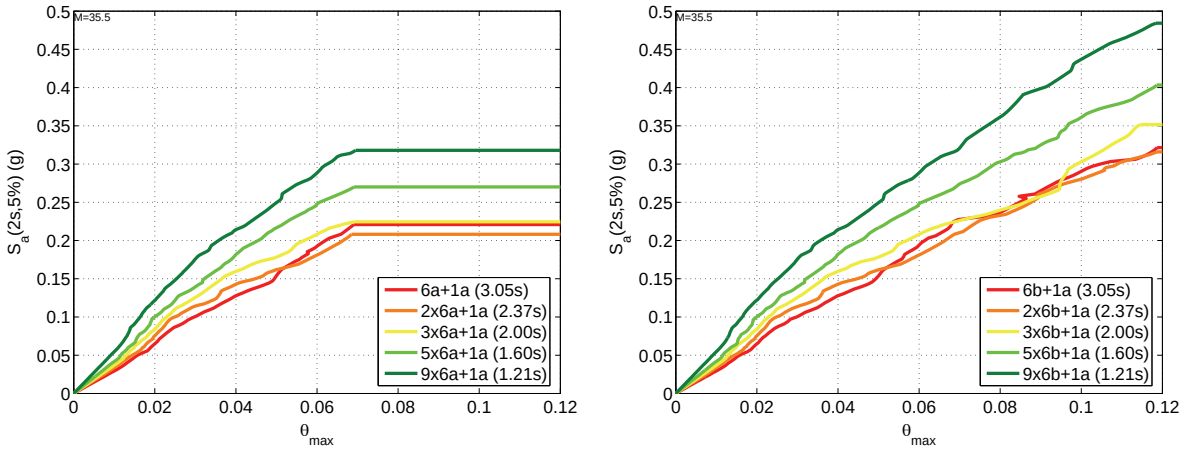

Figure D-32 Median IDA curves plotted versus the intensity measure S_a(2s,5%) for systems Nx6a+1a and Nx6b+1a with mass M=35.46ton.

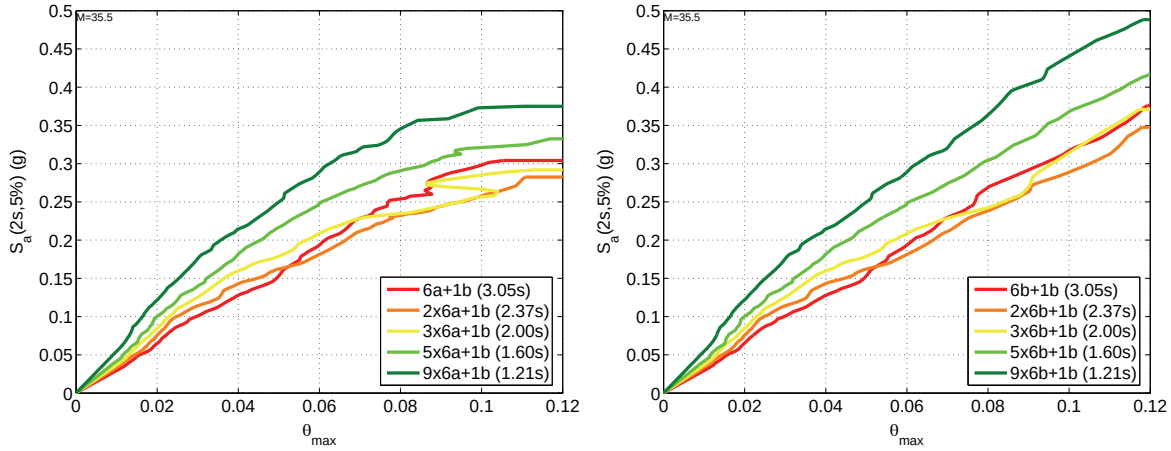

Figure D-33 Median IDA curves plotted versus the intensity measure S_a(2s,5%) for systems Nx6a+1b and Nx6b+1b with mass M=35.46ton.

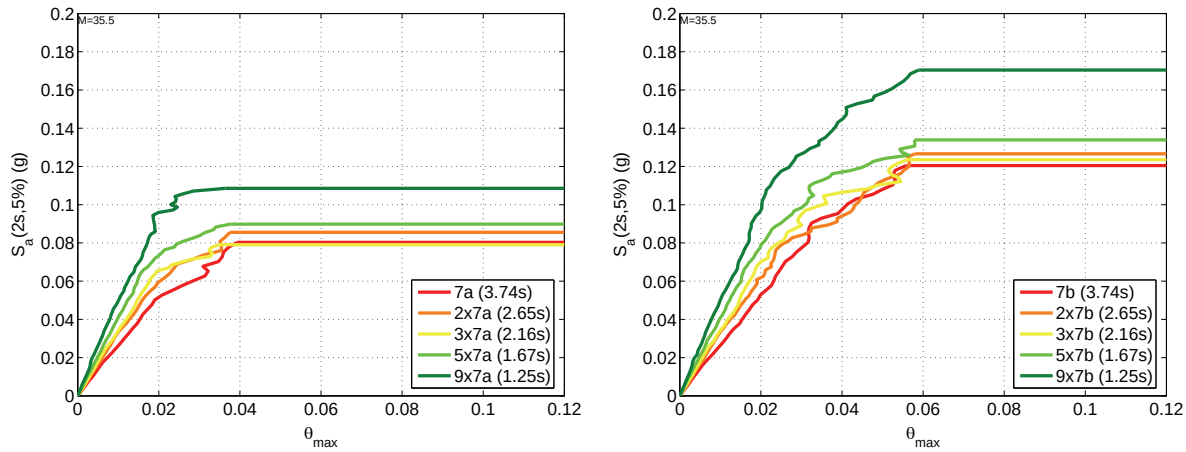

Figure D-34 Median IDA curves plotted versus the intensity measure $S_a(2s,5\%)$ for systems Nx7a and Nx7b with mass M=35.46ton.

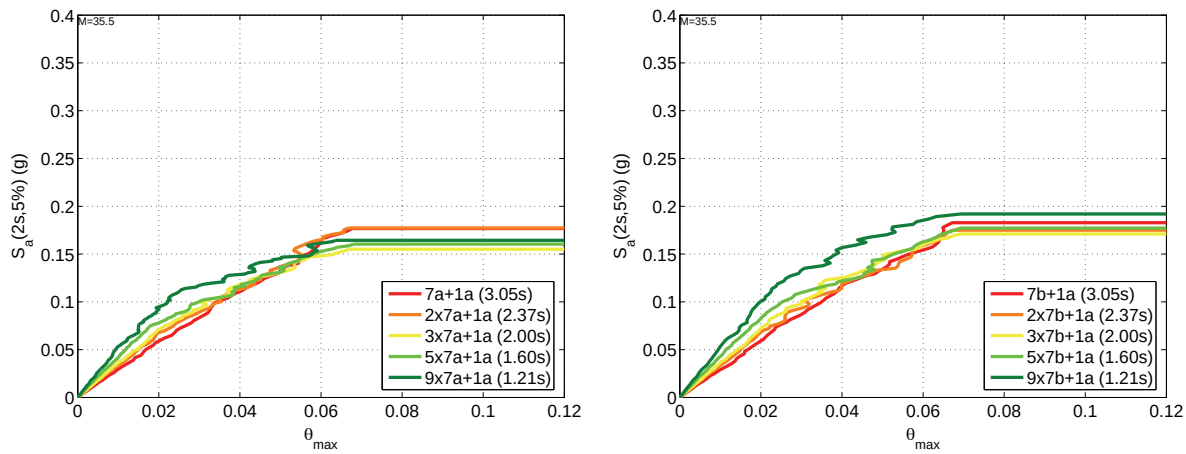

Figure D-35 Median IDA curves plotted versus the intensity measure $S_a(2s,5\%)$ for systems Nx7a+1a and Nx7b+1a with mass M=35.46ton.

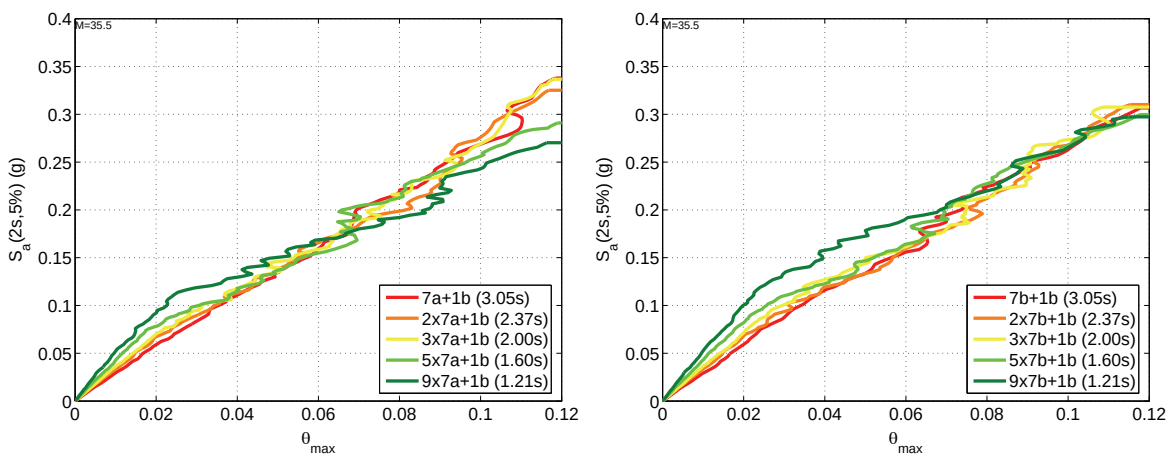

Figure D-36 Median IDA curves plotted versus the intensity measure $S_a(2s,5\%)$ for systems Nx7a+1b and Nx7b+1b with mass M=35.46ton.

Appendix E
Uncertainty, Fragility, and Probability

The concepts presented in this report are compatible with current probabilistic trends in performance-based seismic design. A probabilistic context allows explicit consideration of the variability and uncertainty associated with each of the contributing parameters. An important concept in probabilistic procedures is the development and use of fragility curves.

Use of fragility curves, and explicit consideration of uncertainty in performance assessment, is described in ATC-58 *Guidelines for Seismic Performance Assessment of Buildings* (ATC, 2007). Fragility curves are also used to determine the margin of safety against collapse in FEMA P695 *Quantification of Building Seismic Performance Factors* (FEMA, 2009).

This appendix explains the conversion of incremental dynamic analysis (IDA) results into fragilities, and presents equations that could be used to calculate annual probabilities for collapse, or any other limit state of interest.

E.1 Conversion of IDA Results to Fragilities

Incremental dynamic analysis results can be readily converted to fragilities. Figure E-1 shows an example of IDA results for a single structure subjected to a suite of ground motions of varying intensities.

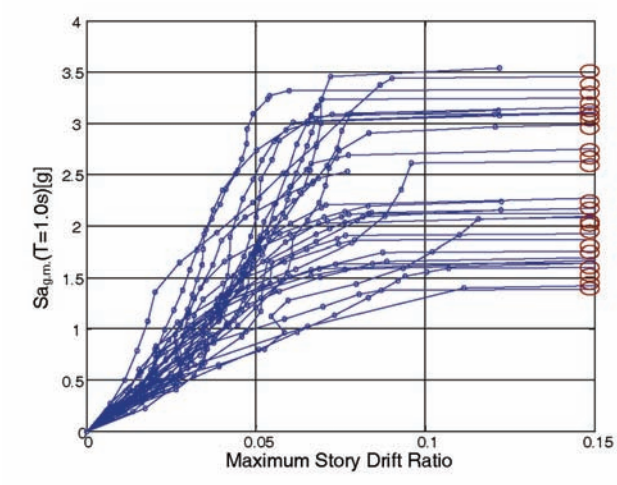

Figure E-1 IDA results for a single structure subjected to a suite of ground motions of varying intensities.

In this illustration, sidesway collapse is the governing mechanism, and collapse prediction is based on dynamic instability or excessive lateral displacements. Using collapse data obtained from IDA results, a collapse fragility can be defined through a cumulative distribution function (CDF), which relates the ground motion intensity to the probability of collapse (Ibarra et al., 2002). Studies have shown that this cumulative distribution function can be assumed to be lognormally distributed. Figure E-2 shows an example of a cumulative distribution plot obtained by fitting a lognormal distribution to the collapse data from Figure E-1.

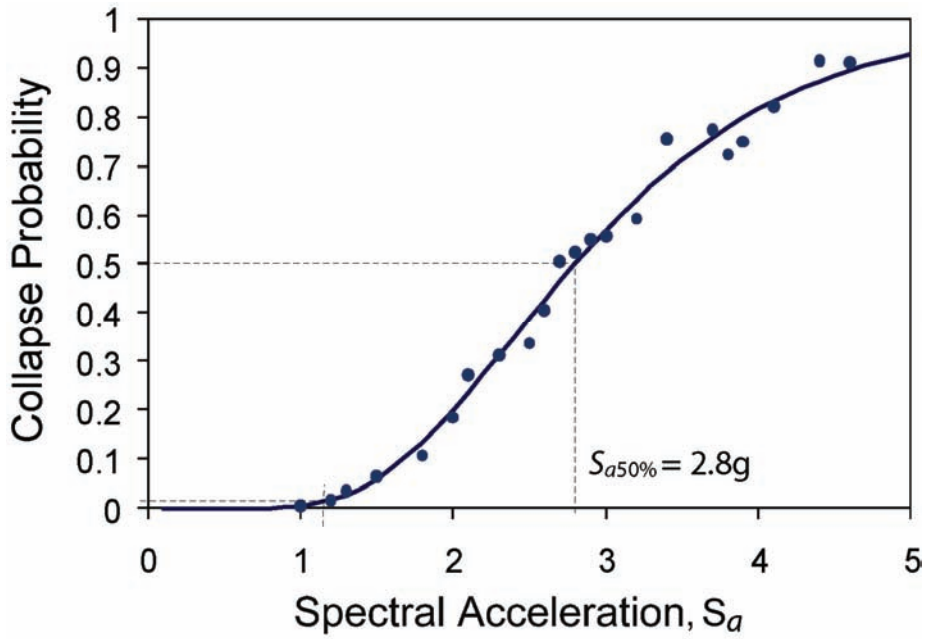

Figure E-2 Cumulative distribution plot obtained by fitting a lognormal distribution to collapse data from IDA results.

Lognormal distributions are defined by a median value and a dispersion parameter. The median collapse capacity, $S_{a50\%}$, indicates a ground motion intensity that has a 50% chance of producing collapse in the system. It also indicates the point at which half of the ground motions will produce collapse at higher intensities, and half will produce collapse at lower intensities. For each mode of collapse, the record-to-record dispersion can be estimated as:

$$\beta_{RTR} = \frac{ln(S_{a84\%}) - ln(S_{a16\%})}{2} \qquad \text{(E-1)}$$

Figure E-3 provides conceptual collapse fragility curves showing the probability of collapse due to loss of vertical-load-carrying capacity (LVCC) or lateral dynamic instability (LDI). These are events are mutually exclusive, meaning that either one or the other can occur, but both events cannot occur at the same time.

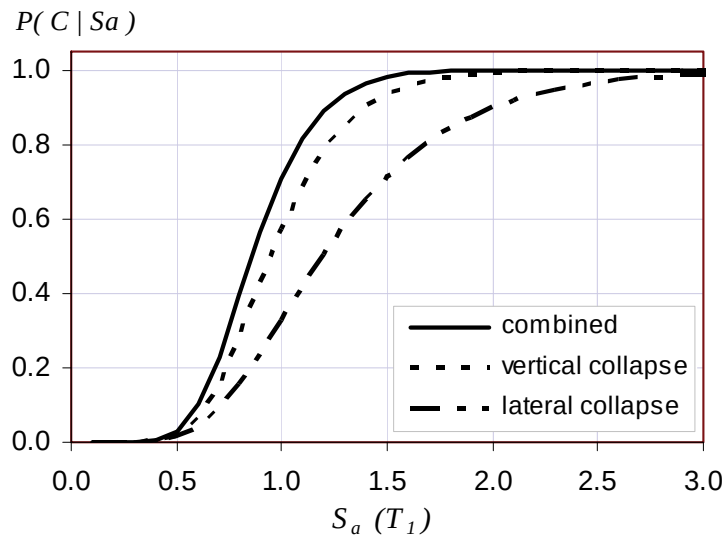

Figure E-3 Conceptual collapse fragility curves for sidesway (lateral) collapse, vertical collapse, and a combination of both.

The total probability of collapse due to either mode can then be represented (Cornell et al., 2005) as:

$$P(C \mid s_a) = P(C_{LDI} \mid s_a) + P(C_{LVCC} \mid NC_{LDI}, s_a) \cdot P(NC_{LDI} \mid s_a \qquad \text{(E-2)}$$

where:

$P(C_{LDI} \mid s_a)$ is the probability of collapse due to lateral dynamic instability at a ground motion intensity level s_a ,

$P(C_{LVCC} \mid NC_{LDI}, s_a)$ is the probability of collapse due to loss of vertical-load-carrying capacity, given that collapse due to lateral dynamic instability has not occurred at intensity s_a , and

$P(NC_{LDI} \mid s_a)$ is the probability of no collapse due to lateral dynamic instability at a ground motion intensity level s_a.

Since $P(NC_{LDI} \mid s_a)$ is equal to $1 - P(C_{LDI} \mid s_a)$, then Equation E-2 can also be written as:

$$P(C \mid s_a) = P(C_{LVCC} \mid NC_{LDI}, s_a) + P(C_{LDI} \mid s_a) - P(C_{LVCC} \mid NC_{LDI}\, s_a) \cdot P(C_{LDI} \mid s_a) \qquad \text{(E-3)}$$

E.2 Calculation of Annualized Probability

The results of an incremental dynamic analysis expressed as a cumulative distribution function can be used in combination with a seismic hazard curve to generate mean annual frequencies (MAF) for collapse (or for other limit states of interest). This process is the integration of the limit state CDF (e.g.,

fragility representing the probability of collapse as a function of spectral acceleration) with respect to the probability of occurrence of the intensity measure (e.g., hazard curve representing the annual probability of exceeding a full range of spectral accelerations). The mean annual frequency of collapse, λ_{col}, or other limit state of interest, can be approximated (Cornell, 2002) as:

$$\lambda_{col} = \lambda_{S_a}\left(\eta_C\right)\exp\left(\frac{1}{2}k^2\beta_{RTR}^2\right) \tag{E-4}$$

where $\lambda_{S_a}\left(\eta_C\right)$ is the mean annual probability of the median spectral acceleration associated with collapse. The parameter k is the slope of the hazard curve, and can be calculated as:

$$k = \frac{\ln\left(\dfrac{H_{S_{aT}(10/50)}}{H_{S_{aT}(2/50)}}\right)}{\ln\left(\dfrac{S_{aT(2/50)}}{S_{aT(10/50)}}\right)} = \frac{1.65}{\ln\left(\dfrac{S_{aT(2/50)}}{S_{aT(10/50)}}\right)} \tag{E-5}$$

Appendix F
Example Application

This appendix presents an example application of a simplified nonlinear dynamic analysis procedure. The concept originated during the conduct of focused analytical studies comparing force-displacement capacity boundaries to incremental dynamic analysis results. In this procedure, a nonlinear static analysis is used to generate an idealized force-deformation curve (i.e., static pushover curve). The resulting curve is then used as a force-displacement capacity boundary to constrain the hysteretic behavior of an equivalent single-degree-of-freedom (SDOF) oscillator. This SDOF oscillator is then subjected to incremental dynamic analysis.

The steps for conducting a simplified nonlinear dynamic analysis are outlined in the following section, and illustrated using an example building. Alternative retrofit strategies are evaluated using the same procedure. Use of the procedure to develop probabilistic estimates of performance for use in making design decisions is also illustrated.

F.1 Simplified Nonlinear Dynamic Analysis Procedure

The concept of a simplified nonlinear dynamic analysis procedure includes the following steps:

- **Develop an analytical model of the system**.

  Models can be developed in accordance with prevailing practice for seismic evaluation, design, and rehabilitation of buildings described in ASCE/SEI Standard 41-06 *Seismic Rehabilitation of Existing Buildings* (ASCE, 2006b). Component properties should be based on force-displacement capacity boundaries, rather than cyclic envelopes.

- **Perform a nonlinear static pushover analysis.**

  Subject the model to a conventional pushover analysis in accordance with prevailing practice. Lateral load increments and resulting displacements are recorded to generate an idealized force-deformation curve.

- **Conduct an incremental dynamic analysis of the system based on an equivalent SDOF model.**

  The idealized force-deformation curve is, in effect, a system force-displacement capacity boundary that can be used to constrain a hysteretic model of an equivalent SDOF oscillator. This SDOF oscillator is then subjected to incremental dynamic analysis to check for lateral dynamic instability and other limit states of interest. Alternatively, approximate incremental dynamic analysis can be accomplished using the idealized force-deformation curve and the *Static Pushover 2 Incremental Dynamic Analysis* open source software tool, SPO2IDA (Vamvatsikos and Cornell, 2006).

- **Determine probabilities associated with limit states of interest.**

  Results from incremental dynamic analysis can be used to obtain response statistics associated with limit states of interest in addition to lateral dynamic instability. SPO2IDA can also be used to obtain median, 16th, and 84th percentile IDA curves relating displacements to intensity. Using the fragility relationships described in Appendix E in conjunction with a site hazard curve, this information can be converted into annual probabilities of exceedance for each limit state. Probabilistic information in this form can be used to make enhanced decisions based on risk and uncertainty, rather than on discrete threshold values of acceptance.

F.2 Example Building

The example building is a five-story reinforced concrete frame residential structure with interior unreinforced masonry infill partitions in the upper stories, and a soft/weak first-story. An exterior elevation of the building is shown in Figure F-1 and first floor plan is shown in Figure F-2. Reinforced concrete columns in each orthogonal direction provide lateral resistance to seismic forces. As indicated in Figure F-2, the first story includes a mixture of components with column-like proportions and components that are more like slender shear walls.

This building is a prototypical example of a soft/weak story structure. Concentration of inelastic deformations in the first story presents an obvious potential story collapse mechanism.

F.3 Structural Analysis Model

To investigate the potential for collapse in this structure, it is reasonable to assume that the response can be represented by a SDOF model. The first story column components are classified for modeling purposes in accordance

with ASCE/SEI 41-06. Most of the columns in this example are classified as shear-controlled or flexure-shear controlled. Wall-like column components are shear-controlled along the strong axis of the member.

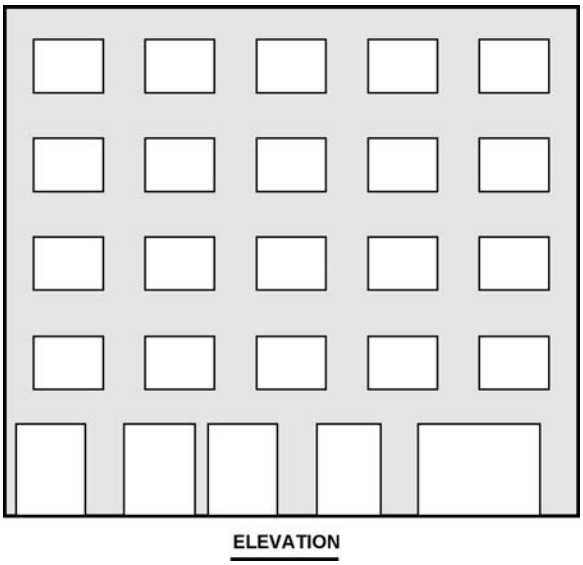

Figure F-1 Example building exterior elevation.

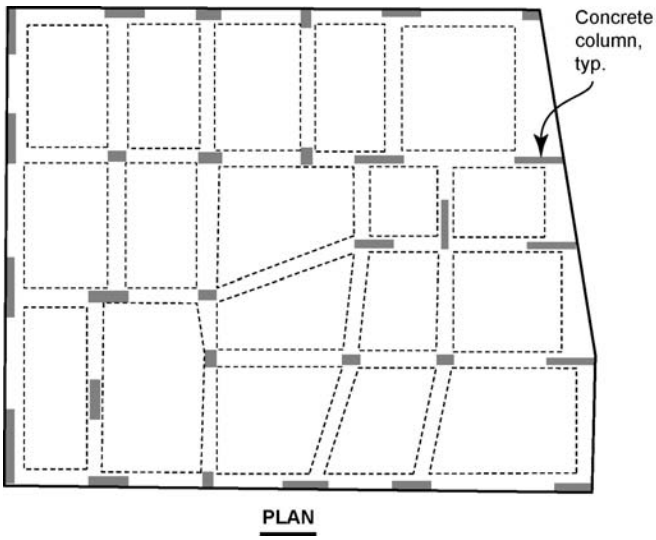

Figure F-2 Example building first floor plan.

Modeling parameters for the column components can be characterized by the conceptual force-displacement relationship ("backbone") specified in ASCE/SEI 41-06. The modeling parameters selected for the components in this example are taken from Chapter 6 of ASCE/SEI 41-06, and depicted in Figure F-3. In both cases, the residual strength, *c*, is taken as zero.

The column components are assembled into a model of the structural system as shown in Figure F-4. Inelastic response is assumed to occur predominantly in the first story. First-story columns are taken as fixed at the base on a rigid foundation. The stiffness of the column components are based on elastic properties in flexure and shear. The model includes soil flexibility, allowing for rigid body rotation due to the response of the structure above. Soil stiffness parameters are taken from Chapter 4 of ASCE/SEI 41-06, assuming a relatively soft soil site (site Class E).

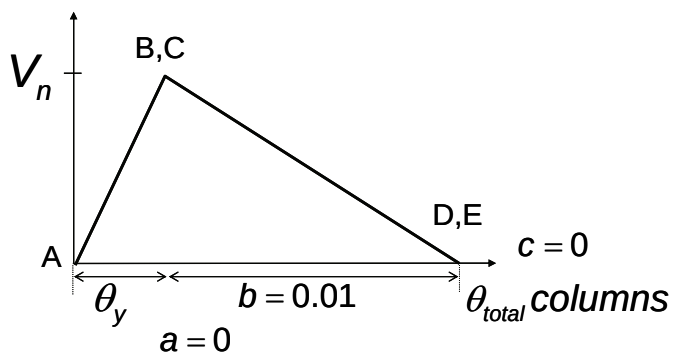

(a)

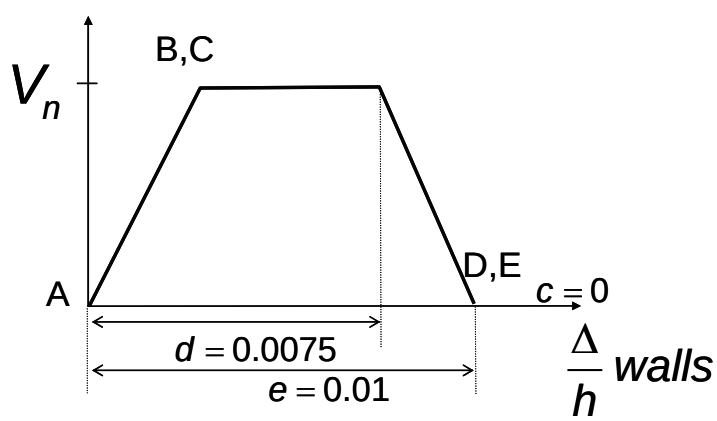

(b)

Figure F-3 Force-displacement modeling parameters for: (a) column components; and (b) wall-like column components.

When developing a SDOF representation of a system, it is important to account for foundation rotation in assessing column distortions. The resulting SDOF model represents the relationship between the total first floor drift, including contributions from the foundation, $\theta_{sys} = \theta_{fdn} + \theta_{cols}$, and the applied inertial loads, V.

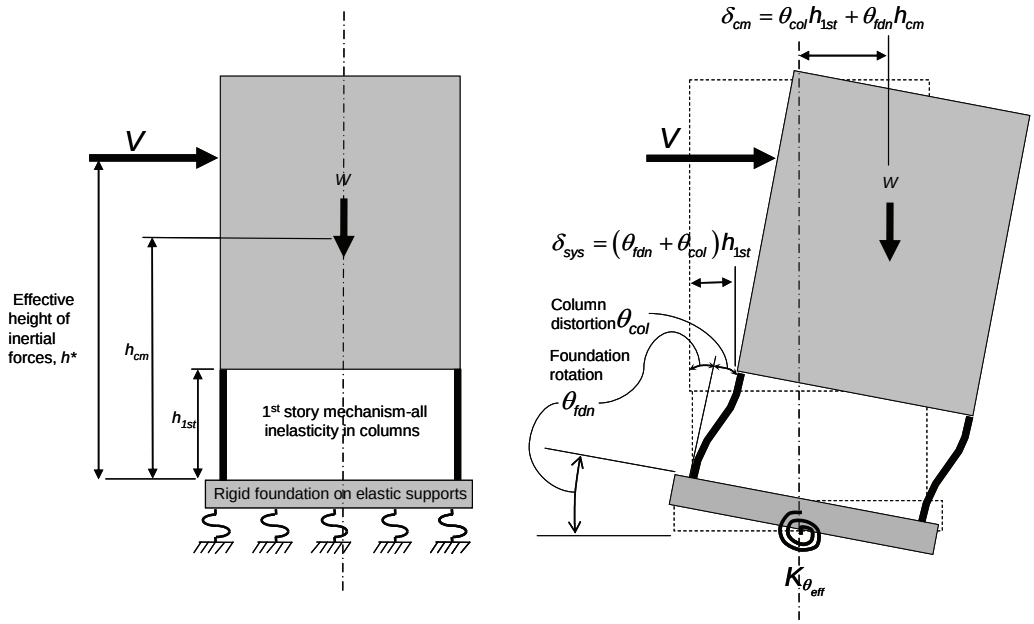

(a.) (b)

Figure F-4 Structural analysis model showing: (a) assumptions; and (b) distortions.

F.4 Nonlinear Static Pushover Analysis

The analytical model is subjected to a conventional pushover analysis. Results are shown in Figure F-5.

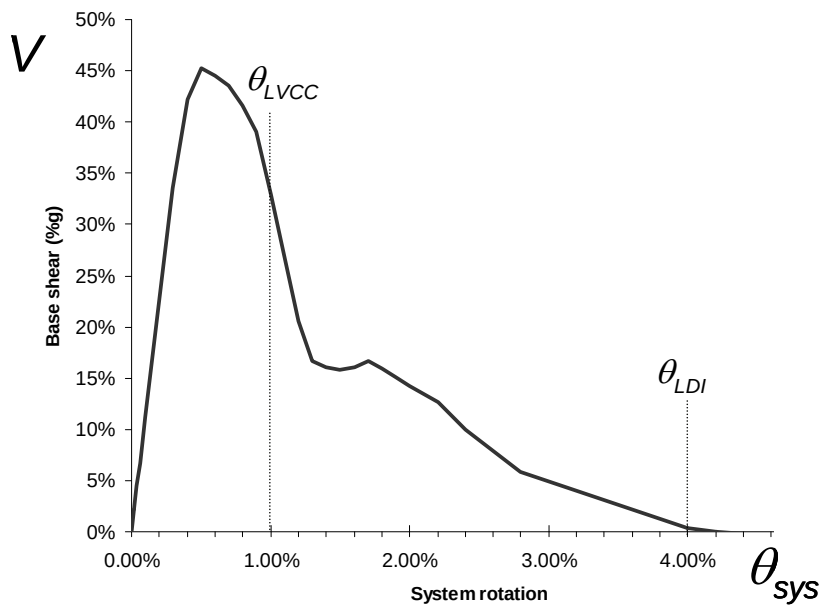

Figure F-5 Pushover curve from nonlinear static analysis.

F.5 Evaluation of Limit States of Interest

Collapse in real structures can be caused by sidesway collapse (lateral dynamic instability) or by loss of vertical-load-carrying capacity. In this example, the following two limit states are defined (both are shown in Figure F-5):

θ_{LVCC} the total system rotation at which loss of vertical-load-carrying capacity occurs (i.e., when first story columns fail due to shear distortion). In this example, the critical column distortion for loss of vertical-load-carrying capacity is taken as 1% inelastic rotation, which occurs when the total system rotation θ_{sys} = 1.2%.

θ_{LDI} the total system rotation at which lateral dynamic instability occurs (i.e., when first story columns lose all lateral-force-resisting capacity). In this example, this is taken to occur when the total system rotation θ_{sys} = 4.0%.

The target displacement for a given intensity is estimated using the Coefficient Method:

$$\delta_t = C_0 C_1 C_2 S_a \frac{T_e^{\,2}}{4\pi^2} g$$

Uniform hazard spectra for the example site are shown in Figure F-6 and Figure F-7.

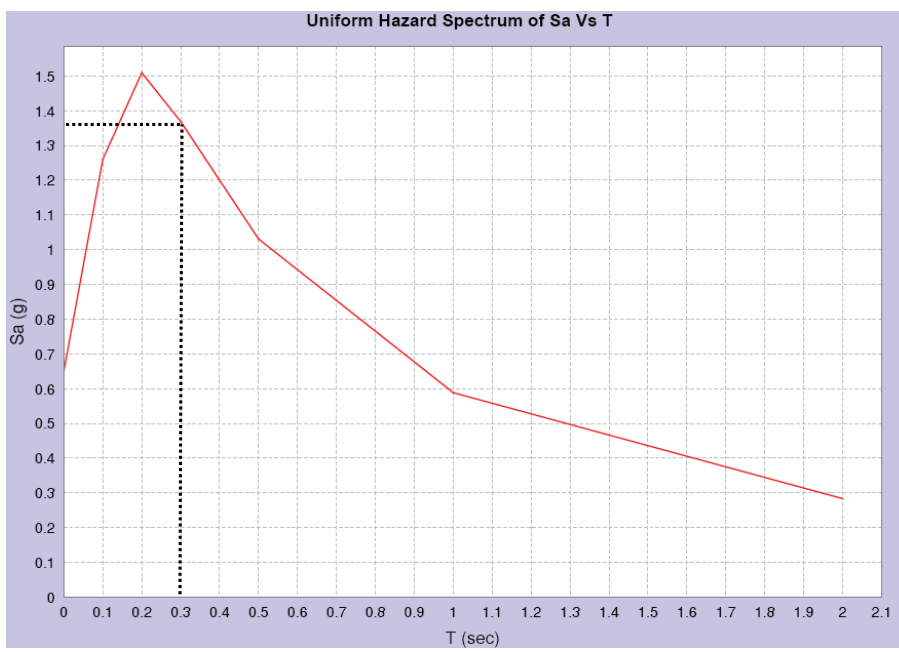

Figure F-6 Uniform hazard spectrum for intensity corresponding to 10% chance of exceedance in 50 years (from USGS).

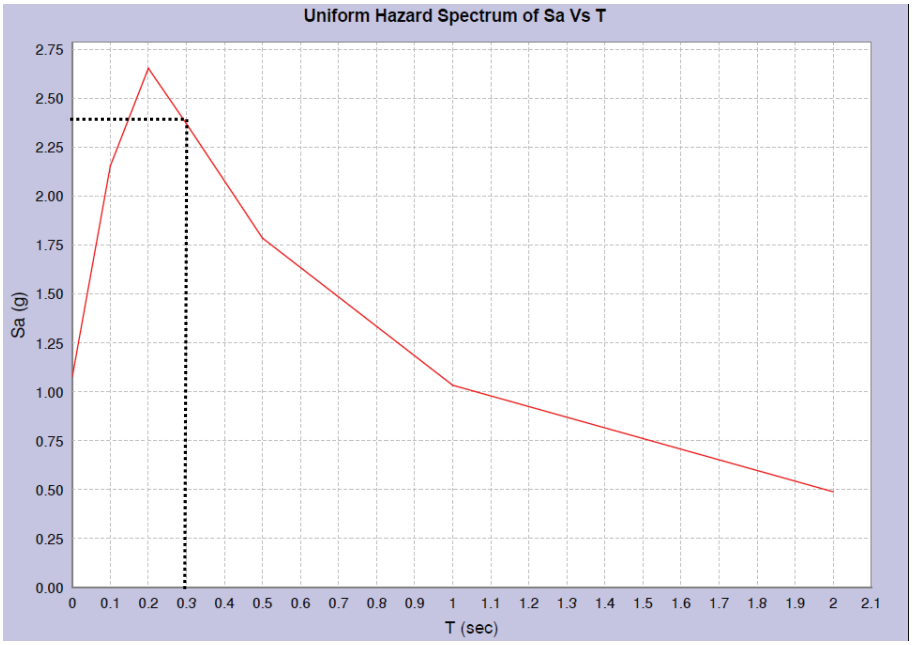

Figure F-7 Uniform hazard spectrum for intensities corresponding to 2% chance of exceedance in 50 years (from USGS).

For an intensity corresponding to a 10% chance of exceedance in 50 years (i.e., 475-year return period), and a period T = 0.3s:

$$S_a = 1.36g$$

The strength of the model is:

$$F_y = 0.45g$$

which results in:

$$R = \frac{S_{aT}g}{F_y} = 3.0 \text{ for the 10\%/50 year hazard level.}$$

The coefficients are:

$C_0 =$ first mode participation factor = 1.0,

$$C_1 = 1 + \frac{R-1}{aT_e^2} = 1.3,$$

where a = 50, and

$$C_2 = 1 + \frac{1}{800}\left(\frac{R-1}{T_e}\right)^2 = 1.04.$$

This results in a target displacement of:

$\delta_t = 1.6$ inches, or $\theta_{sys} = 1.6/100 = 1.6\,\%$.

This is greater than the acceptable limit for loss of vertical-load-carrying capacity (θ_{LVCC}) taken as θ_{sys} = 1.2%.

To check for lateral dynamic instability, the proposed equation for R_{di} is:

$$R_{di} = \left(\frac{\Delta_c}{\Delta_y}\right)^a + b\frac{T_e}{3|\gamma|} + \frac{F_r}{F_c}\left(\frac{\Delta_u - \Delta_r}{\Delta_y}\right)\sqrt[3]{T_e}$$

where T_e is the effective fundamental period of vibration of the structure, Δ_y, Δ_c, Δ_r, and Δ_u are displacements corresponding to the yield strength, F_y, capping strength, F_c, residual strength, F_r, and ultimate deformation capacity at the end of the residual strength plateau. Determination of these parameters requires a multi-linear idealization of the pushover curve, as shown in Figure F-8.

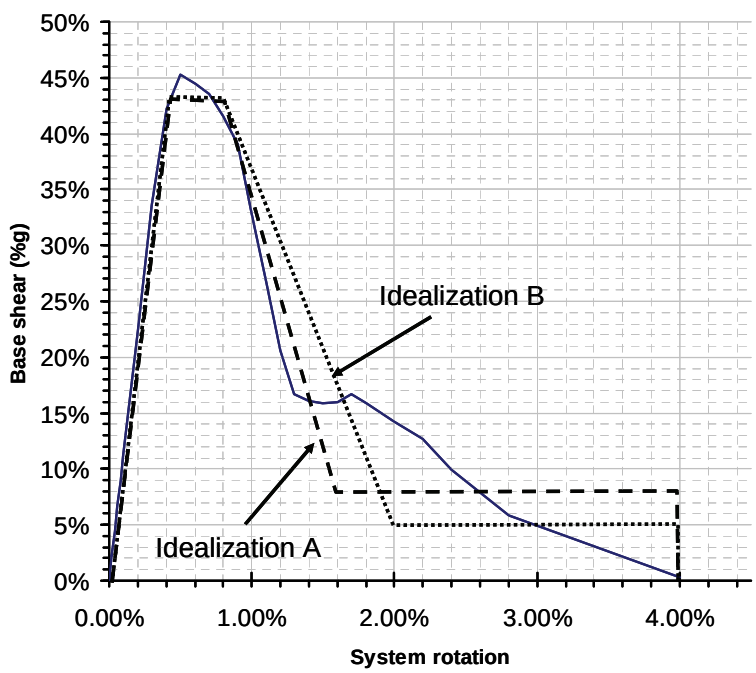

Figure F-8 Pushover curve from nonlinear static analysis and two idealized system force-displacement capacity boundaries.

Parameters a and b are functions given by:

$$a = 1 - \exp(-dT_e)$$

$$b = 1 - \left(\frac{F_r}{F_c}\right)^2$$

and parameter d is a constant equal to 4 for the example building (assuming the presence of stiffness degradation).

Using the above expressions along with parameters from Idealization 'A' in Figure F-8, results in:

$$R_{di} = 2.6$$

which is less that the calculated value of R = 3.0 for intensities corresponding to the 10%/50 year hazard level. The parameter R is a ratio equal to the strength necessary to keep a system elastic for a given intensity, divided by the yield strength of the system. Higher values of R imply lower values of system yield strength. Values of R that exceed R_{di} mean that the structure does not meet the minimum strength necessary to avoid lateral dynamic instability at this hazard level.

At higher intensities (e.g., 2%/50 year hazard level) the calculated value of R would be even higher ($R = 5.3 >> R_{di} = 2.6$), illustrating how the comparison between system strength and the limit on lateral dynamic instability would change for a different hazard level.

In summary, the example structure does not meet acceptability criteria for loss of vertical-load-carrying capacity and lateral dynamic instability at the 10%/50 year hazard level. Thus, a nonlinear response-history analysis must be performed.

F.6 Incremental Dynamic Analysis

The resulting force-displacement relationship from the pushover curve can be used to generate a force-displacement capacity boundary for the system. An incremental dynamic analysis (IDA) can then be applied to a SDOF oscillator constrained by the resulting force-displacement capacity boundary. Performing an incremental dynamic analysis will allow determination of the ground motion intensity at which various limit state deformations occur.

For the example building, an approximate incremental dynamic analysis is performed using the open source software tool, SPO2IDA. Use of SPO2IDA along with Idealization 'A' in Figure F-8 results in the median, 16th, and 84th percentile IDA curves shown in Figure F-9. The figure also includes the estimate of R_{di} for lateral dynamic instability.

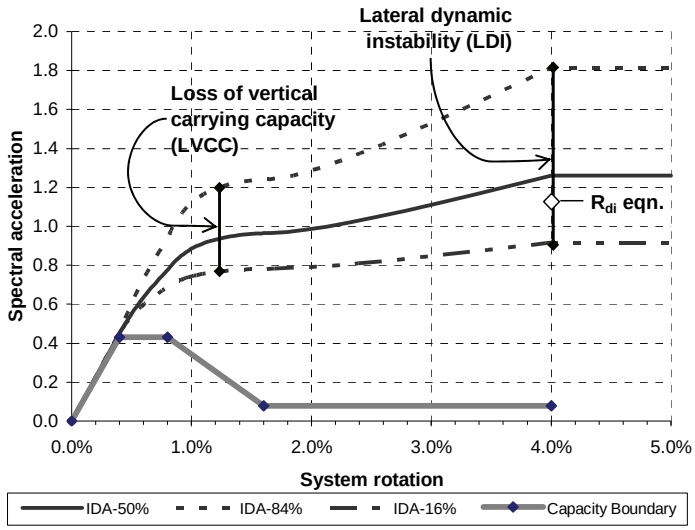

Figure F-9 Results of approximate incremental dynamic analysis using SPO2IDA.

F.7 Determination of Probabilities Associated with Limit States of Interest

From Figure F-9, median values of intensity causing loss of vertical-load-carrying capacity (LVCC) or lateral dynamic instability (LDI) in the example building can be obtained. Using the expressions in Appendix E, the dispersion and mean annual frequencies (MAF) associated with these limit states can be determined. The resulting data is presented Table F-1.

Table F-1 Mean Annual Frequencies for Collapse Limit States

Limit state/collapse mode	S_{a50}	MAF S_{a50}	β	MAF collapse
Loss of vertical load carrying capability	0.92	0.0050	0.20	0.0060
Lateral dynamic instability	1.26	0.0025	0.32	0.0040
LVCC or LDI	0.88	0.0060	0.17	0.0069

For the example building, fragilities associated with loss of vertical-load-carrying capacity (LVCC) or lateral dynamic instability (LDI) are derived from the median values of spectral acceleration and dispersions in Table F-1, as illustrated in Figure F-10.

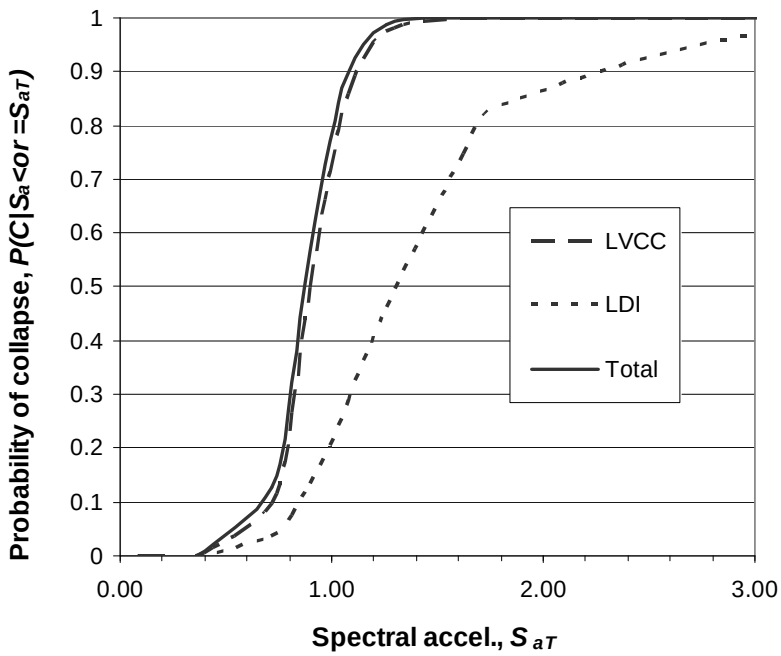

Figure F-10 Example building collapse fragilities for loss of vertical-load-carrying capacity (LVCC), lateral dynamic instability (LDI), and a combination of both.

The probabilities of experiencing the limit states of interest for the example building are derived in combination with a site-specific seismic hazard curve. For a representative soft site, the USGS hazard curve for a period of 0.3 seconds is shown in Figure F-11.

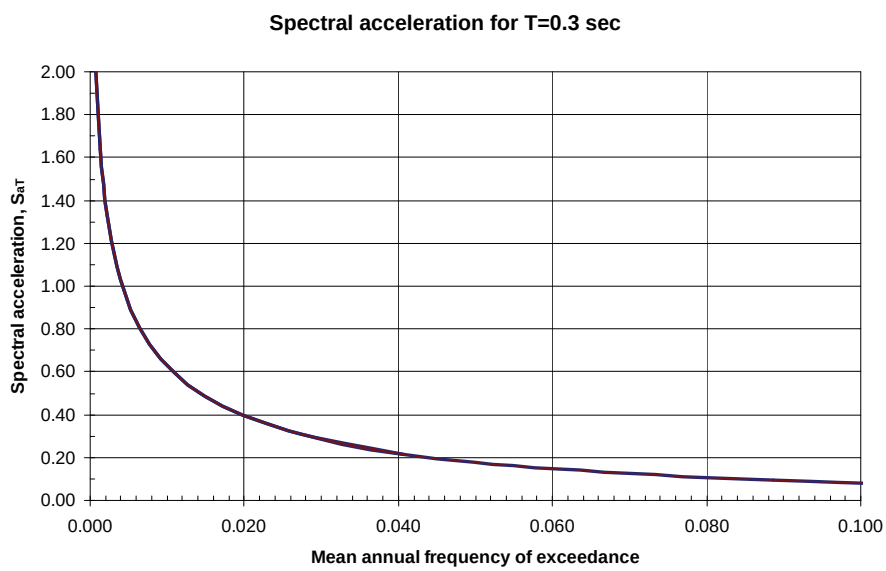

Figure F-11 Hazard curve for representative soft site (from USGS).

Using the expressions in Appendix E, the mean annual frequency (MAF) of collapse of the example building can be calculated. The MAF of collapse, shown in Table F-1, is approaching 1% annually, which can be considered high.

F.8 Retrofit strategies

As indicated by results of focused analytical studies presented in Chapter 4, the probability of collapse, as measured by the potential for lateral dynamic instability, can be reduced by adjusting the force-deformation characteristics of the system. Retrofit strategies to reduce the annual probability of collapse could include: (1) the addition of secondary lateral system; or (2) improvement of primary system strength and ductility.

F.8.1 Addition of a Secondary Lateral System

Lateral dynamic instability can be improved through the addition of a flexible and ductile secondary lateral system. In order to be effective, the secondary system does not need to provide much additional lateral strength to the overall system.

Figure F-12 shows a revised pushover curve for the example building after retrofit using a ductile moment frame system with a lateral strength approximately equal to 10% of the building weight. Calculations similar to the above show that this strategy would reduce the mean annual frequency of collapse due to lateral dynamic instability to about 0.2%.

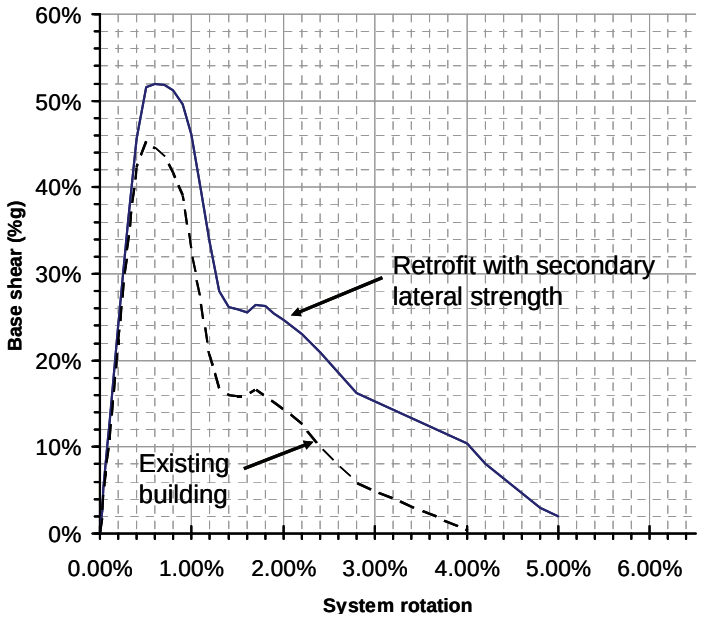

Figure F-12 Revised pushover curve for the example building after retrofit with a secondary lateral system.

F.8.2 Improvement of Primary System Strength and Ductility

Lateral dynamic instability can also be improved by providing additional deformation capacity in the system. This can be accomplished by wrapping the concrete columns with fiber reinforced polymers (FRP) to increase strength and ductility of the primary seismic-force-resisting system.

Figure F-13 shows a revised pushover curve for the example building after retrofitting the existing columns with FRP. Calculations similar to the above show that this strategy would reduce the mean annual frequency of collapse due to lateral dynamic instability to about 0.03%, which is an order of magnitude improvement over the existing structure.

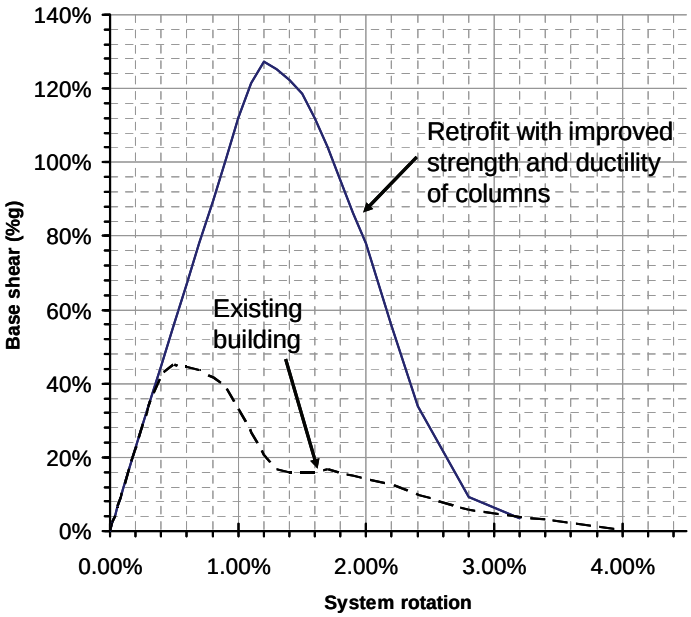

Figure F-13 Revised pushover curve for the example building after retrofit for improved strength and ductility of columns.